NASA Technical Memorandum 106989

Structures Division 1994 Annual Report

Structural Mechanics • Fatigue and Fracture •
Structural Dynamics • Structural Integrity

National Aeronautics and
Space Administration

May 1996
Lewis Research Center

Introduction

The 1994 Annual Report of the Structures Division of the NASA Lewis Research Center gives a brief, but comprehensive, review of the work completed and the technical accomplishments of the division during the 1994 calendar year. The Structures Division consists of four branches: Structural Mechanics, Fatigue and Fracture, Structural Dynamics, and Structural Integrity. The report is organized to match the functional branches within the division. This publication covers 54 separate topics with a bibliography of 66 citations.

The research work we undertake is dictated primarily by NASA mission requirements and the intermediate and long-range aeropropulsion goals of U.S. industry. The intent of this research is to both enable and facilitate the competitiveness of the U.S. aeropropulsion industry and the performance of space propulsion systems. The focus of most of our work is on developing enabling technology for NASA missions and improving commercial aeronautical engines and turbomachinery. Much of this technology also has use in nonaerospace applications. It finds its way into engineering design books, technical society standards and codes, and computer-aided design (CAD) and analysis codes.

The work reported was performed both in-house at the Lewis Research Center and on contracts and grants with industry and universities under sponsorship of Lewis. Although not always the case, most of the reported work was planned and begun 5 to 10 years before its completion. It was undertaken in consultation with representatives of the aerospace industry, academia, and NASA. Cooperative technology programs are concurrently carried out with both industry and universities to transfer and implement this NASA-developed technology.

The staff of the Structures Division includes a number of internationally recognized engineering authorities in their fields of expertise. Many of them, besides performing research and writing the journal and NASA articles listed in the bibliography, have written or contributed to engineering and scientific books used in industry and academia. These books incorporate much of the work that they and their colleagues performed at Lewis. A number of the staff members have been recognized for their contributions by being named a fellow in their respective engineering professional societies. The honor of fellow is awarded to less than 1 percent of all engineers is recognition of their outstanding engineering and scientific contributions and professional achievements.

We hope that you find this report useful. Your comments or questions regarding the report or our work are welcome. You may contact me or any of the Lewis contacts named for additional information.

Louis J. Kiraly
Acting Chief, Structures Division

Contents

Structural Mechanics

Fatigue and Fracture

Structural Dynamics

Structural Integrity

Structural Mechanics

Dominant Parameters for Reliable Combustor Liner Design Identified by Probabilistic Assessment

Aerospace propulsion systems are a complex assemblage of structural components that are subjected to a variety of cyclic and transient loading conditions. Inherent variability of material properties and fabrication processes, as well as geometrical tolerances introduce additional uncertainties. Deterministic structural analysis methods are not adequate to properly evaluate the design parameters' variability. Furthermore, these methods lead to conservative designs because they use safety factors.

As an alternative to the deterministic approach, NASA Lewis is developing probabilistic structural analysis methods (PSAM's), which enable a user to assess the effects of fluctuating loads, variable material properties, and uncertain geometries on the scatter of structural responses (eigenvalues, frequencies, effective stresses, etc.). PSAM's are a more reliable and systematic way to quantify sensitivities associated with the corresponding uncertainties in the design variables and the significance of the design variables to the system model. A PSAM is embedded in the computer code Numerical Evaluation of Stochastic Structures Under Stress (NESSUS).

A typical hot structural component within an engine, such as a composite combustor liner, is computationally simulated and probabilistically evaluated in view of the numerous uncertainties associated with the structural, material, and thermomechanical load variables (primitive variables) that describe the combustor. Results show that the scatter in the combined stress is not uniform along the length of the combustor and that the coefficient of thermal expansion, the hoop modulus of the liner material, and the thermal load profile dominate stresses near the support. Furthermore, altering the support conditions to allow unrestrained radial growth reduced the stress level near the support location by more than 50% to that of fixed support conditions at 50% probability level (fig. 1).

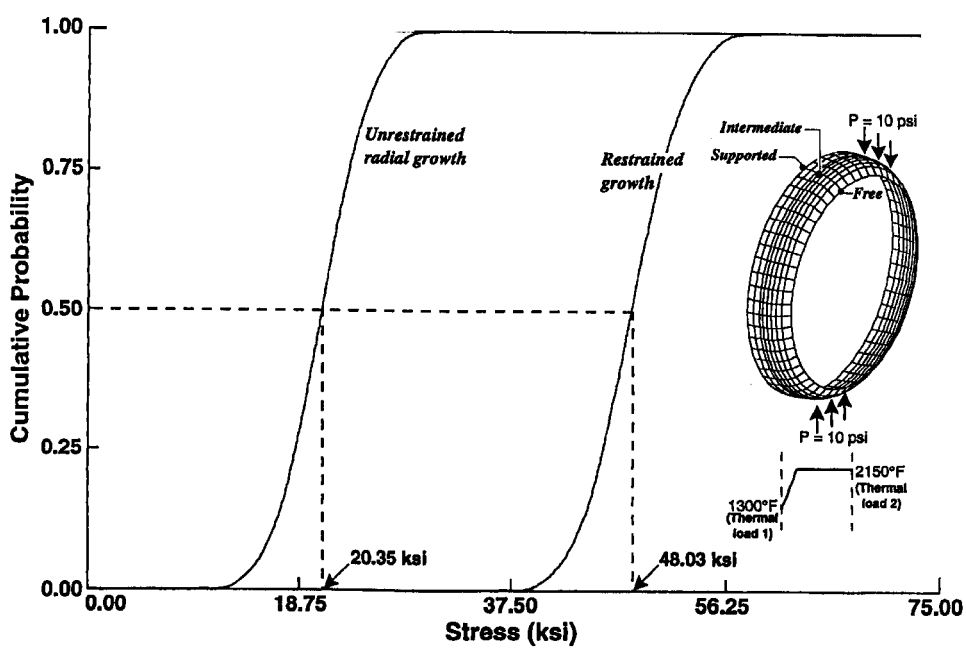

Figure 1.—Substantially reduced stresses near Enabling Propulsion Materials Program combustor support from selecting support compliance.

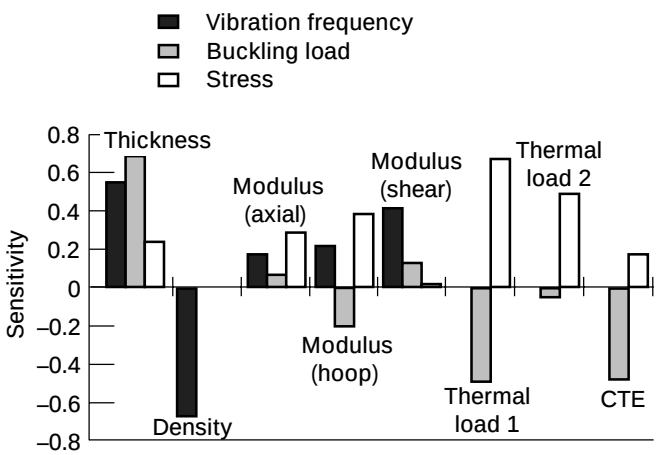

Figure 2.—Identification of dominant parameters by probabilistic assessment. Probability level, 0.001.

Collectively, the results give quantifiable guidance on dominant parameters for reliable combustor liner design (fig. 2).

Lewis contact: Shantaram S. Pai, (216) 433–3255

Multilevel Substructuring Solution Strategy Implemented on Workstation Network by Using Parallel Virtual Machine Code

Efforts continue in the development of parallel finite element (FE) analysis capabilities that are easy to use, computationally efficient, economically viable, and readily transportable from one computer architecture to the next. In an attempt to address these goals, a parallel multilevel substructuring (MLS) FE program has been developed to organize the parallelization of the overall solution process. This program uses parallel virtual machine (PVM) code to exploit the modular flexibility that the MLS solution strategy can provide in scheduling resources on a distributed-memory network, such as the NASA Lewis Advanced Cluster Environment (LACE) system. The LACE system is a clustered set of 32 IBM RS6000 workstations.

Integrating PVM and MLS allows concurrent data input, element stiffness matrix generation and assembly, solution of system equations, postprocessing (e.g., stress and strain calculations), and data output phases of the FE solution process. Concurrent computation can be achieved on a distributed-memory network such as the LACE system because each substructure can be manipulated virtually in its entirety on its own workstation during all FE solution phases.

In addition to its computational advantages, MLS has many favorable analytical capabilities. One in particular is the ability to isolate the numerical treatment of nonlinear material behavior. Specifically, when using a Newton-Raphson solver, only the stiffness matrices of the substructures that are affected by nonlinearity need be updated during the nonlinear iteration process. As a consequence the statically condensed coefficient matrices of the linear substructures need only be calculated once and can simply be reassembled with the updated nonlinear condensed systems as necessary. Note that the recalculation of the stiffness matrices for entire “branches” and/or levels of the MLS model hierarchy during the nonlinear iterations can be circumvented when using this type of solution strategy.

To demonstrate the validity of the MLS solution strategy as a viable algorithmic approach for the efficient parallelization of the overall FE analysis solution process, we elasto-plastically analyzed two types of turbine blade subjected to centrifugal forces. The first model (fig. 1) has 1575 nodes,

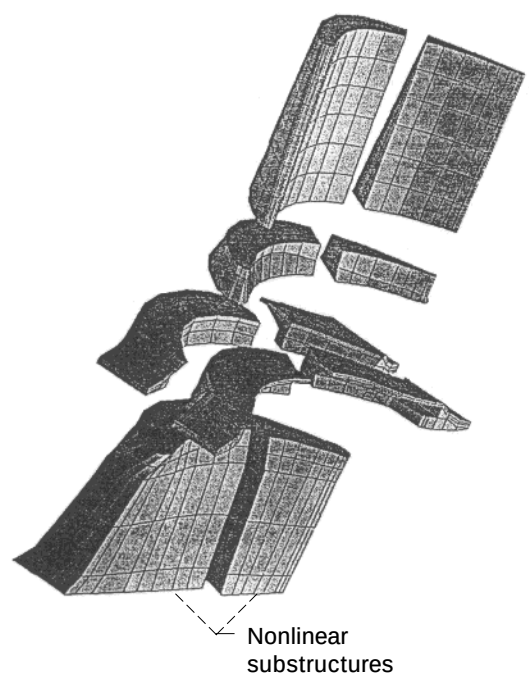

Figure 1.—First level of three-level turbine blade model.

4533 equations, 1025 elements, and a “global” mean half-bandwidth of 253. The other model (fig. 2) has 12 767 nodes, 36 518 equations, 10 955 elements, and a “global” mean half-bandwidth of 728. As figures 1 and 2 show, the linear and nonlinear parts of the analysis can be readily isolated from each other when using MLS. Note that these figures represent just the first level of their respective MLS decompositions.

Three versions of the analysis were performed for each model on the LACE network to evaluate the performance of the MLS program: (1) an analysis of the standard, “global” version of the FE model on a single workstation, (2) an analysis of the MLS version of the model on a single workstation, and (3) an analysis of the model using multiple workstations. Figures 3 and 4 convey the results from this study. In particular, they show the wallclock times obtained for two iterations of the solution process for each of the three benchmark analyses conducted for each problem. These results show that a properly constructed MLS decomposition will reduce the amount of time needed to perform analysis. For example, from figure 3 the time required for the first iteration of the analysis for the global and MLS versions of the model shown in figure 1 using one workstation was reduced from 78 to 62 wallclock seconds (WCS). This difference was more disparate for the model shown in figure 2. From figure 4 the time was reduced from 3474 to only 1487 WCS when using only one workstation.

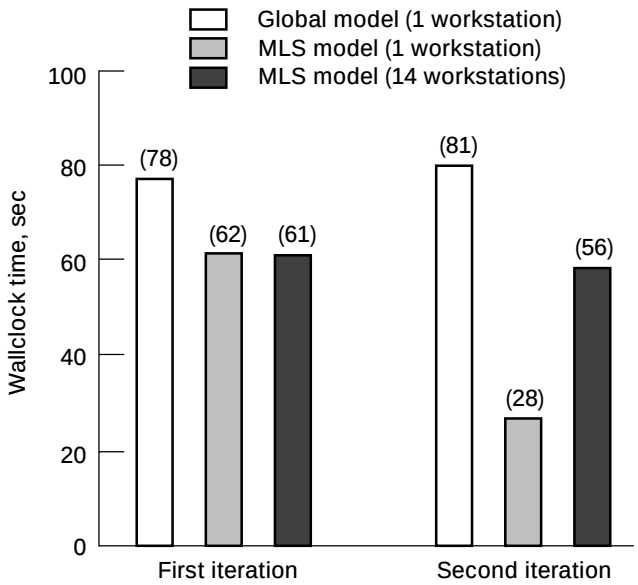

Figure 3.—Run times for turbine blade analysis on single and multiple workstations of LACE system.

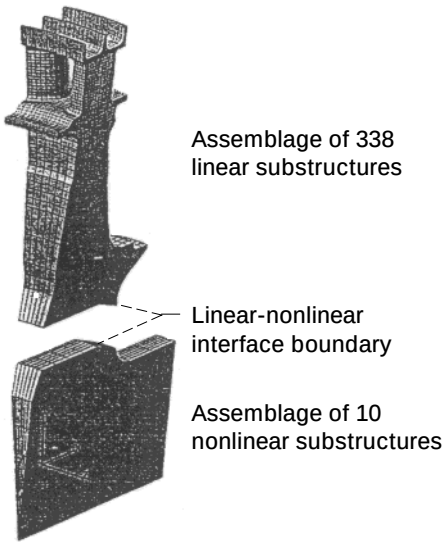

Figure 2.—First level of seven-level rotor blade model.

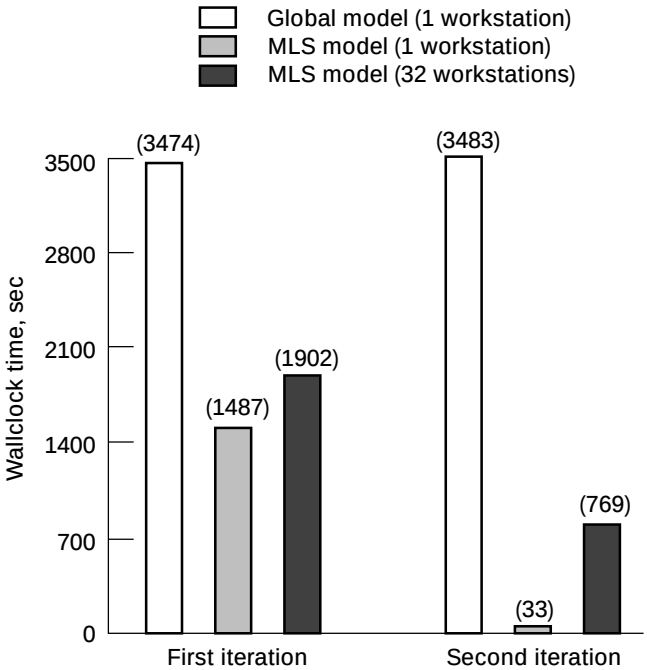

Figure 4.—Run times for rotor blade analysis on single and multiple workstations of LACE system.

The ability to isolate nonlinear material behavior within the requisite substructures was also shown to yield significant computational savings. Comparing the times spent performing the second iteration of the analysis for the global and MLS models on one workstation clearly illustrates this. For instance, the MLS version of the first model required only 28 WCS as opposed to 81 WCS for the global model, and the MLS version of the second model required only 33 WCS as opposed to 3483 WCS for the global model.

The current parallel implementation of the MLS program on the LACE network using PVM was shown to be very inefficient. This inefficiency can be attributed to many factors: (1) using an oversimplified data communication methodology, (2) spawning multiple processes simultaneously on individual workstations, and (3) using an Ethernet to perform the data transfer functions. These deficiencies are being rectified.

Lewis contact: Shantaram S. Pai, (216) 433–3255

Multidisciplinary Design Optimization Tool Minimizes Takeoff Gross Weight for Both Subsonic and Supersonic Aircraft Concepts

Configuration analysis of aircraft, which involves weight estimation, aerodynamics, mission performance, engine propulsion parameters, takeoff and landing conditions, etc., is truly a multidisciplinary problem. A computer software flight optimization system (Flops) has been developed to access new technologies in the conceptual configuration designs of subsonic and supersonic aircraft. For system optimization the Flops software was coupled to the design tool CometBoards (an acronym for comparative evaluation test bed of optimization and analysis routines for the design of structures). Salient features of the Flops and CometBoards optimization system include constraint formulation, design variable formulation, and a global scaling strategy. The resulting multidisciplinary design software was used to generate optimum configurations for subsonic and supersonic aircraft.

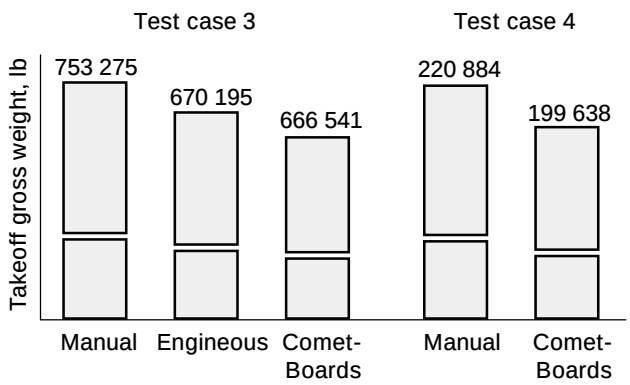

Figure 1.—Optimum designs for subsonic and supersonic aircraft.

It was observed that the optimization system converged to the same global solutions for both subsonic and supersonic aircraft even when begun from different initial design points. The optimum weights obtained for both aircraft are depicted in figure 1. The optimum weights of the subsonic aircraft compare well with the solution that was obtained by another code, Engineous. For the supersonic case the optimum weight is about 10% lighter than the weight used to begin the optimization iterations.

Lewis contacts: Dale A. Hopkins, (216) 433–3260; Surya N. Patnaik, (216) 433–8468

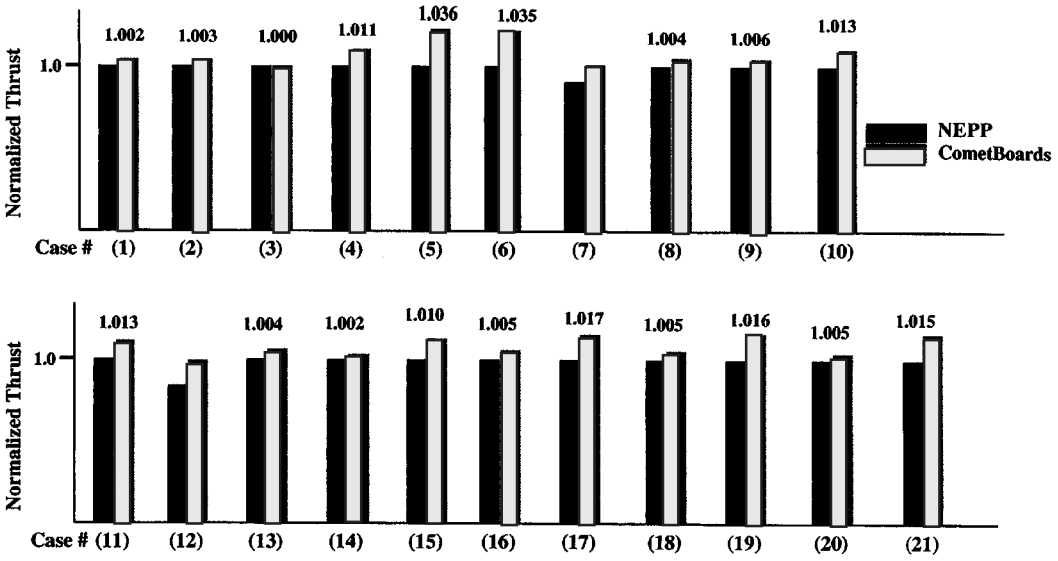

Figure 1.—Optimum thrust for HSCT engine with 21 mission points.

Cascade Optimization Strategy Maximizes Thrust for High-Speed Civil Transport Propulsion System Concept

Designing a High-Speed Civil Transport airbreathing propulsion system for multimode or variable-cycle operations over a wide flight regime is a complex problem. A computer simulation called NASA Engine Performance Program (NEPP) has been developed for analyzing such aeropropulsion engines. Optimizing engine net thrust for multiple mission points (defined through altitudes, Mach numbers, flow rates, etc.) with constraints specified on pressure ratios, temperatures, speed corrections, mass flows, etc., has been cast as a nonlinear programming problem through a soft coupling of the NEPP code and the design tool CometBoards (an acronym for comparative evaluation test bed of optimization and analysis routines for the design of structures). The design parameters, constraints, and merit function of the resulting nonlinear optimization problem vary over a wide range, especially due to the multiple mission requirements for such engines. Using the most robust optimization algorithm (available in CometBoards) could provide a feasible optimum solution only for a portion of the mission.

To generate an optimum solution for the entire flight regime, we have developed a scheme called cascade optimization strategy. Multiple optimization algorithms; pseudorandom damping; and scaling of objectives, design variables, and constraints are a few of the salient features of the cascade strategy. The cascade strategy produced a feasible optimum solution for engines with over 100 mission points. The cascade scheme converged to the same global optimum solution even when begun from different design points. Figure 1 depicts the optimum thrust for an engine with 21 mission points. For the problem the cascade strategy produced superior feasible optimum solutions for the entire mission.

Lewis contacts: Dale A. Hopkins, (216) 433–3260; Surya N. Patnaik, (216) 433–8468

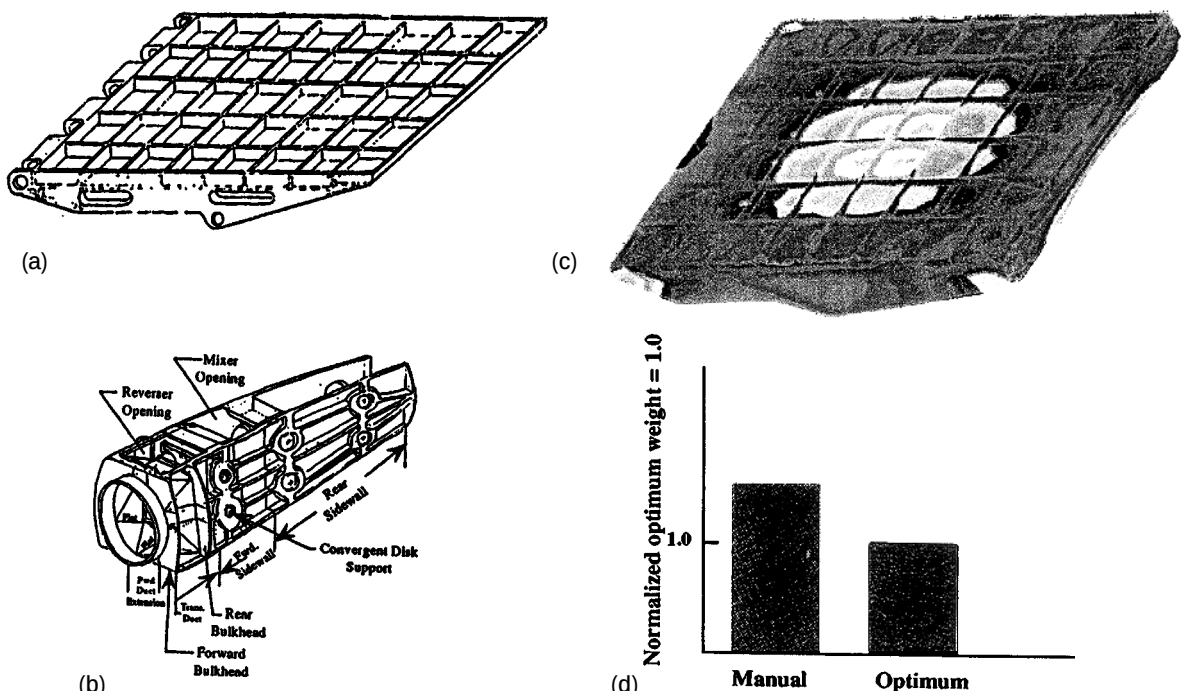

Figure 1—Optimum design of rear divergent flap by CometBoards. (a) Rear divergent flap. (b) Downstream mixing nozzle. (c) Von Mises stress contours. (d) 39% Weight reduction through CometBoards.

Optimization Improves Design of Mixed-Flow Turbofan Engine Exhaust Nozzle Component

A mixed-flow turbofan engine exhaust nozzle system for High-Speed Civil Transport aircraft (depicted in fig. 1) has several components, such as rear and forward divergent flaps, rear and forward sidewalls, bulkheads, duct extensions, and approximately six disk supports. Nozzle design complexity increases with flight Mach number, pressure ratios, temperature gradients, dynamic response, and degradation of material properties at elevated temperatures. Design optimization of a rear divergent flap of the downstream mixing nozzle was attempted through the design code CometBoards (an acronym for comparative evaluation test bed of optimization and analysis routines for the design of structures). The static and dynamic analyses for the flap were performed with two analysis codes (LEHOST and MSC/NASTRAN).

Qualitative behavior of the flap was explored through its dynamic animation. Scrutiny of the animation revealed that skin panels, stiffeners, tapered sidewalls, and edge beams may be candidates for optimizing flap design. The flap was optimized for minimum weight conditions and for static and dynamic constraints for the potential design variables. Features of CometBoards, such as design variable formulation and constraint grouping strategy, were followed to reduce excessive analysis parameters and constraints that resulted from the finite element model, which had over 5000 degrees of freedom. The optimum solution obtained is depicted in figure 1. At the optimum, stress, displacement, and frequency constraints are active. The optimum weight is 39% lower than for the manual design.

Lewis contacts: Dale A. Hopkins, (216) 433–3260; Surya N. Patnaik, (216) 433–8468

More Accurate Stress Mode in Turboprop Blades Obtained From New Integrated Force Method

The novel integrated force method has been extended for dynamic analysis of structures wherein force mode shapes are considered as the primary unknowns of the resulting eigenvalue

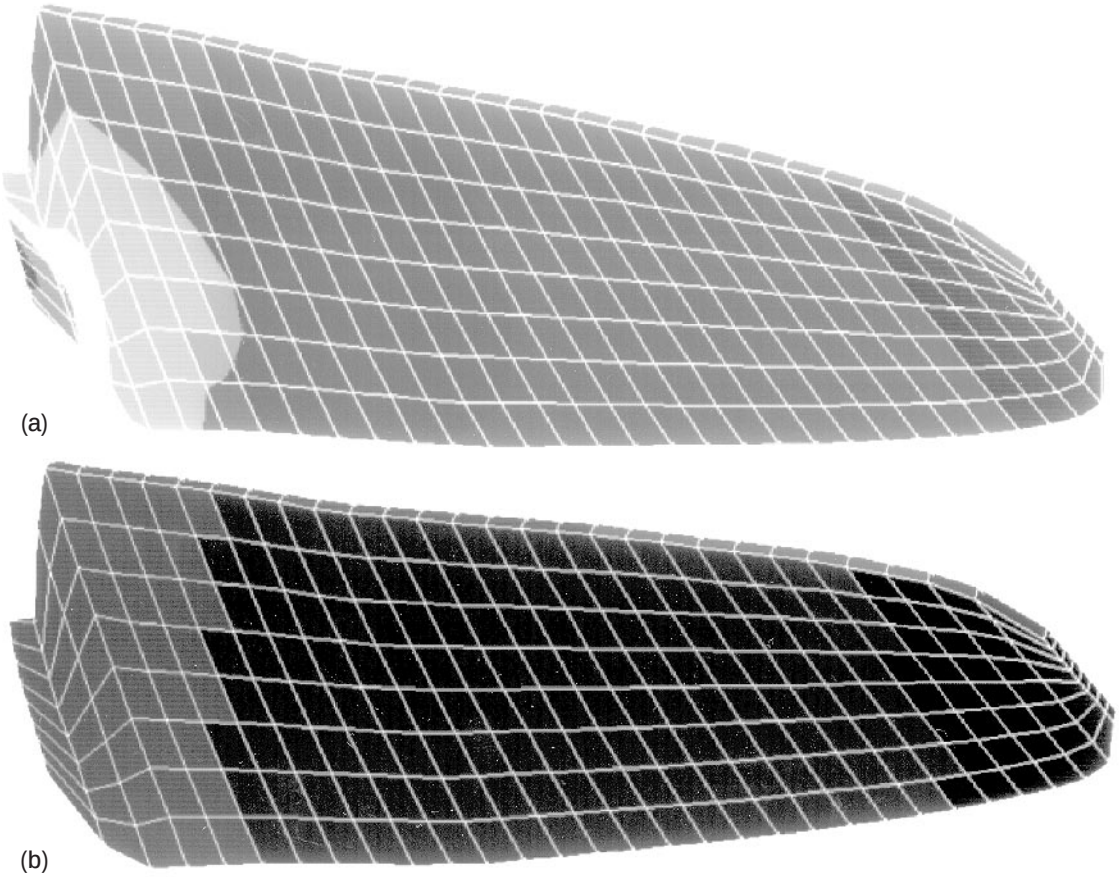

Figure 1.—Dynamic animation of turboprop blade. (a) Stress mode. (b) Displacement mode.

problem. Like static analysis the force method produces accurate stress mode shapes. The displacement modes, in the force method, can be backcalculated from the force mode shapes. The integrated force formulation in other words provides accurate stress and displacement modes.

A computer software called IFM/ANALYZERS, developed at NASA Lewis, can analyze structures that can be modeled by using solid elements. Approximately one dozen solid elements with and without midside nodes, which are available in IFM/ANALYZERS, can model components of airbreathing engines with arbitrary shapes. IFM/ANALYZERS also provides dynamic animations for both force and displacement modes. Animation of displacement and stress modes, which complement each other, can be effectively used to characterize failures due to fatigue and fracture especially under dynamic loads. Dynamic animations of a turboprop blade using eight-node brick elements is shown in figure 1. Note the high displacement amplitude at the tip of the cantilevered blade and the corresponding high stress amplitude at its root. Both displacement and stress animations complement each other and depict the comprehensive behavior of the turboprop blade.

Lewis contacts: Dale A. Hopkins, (216) 433–3260; Surya N. Patnaik, (216) 433–8468

Mechanics Enable Robust Simulation of Smart Composite Plate Structures With Piezoelectric Actuators and Sensors

Mechanics were developed at NASA Lewis for smart composite laminates with embedded piezoelectric actuators and sensors. A layerwise formulation applied on both displacements and electric potential has provided robust features not found in previously developed models, including the capability to model (1) active and sensory response, (2) global response (deflected shapes, voltage at sensors, and natural frequencies),

(3) local through-the-thickness response (intralaminar and interlaminar stresses, interfacial phenomena between structure and piezoelectric devices, etc.), and (4) thin and thick laminates. Specialty beam and plate finite elements (based on laminate mechanics) and prototype software were developed. The finite elements can model either continuous or discrete piezoelectric actuators and sensors.

Figure 1 illustrates one of the extreme capabilities of the mechanics, that is, the prediction of local dynamic response of a thick composite plate with surface-bonded piezoceramic layers. Numerous other evaluations of beam and plate structures have analytically and experimentally verified the mechanics and have demonstrated the versatility of the computational models for the analysis and development of adaptive piezoelectric components in advanced propulsion systems.

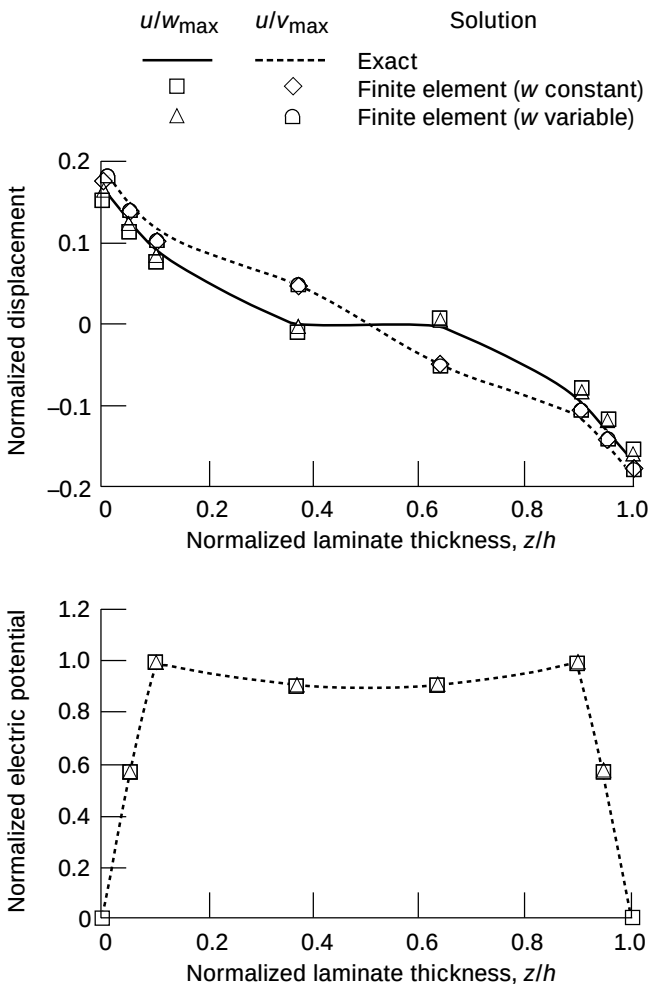

Figure 1.—Through-the-thickness distribution of displacement and electric potentials of fundamental mode in thick [p/0/90/0/p] square plate, where u *and* v *indicate displacement in the* x *and* y *directions, respectively, and* w *is the through-the-thickness displacement. Span/thickness ratio, 4.*

Bibliography

Heyliger, P.; Ramirez, G.; and Saravanos, D.: Coupled Discrete-Layer Finite Elements for Laminated Piezoelectric Plates. Communications in Numerical Methods in Engineering, vol. 10, 1994, pp. 971–981.

Saravanos, D.A.; Heyliger, P.R.; and Hopkins, D.A.: Mechanics for the Coupled Dynamic Response of Active/Sensory Composite Structures. AIAA Paper 94–1756–CP, 1994, pp. 199–209.

Lewis contacts: Dimitris A. Saravanos, (216) 433–8466; Dale A. Hopkins, (216) 433–3260

Active Piezoelectric Structures Provide Tip Clearance Management

Managing blade tip clearance in turbomachinery stages is critical to the development of advanced propulsion systems. Active casing structures with embedded piezoelectric actuators appear to be a promising solution. Their advantages include the capability for static and dynamic tip clearance control; the capability to compensate for uneven deflections; compact design; and electro-mechanical coupling at the material level. To assess the feasibility of this concept, we used in-house-developed computational capabilities for the analysis of composite structures with piezoelectric actuators and sensors to simulate the response of typical active casing structures. Additional efforts were also directed toward the development of controller schemes for regulating tip clearance.

The simulations provided valuable information regarding preliminary actuator configurations (number and location) and the corresponding voltage patterns required to induce (or compensate for) casing deformations contributing to variations in the tip clearance. Figure 1(a) shows an example of an active casing ring with four discrete piezoceramic actuators attached on the outer surface. Figure 1(b) shows the applied electrostatic voltage on the piezoceramic actuators required to statically ovalize the casing and the induced radial displacements. The results have demonstrated that active piezoelectric casings can modify the blade tip clearance significantly enough to ensure an effect on stage efficiency.

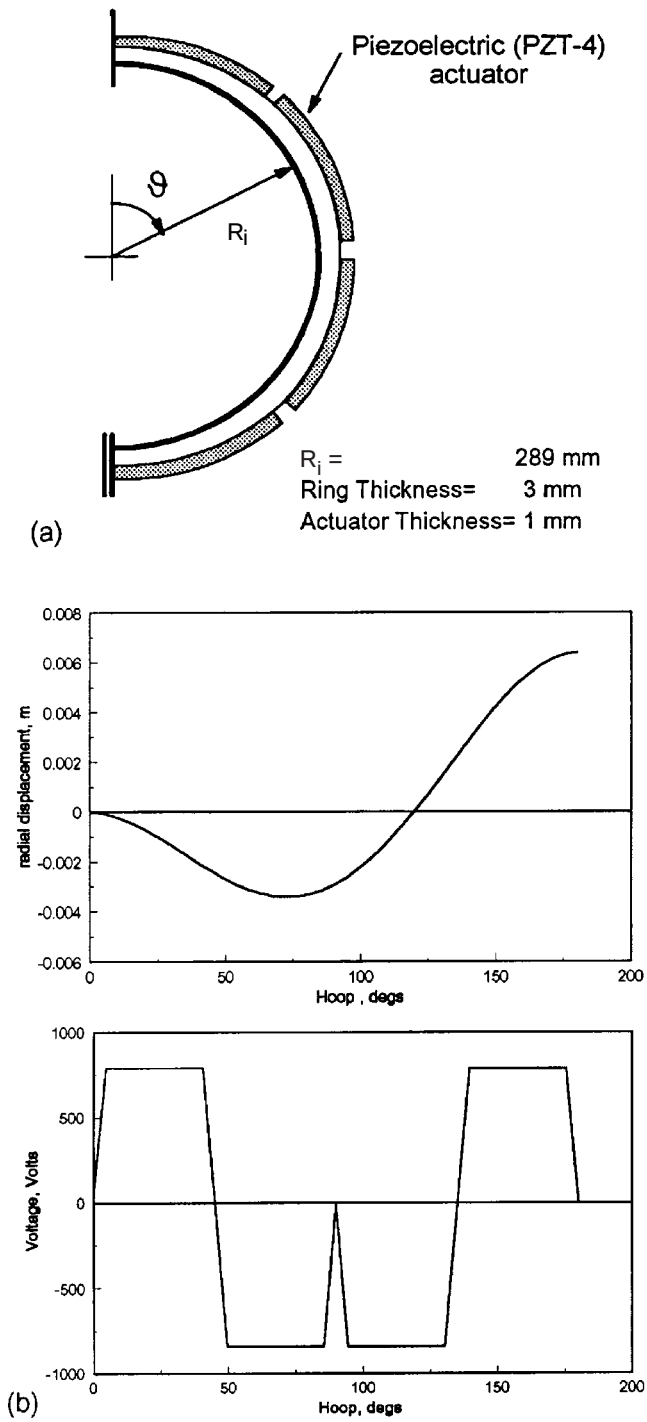

Figure 1.—Active ring structure with piezoelectric actuators. (a) Typical configuration. (b) Induced radial deflections and applied electric voltage at actuators.

Bibliography

Saravanos, D.A.; Lin, Y.J.; Choi, B.B.; and Hopkins, D.A.: On Smart Composite Structures for Active Tip Clearance Control. Adaptive Structures and Composite Materials: Analysis and Application. American Society of Mechanical Engineers, New York, 1994, pp. 145–150.

Lewis contacts: Dimitris A. Saravanos, (216) 433–8466; Dale A. Hopkins, (216) 433–3260

Sensory Composite Laminates Detect Delaminations

The development of sensory composite laminates with real-time, nondestructive "health-monitoring" capabilities will drastically improve the reliability of many structural applications. In an attempt to address this void in present technology, NASA Lewis has investigated the feasibility of delamination detection by distributed piezoelectric sensors. At least two detection approaches were pursued by monitoring changes in the modal damping and frequencies of composite structures and changes in the patterns of voltage distribution across a grid of distributed piezoelectric sensors. To understand the complicated physics of the problem, we have formulated mechanics that enable prediction of how delaminations affect natural frequencies, modal damping, and the electric signal at the piezoelectric sensors of vibrating composite beams. We also characterized the effects of delamination on the dynamic characteristics by testing graphite/epoxy specimens incorporating different sizes of delaminations and correlated them with the analytical predictions.

The changes in the natural frequencies and modal damping were reasonable indicators of intermediate and large delamination cracks (fig. 1), but such changes strongly depend on the laminate configuration and mode order. Delaminations also affected the electric signal of distributed piezoelectric sensors attached on the free surfaces of a vibrating laminate. Characteristic voltage patterns have been predicted to develop along the delaminated length (fig. 2) and may be used to detect even small delaminations, with limitations imposed only by the size and density of the sensors. The work has demonstrated the feasibility of delamination

detection based on changes in the damping, natural frequencies, and voltage amplitude of piezoelectric sensors.

Bibliography

Saravanos, D.A.; Birman, V.; and Hopkins, D.A.: Detection of Delaminations in Composite Beams Using Piezoelectric Sensors. AIAA Paper 94–1754–CP, 1994, pp. 181–191.

Lewis contacts: Dimitris A. Saravanos, (216) 433–8466; Dale A. Hopkins, (216) 433–3260

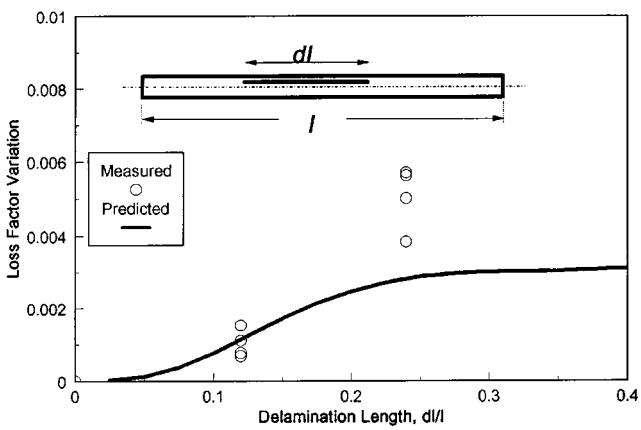

Figure 1.—Effect of delamination on damping of third mode of $[0/90/45\text{-}/45]_s$ beam.

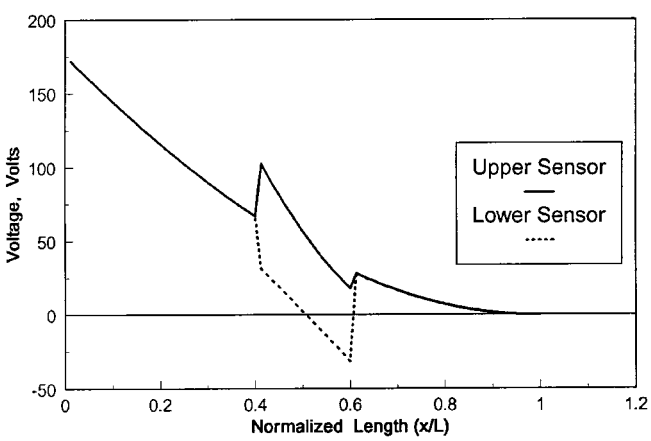

Figure 2.—Effect of delamination on voltage amplitude of piezoelectric sensors. $[0/90/45\text{-}/45]_s$ graphite/epoxy beam with delamination equal to 20% of beam length.

Boundary Element Method Simulates Thermal Behavior of Functionally Graded Material

The special boundary element methods developed in a joint program between the NASA Lewis Structures Division and the State University of New York at Buffalo have been used to conduct thermal analyses of functionally graded materials on the micromechanical (constituent) scale. Functionally graded materials are materials in which the internal microstructure or properties are explicitly tailored to obtain an optimal response. The analyses were carried out by using the computational tool Boundary Element Solution Technology—Composite Modeling System (BEST–CMS). The unique features of the boundary element formulations used here are derived from the streamlined manner in which the composite constituents are represented. A BEST–CMS model requires only the external surfaces of the matrix and the centerlines of the fibers to be discretized. Circular shape functions are then used within the BEST–CMS code to convert the two-dimensional integrations of the composite fibers to one-dimensional integrations. The advantages of using this approach as opposed to traditional finite element methods is that the complexity of the model is significantly reduced and the model generation process is simplified, particularly for composites with complex interior architectures. For this particular study the through-the-thickness temperature profiles were computed for a representative metal-matrix composite subjected to a thermal gradient with varying numbers of fibers and fiber spacing in the thickness direction. The computed temperature profiles were then compared with those obtained by using an alternative analytical theory, Higher Order Theory for Functionally Graded Materials (HOTFGM), in which the heterogeneous microstructure is explicitly coupled to the global analysis. HOTFGM allows unique responses in each of the composite phases that differ from the response that would be seen in a homogenized continuum.

Figure 1 shows the through-the-thickness temperature profile computed by using BEST-CMS and HOTFGM for a material with three uniformly spaced fibers through the thickness subjected to a 500 deg C temperature gradient. In a general sense the boundary element results capture the variation from linearity in the thermal profile predicted by HOTFGM. The nonlinearity results from the specification that the material is to be treated as a heterogeneous medium, not as

a homogeneous continuum. The disparity in the results between the two analyses is primarily due to assumptions inherent to the insert element formulation used to model the fibers in the boundary element model. This hypothesis is verified in figure 2, where results computed by using a boundary element model in which the fibers are explicitly modeled with quadrilateral surface elements are compared with the HOTFGM results. The two sets of results match almost exactly.

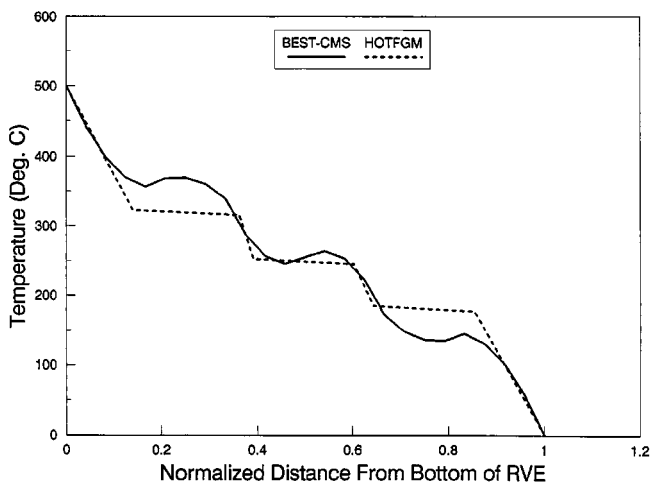

Figure 1.—Through-the-thickness temperature profile computed by using insert element formulation to model composite fibers in boundary element model.

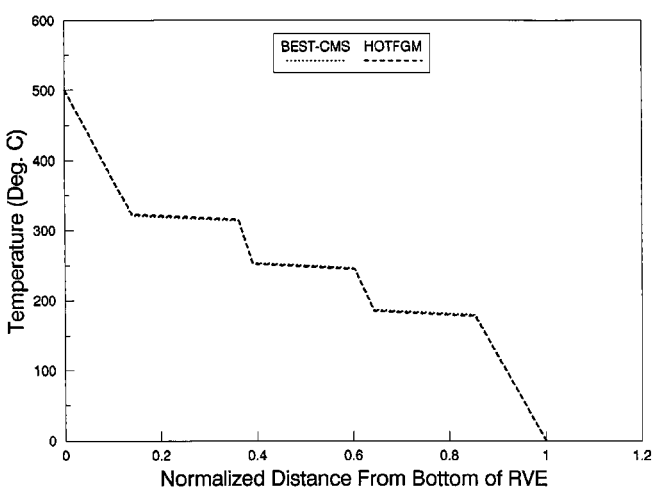

Figure 2.—Through-the-thickness temperature profile computed by using quadrilateral surface elements to model composite fibers in boundary element model.

The results obtained here demonstrate that the boundary element method can model the thermal behavior of functionally graded materials, with the accuracy level being determined by the complexity with which the composite fibers are modeled. The consistency between the boundary element results and the HOTFGM results also helps to verify the accuracy of the HOTFGM theory.

Lewis contact: Robert K. Goldberg, (216) 433–3330

Micromechanics Equations Developed for Particulate-Matrix Composites

Particulate-matrix composites are used in many aerospace and nonaerospace applications. The high costs and technical difficulties involved with fabricating fiber-reinforced composites sometimes limit their use in many applications. Particulate-reinforced composites can be a viable alternative. They can be used as dual- or multiphase composite materials and have the advantages of monolithic materials. They are easily processed to near net shape and have the strength and fracture toughness characteristic of continuous-fiber-reinforced materials. They can also be used as the matrix material in a continuous-fiber-reinforced composite. The characterization of these materials is fundamental to their reliable use in structural components.

Recently, NASA Lewis has developed a set of micromechanics equations to characterize these materials. Their development followed the same lines as the continuous-fiber-reinforced equations. Although the reinforcing particles have different sizes and shapes, they are assumed to be dispersed uniformly as equivalent spherical particles. A perfect bond is assumed to exist between the reinforcing particle and the matrix (binder) material. The micromechanics equations for particulate composites are then used in conjunction with composite micro- and macromechanics equations. The computer program Integrated Composite Analyzer (ICAN), developed at NASA Lewis for polymer-matrix composites reinforced with continuous fibers, has been augmented for particulate-reinforced composites as well. It allows the simulation of composite behavior where the matrix itself consists of two or more distinct phases (fig. 1).

The references show the derivation of micromechanics equations for particulate-matrix

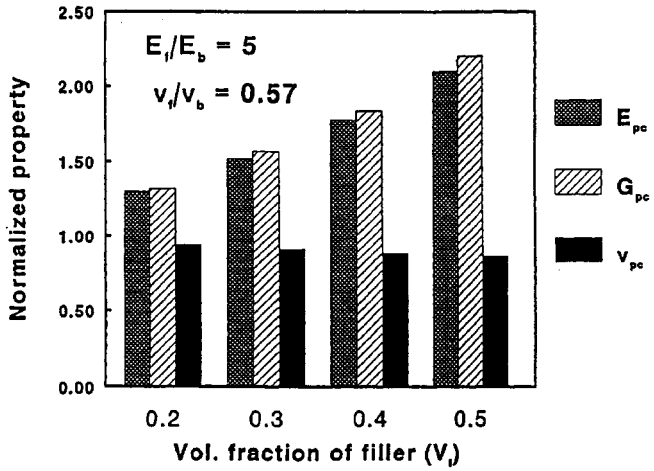

Figure 1.—Properties of particulate composite (normalized with respect to binder properties).

composites. Work is in progress to incorporate a third constituent (i.e., an interphase region between the reinforcing particle and the binder material) and to predict the strength of these materials.

Bibliography

Mital, S.K.; and Chamis, C.C.: Thermal and Mechnical Behavior of Particulate Composite Materials. Proceedings the Energy-Sources Technology Conference, American Society of Mechanical Engineers, New York, 1994, pp. 275–283.

Murthy, P.L.N.; Ginty, C.A.; and Sanfeliz, J.G.: Second-Generation Integrated Composite Analyzer (ICAN) Computer Code. NASA TP–3290, 1993.

Lewis contact: Christos C. Chamis, (216) 433–3252

Integrated Composite Analyzer Enhanced for Polymer-Matrix Composites

Preliminary design and analysis of fiber composite structures can be done in a cost-effective manner by using computer codes. Over the last two decades at NASA Lewis research in composite micromechanics and macromechanics, which includes the effects of temperature and moisture, has resulted in the development of several computer codes for composite mechanics and structural analysis. The recent addition to this list of computer codes is the enhanced version of Integrated Composite Analyzer (ICAN, version 3.0) for polymer-matrix composites for both personal computers and mainframes. The original version of ICAN was released in 1984; and a second-generation version, in 1993.

This current version of ICAN is about 40% larger than the original, yet it is still manageable and more user friendly. The code is written in FORTRAN 77 and runs on many platforms, including mainframes, supercomputers, desktop workstations, and personal computers. Some of its salient features are as follows:

1. The output can be tailored to specific needs by choosing the appropriate options.

2. The property input can be given at the constituent level (fiber and matrix) or at the ply level (if only ply-level properties are available).

3. Symmetric layups require reduced input information as the code is augmented for automatic generation of the complete laminate configuration based on symmetry.

4. Several modules have been added to perform durability or fatigue analyses for thermal as well as mechanical cyclic loads. The code can currently assess degradation due to mechanical and thermal cyclic loads with or without a defect.

5. A completely redesigned, dedicated data bank of constituent material properties as well as ply-level properties is now available. An important feature of the current data bank is a complete description of the property, its symbol and units, and its value.

Work is in progress to incorporate the micromechanics for particulate-matrix composites into ICAN.

The computer software and documentation are available through the Computer Software Management and Information Center (COSMIC), Suite 112, Barrow Hall, Athens, GA 30602.

Bibliography

Murthy, P.L.N.; Ginty, C.A.; and Sanfeliz, J.G.: Second Generation Integrated Composite Analyzer (ICAN) Computer Code. NASA TP–3290, 1993.

Lewis contact: Jose G. Sanfeliz, (216) 433–3348

Computational Structural Analysis Tool Developed for Parallel Processing Environments

Alpha STAR Research and NASA Lewis under a Small Business Innovative Research (SBIR) phase II contract developed a computational tool that meets industry's future demand for expedience and reduced cost in the design and analysis of high-temperature structures. This unique software, GENOA, is dedicated to high-speed analysis of next-generation aerospace systems. GENOA is focusing on computational integration and synchronization for probabilistic analysis, structural/material mechanics, and parallel computing to combine their latest innovative capabilities into a commercially viable software package. Because of the inherent complexity of high-temperature composite structures, parallel processing and dynamic load-balancing optimization are used to speed up the simulation processing of the diverse field of specialized analysis techniques and mathematical models. At times these models require hierarchical multiple levels of interactive analysis, using time-consuming convergence criteria that further drive computing and design costs upward.

To reduce CPU time and memory limitations, an effective optimized parallelization of the solution scheme was introduced. The framework of creating a parallelized and optimized system is introduced with divisions of principal algorithms for the machine-independent types of computer architecture: multiple-instruction multiple data, single-instruction multiple data, and open software foundation. Figures 1 and 2 show the turboblade finite element model for the space shuttle main engines and the analysis times achieved by the Lewis Advanced Cluster Environment (LACE).

Lewis contact: P.L.N. Murthy, (216) 433–3332

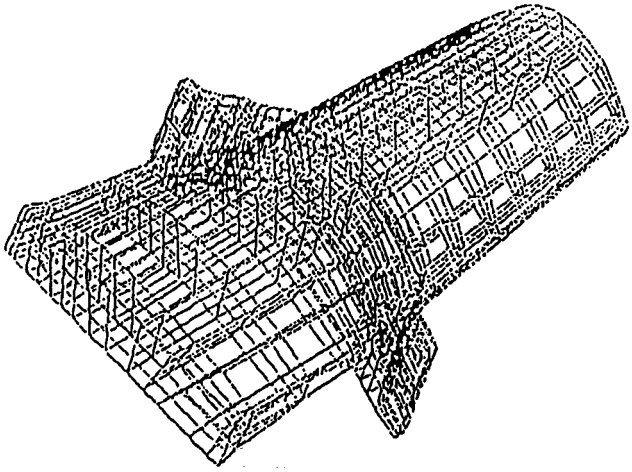

Figure 1.—Small turbine blade model specification: 8-noded brick element; 1575 nodes; 1025 elements; 3 degrees of freedom per node.

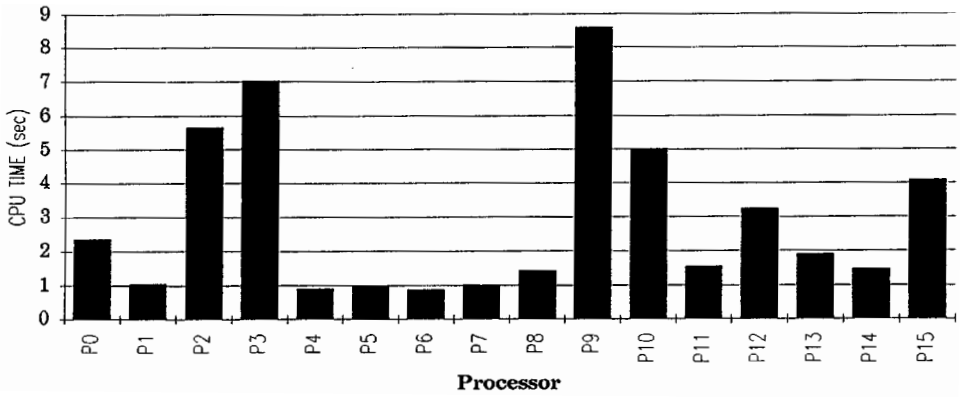

Figure 2.—Benchmark of small turbine model on 16 IBM/RS6000 processors at LACE. CPU time for preprocessing (calculation of stiffness matrices), 11.85 sec; highest CPU time for solving between processors, 8.60 sec; CPU time for postprocessing (calculation of stress and strain), 4.71 sec; total CPU time, 120 sec.

Multicriteria Design Optimization Uses Genetic Search Algorithms

Most optimization applications use only one objective function to describe the problem at hand. For example, a manufacturer might wish to know how to maximize the profit from producing an item. Some applications, however, require two or more cost functions to be maximized. For example, a manufacturer might wish to maximize the profit while also minimizing the number of accidents. Because it would be difficult to put a dollar value on the cost of accidents, the two functions must be optimized separately. In most cases there is no single point that maximizes both functions simultaneously; rather, the optimal solution is a set of points, called Pareto points. The goal of any multiobjective optimization technique is to find the set of Pareto points for two or more cost functions.

The advantages of genetic search algorithms are that they are quite robust and do not require knowledge of the gradients. Most genetic algorithms are single-objective optimizers. However, NASA Lewis has developed a new multiobjective optimization procedure based on a genetic algorithm. This procedure was implemented in a computer program called GENMO.

As illustrated by figure 1 all nondominated points are given rank 1; and all dominated points, rank 2. Any designs that are infeasible are also given rank 2. All rank 2 points are thrown away. The rank 1 points and the children bred from these points are carried over into the next generation. New design points, "immigrants," are added to keep the total population constant. The process is repeated until the entire population is made up of rank 1 points. These points are then the Pareto points for the optimization problem. To test the new algorithm, we ran three example cases from the areas of turbomachinery aeromechanics, ceramic composites, and polymer-matrix composites.

In the turbomachinery aeromechanics area, optimization runs were performed to maximize the torsional flutter margin and to minimize the torsional response amplitude of a cascade of blades in subsonic unsteady flow. The design variables were the bending-torsion frequency ratio and the location of the center of gravity. The Pareto optimal curve generated indicated that the optimum location of the center of gravity is slightly forward of the quarter-chord point.

The second example involved the optimization of a five-ply symmetric ceramic laminate to minimize thermal residual stresses and cost simultaneously by using ply thicknesses and volume fractions. The Pareto curve generated has a so-called "min-max" point that may be considered to be the optimal solution to the optimization problem.

The third example problem is concerned with

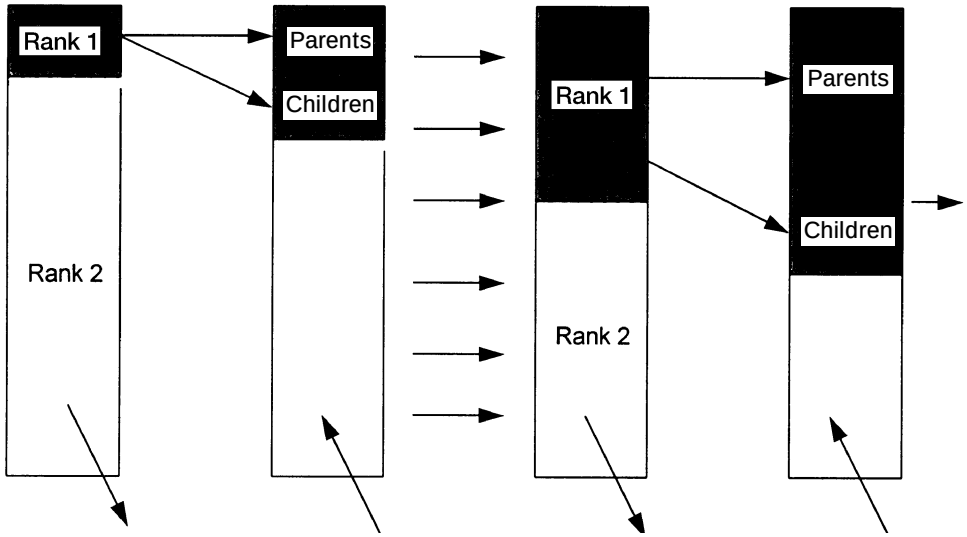

Figure 1.—Schematic of new genetic algorithm.

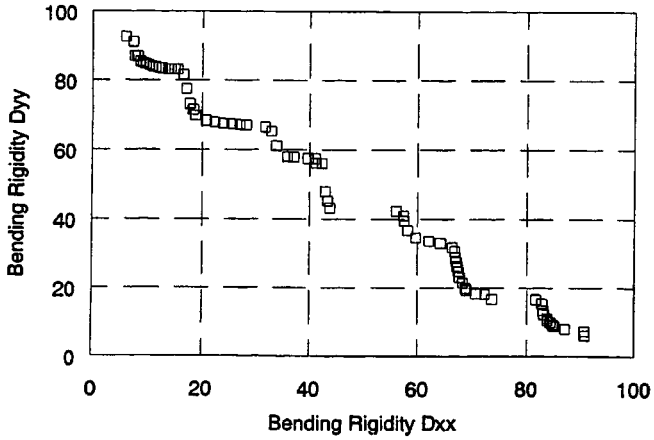

Figure 2.—Pareto curve for best compromised inplane bending rigidities.

maximizing the inplane bending rigidities of a eight-ply symmetric graphite/epoxy laminate. The design variables are the ply orientations, which are allowed to vary between +90° and –90°. The number of objective functions are two, the reduced bending rigidities in the *xx* and *yy* directions. No behavior constraints are imposed. The reduced bending rigidities are calculated by using the computer code Integrated Composite Analyzer (ICAN), which is integrated with the multicriteria design optimization code. The Pareto curve generated is shown in figure 2. The conflicting nature of the objective functions is clearly seen, and it appears that the nondominated solution giving the best possible planar rigidities follows a "stepped pattern," as shown in figure 2.

Bibliography

Belegundu, A.D.; Murthy, D.V.; Salagame, R.R.; and Constans, E.W.: Multi-Objective Optimization of Laminated Ceramic Composites Using Genetic Algorithms. Presented at the 5th Symposium on Multidisciplinary Analysis and Optimization, Panama City Beach, FL, Sept. 7–9, 1994.

Lewis contact: P.L.N. Murthy, (216) 433–3332

New Code Analyses Ceramic-Matrix Composite Stress-Strain Behavior Including Progressive Fracture and Load Redistribution

Ceramic-matrix composites (CMC's) are being considered for high-speed engine applications because of their strength, fracture toughness, and creep resistance in demanding service environments. To analyze the behavior of these composites, NASA Lewis has developed a unique and novel fiber-substructuring technique and is incorporating it into a stand-alone computer code called Ceramic Matrix Composite Analyzer (CEMCAN). In this technique the fiber in the conventional unit cell or the representative volume element (RVE) is substructured into several slices, and the micromechanics equations are applied at the slice level. This technique can account for varying degrees of interfacial bonding around the fiber circumference or through the thickness, local matrix cracking and fiber breaks, different fiber shapes, etc., and it integrates the effects of all these aspects on composite properties and response. It also provides greater detail in stress distribution.

Elastic properties of unidirectional, cross-ply, and some angle-ply laminates made of SiC/RBSN composite (silicon carbide SCS–6 fibers in reaction-bonded silicon nitride matrix) were predicted and compared with measured properties. The comparison for thermal and mechanical properties is excellent. Recently, a nonlinear analysis capability that incorporates local stress redistribution due to progressive fracture has been added to the CEMCAN computer code. Any material nonlinearity is accounted for at the constituent level. This capability also allows for the inclusion of the residual stresses that arise from the difference between the processing and use temperatures and the mismatch in the coefficients of thermal expansion between fiber and matrix materials. It simulates the stress-strain state in the as-fabricated material prior to loading. Another added capability is the microstress redistribution as the fracture initiates and propagates in a laminate. If a constituent fails in a slice, its microstresses are redistributed to the regions that have not failed.

Results indicate that fiber substructuring provides greater local detail than other micromechanics-based theories at a high computational efficiency. It allows for the simulation of partial interphase bonding and integrates its effect on the laminate properties and response. Tensile stress-strain to failure for several laminates was also predicted (fig. 1), and failure modes were compared with experimental observations. CEMCAN provides the user with a "virtual test laboratory" in that new candidate materials, different laminate configurations, or different service environments can be quickly

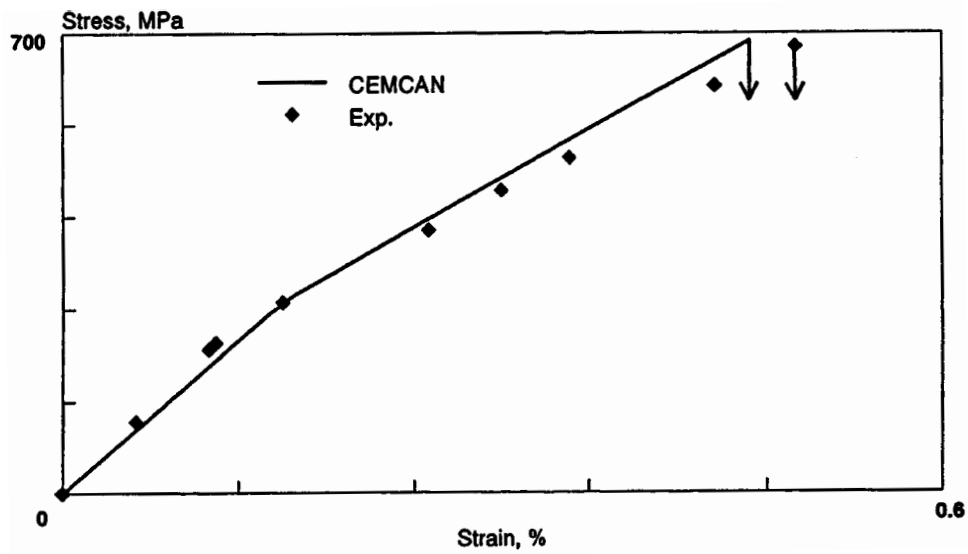

Figure 1.—Room-temperature stress-strain for SiC/RBSN $[0]_8$ composite; fiber volume ratio, 0.36.

evaluated with a selected number of tests needed for the calibration of certain properties for a given material system.

Bibliography

Mital, S.K.; Murthy, P.L.N.; and Chamis, C.C.: Ceramic Matrix Composites Properties/Microstresses With Complete and Partial Interphase Bond. NASA TM–106136, 1993.

Mital, S.K.; Murthy, P.L.N.; and Chamis, C.C.: Modeling of Stress/Strain Behavior of Fiber-Reinforced Ceramic Matrix Composites Including Stress Redistribution. NASA TM–106789, 1994.

Lewis contact: Christos C. Chamis, (216) 433–3252

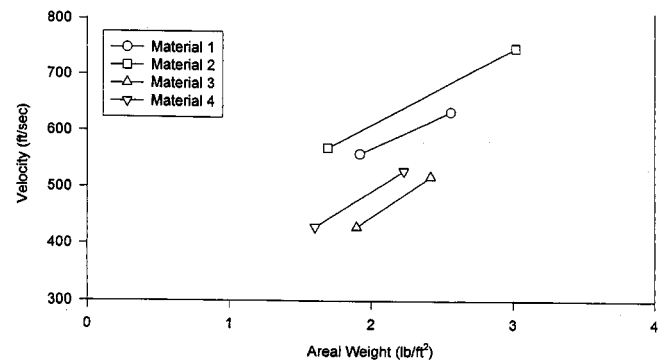

Figure 1.—Velocity required for standard projectile to penetrate four candidate materials at 370 °C (700 °F).

Ballistic Properties of Metal Fan Containment Materials Being Evaluated for High-Speed Civil Transport

Under the Enabling Propulsion Materials (EPM) Program (a partnership between NASA, Pratt & Whitney, and General Electric Aircraft Engines) the Materials and Structures Divisions are involved in developing a fan containment system for the High-Speed Civil Transport. The program calls for a baseline system to be designed by the end of 1995, with subsequent testing of innovative concepts. Five metal candidate materials are currently being evaluated for the baseline system in the ballistic impact facility. This facility was developed to provide cost-efficient and timely impact test data to the EPM program. The facility allows both room- and elevated-temperature ballistic impact tests, with post-test analysis and the ability to conduct mathematical modeling of the impact event to guide experimental testing.

To date, four of the five candidates have been tested (see fig. 1). The fifth material will be tested at Lewis as soon as it is made available. Results of the tests will be used to select materials for further large-scale testing, as well as by engine designers to aid in the design of the baseline fan containment system.

Lewis contacts: J. Michael Pereira, (216) 433–6738; Matt Melis, (216) 433–3322

New Fiber Demonstrated Excellent Ballistic Impact Properties

Fabric-based fan containment systems for jet engines can save hundreds of pounds of engine weight over standard metallic containment systems. As part of the High-Speed Civil Transport (HSCT) Enabling Propulsion Materials Program, work is under way in the Materials and Structures Divisions to evaluate the elevated-temperature ballistic performance of fiber systems. In the past year an elevated-temperature ballistic impact facility was developed for testing fan containment materials and concepts. Fabric materials were evaluated in this facility by shooting square specimens, clamped on four sides, with a 1.27-cm (0.5-in.) diameter, 2.54-cm (1-in.) long cylindrical projectile. The projectiles were shot from a gas gun using a helium propellant. Some of the specimens were heated to 260 °C (500 °F) with quartz lamps. The energy absorbed by the fabric was measured from the change in velocity of the projectile after it penetrated the fabric. The ability to perform computer simulations of the impact event has also been developed as an aid in guiding the experimental program.

One of the fabric candidates has shown excellent results (see fig. 1). This candidate has demonstrated the ability to absorb over twice the energy of currently used fabric systems. It has also shown good results at elevated temperatures. This material is being evaluated for use both in the HSCT program and in subsonic applications.

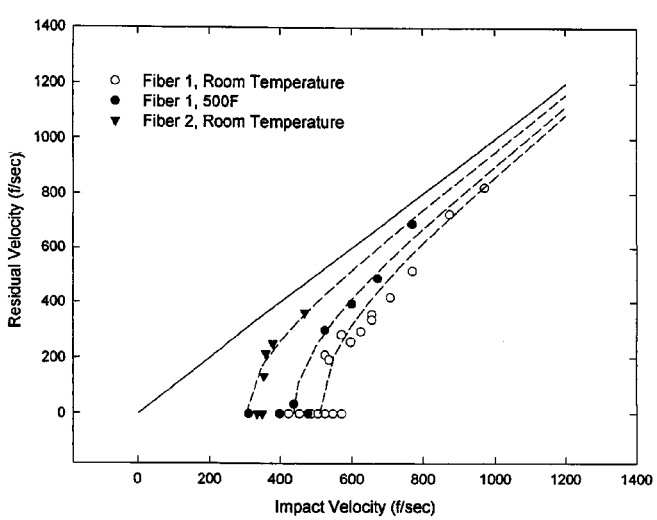

Figure 1.—Postimpact velocity as function of impact velocity for two fabric systems, one at 260 °C (500 °F).

Bibliography

Ferri, R.; and Pereira, J.M.: Strength and Stiffness Properties of Graphite/Epoxy Laminates With Interlaminar Damping Layers. Proceedings of the 39th SAMPE Symposium, 1994, pp. 2544–2551.

Pereira, J.M.; Kautz, H.E.; Roth, D.J.; and Duke, J.: Measurement of Mechanical Damage in Ceramic Matrix Composites Using Vibration and Acousto-Ultrasonic NDE. Proceedings of the 7th Annual HiTEMP Review, NASA CP–10146, Vol. I, 1994, pp. 23–1 to 23–12.

Saigal, A.; and Pereira, J.M.: Mechanical Behaviour and Residual Stresses in Unidirectional Tungsten Fibre-Reinforced Copper Matrix Composites. International Symposium on Recent Developments in Light Metals. Canadian Inst. Mining Met., 1994.

Lewis contacts: J. Michael Pereira, (216) 433–6738; Matt Melis, (216) 433–3322

Human Factor in Structural Reliability Probabilistically Simulated

Structural failures have occasionally been attributed to human factors in engineering design, analysis, maintenance, and fabrication processes. Every facet of the engineering process (planning, designing, manufacturing, inspection, maintenance, communication, and coordination between different engineering disciplines) is heavily governed by human factors and the degree of uncertainty associated with them. Societal, physical, professional, psychological, and many other factors introduce uncertainties that significantly influence the reliability of human performance. Such factors are called primitive variables. Quantifying the effect of human factors and associated uncertainties in structural reliability requires (1) identification of the fundamental factors that influence human performance and (2) models that describe the

interaction of these factors.

The human factor has long been a subject of study. Traditionally, there have been two approaches to quantifying the effect of human factors: (1) qualitatively describing its effects on a certain outcome and (2) curve fitting the data obtained through surveys. There is a clear need for quantifying the fundamental factors (primitive variables) that influence human behavior and its subsequent effects on the probabilistic assessment of structural reliability and risk. An initial formal approach, based on probabilistic concepts and a multifactor interaction equation of product form (fig. 1) was used to probabilistically simulate human behavior. For the initial simulation the fundamental factors assumed to affect human performance are health, home life, marital status, work load, job satisfaction, and professional status. The effect of remuneration is not mentioned specifically, but it is implied in all six factors. It is ludicrous to presume that these are the only factors that influence human performance; however, they constitute a reasonable initial set of factors that are very important in both professional and personal fulfillment. Because these factors vary widely with time, human performance inherits the associated uncertainty. Therefore, it is appropriate to simulate human performance from a probabilistic standpoint.

The results of an initial investigation of the use of probabilistic simulation to quantify the human factors in structural reliability are as follows:

1. A multifactor interaction equation (MFIE) of product form may be used to relate human performance to some easily identifiable factor that can influence it.

2. An initial assessment may include factors such as professional status, home life, job satisfaction, health conditions, marital satisfaction, and work load.

3. The range of uncertainty in the human factor can be evaluated probabilistically by assuming uncertainties in the values for each factor and its corresponding exponent in MFIE.

4. Exponent intervals can be selected to yield reasonable values for the human factor.

5. A hypothetical table can be devised to convert qualitative performance evaluation to quantifiable ranges of uncertainty for specific probability.

6. An MFIE can be adapted to individual

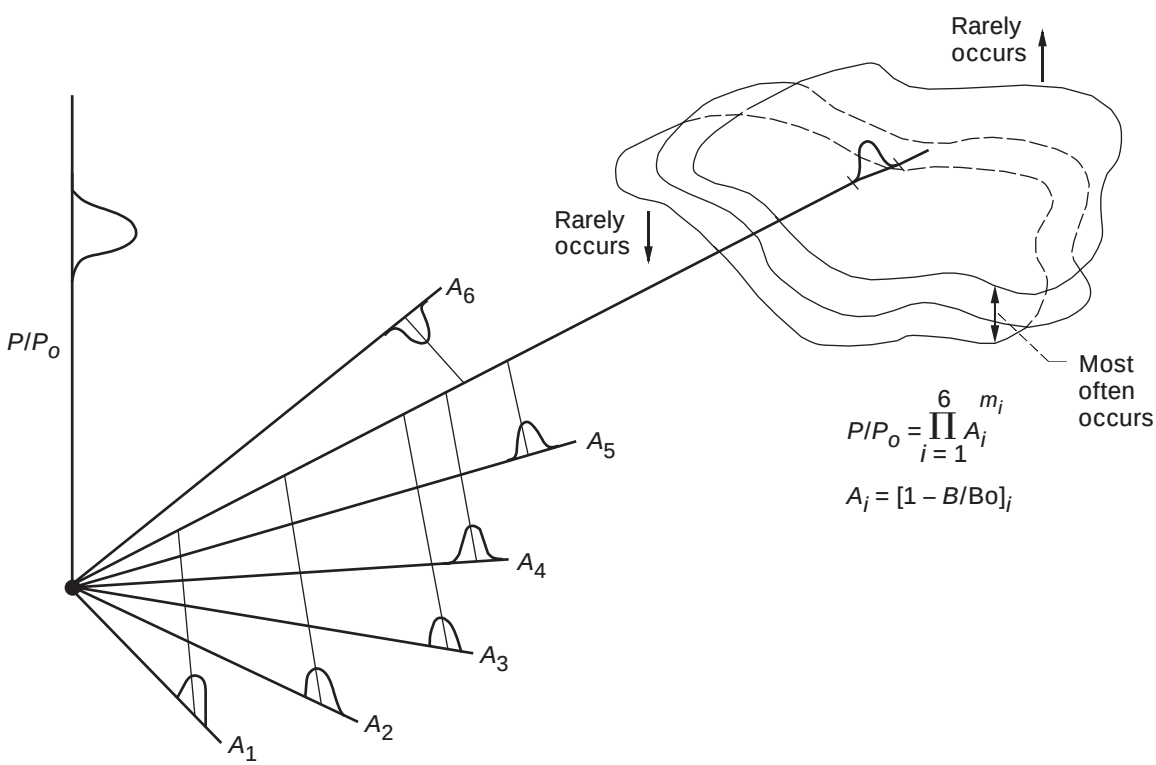

Figure 1.—Human behavior space (assuming six uncertainty factors, N=6.)

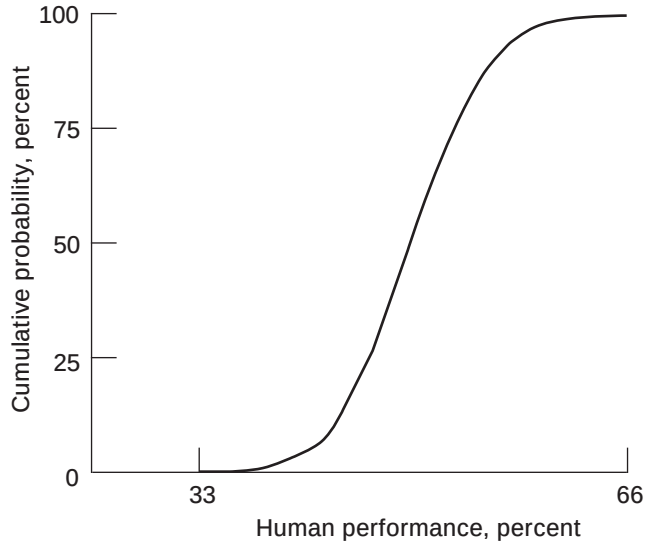

Figure 2.—Effect of variation in exponent.

performance by observing a person over a period of time and entering more specific data into the equation.

Typical results obtained (fig. 2) show that human performance ranges from 33 to 66% out of 100% maximum.

Bibliography

Chamis, C.C.; and Singhal, S.N.: Probabilistic Simulation of the Human Factor in Structural Reliability. NASA TM–106498, 1994.

Lewis contact: Christos C. Chamis, (216) 433–3252

Ice Formation and Material Behavior Computationally Simulated

Ice forms in nature in various ways and comes in contact with man-made structural systems and their components. Ice formation on structures can cause undesirable loading, which affects their performance. In severe environments with constantly changing conditions, such as temperature and time, the properties of ice vary significantly. To effectively counteract damaging ice effects, it is necessary (1) to understand the mechanism of ice formation, (2) to identify the different variables (factors) and environmental conditions that affect the properties of ice, (3) to characterize the material properties of ice, and (4) to analyze how ice properties are affected by the combination of (1) to (3).

Experimental investigations of the material behavior of ice are expensive, test specific, and not always reliable. For instance, the strength of ice as measured under laboratory conditions can be different by an order of magnitude from the strength of multiyear sea ice. General-purpose computational simulation models are needed for cost-effective and reliable quantitative assessment of the material behavior of ice. NASA Lewis has been developing computational simulation methods and corresponding computer codes for more than two decades to analyze composite materials and/or structures (ref. 1). These methods and codes are applicable for evaluating ice behavior. We have demonstrated the capability of these computer codes to predict ice thickness and properties in prevailing environments. Chosen for the demonstration was a sample case of ice formation in a body of water to evaluate (1) the time-variant thickness of ice formed under prevailing environmental conditions and (2) the mechanical and thermal properties of ice at different temperatures through the ice thickness.

Available computational methods were used to simulate the layer-by-layer formation of ice and to characterize its material behavior. The material behavior of ice formed under prevailing environments over a period of time was modeled by a multifactor interaction model. The model is general in that it is applicable to all types of ice, isotropic or anisotropic, formed under all conditions. The enabling computer codes were demonstrated for a sample case that illustrated the procedure and the importance of layer-by-layer simulation of ice formation and behavior under the prevailing environments. The results (fig. 1) showed that the modulus of elasticity and

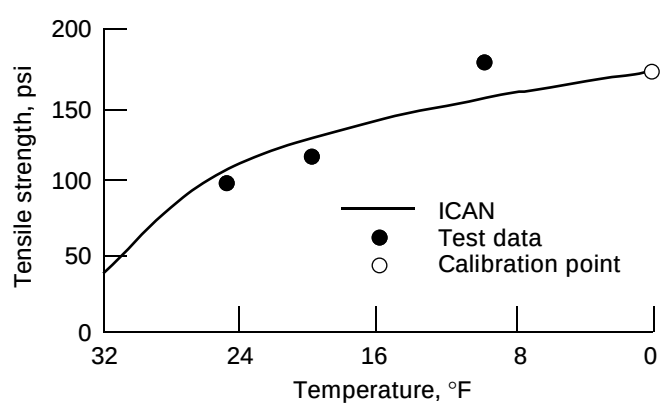

Figure 1.—Temperature variation of tensile strength of ice layers.

tensile strength of ice layers and the entire ice block increase with time as the ice temperature decreases. The density of the ice layers and of the entire ice block decrease as the ice gets colder. Results such as these can be quickly generated by using computer codes (such as those described in ref. 1). Collectively, the results demonstrated that the formation process and properties of ice can be computationally simulated, making it a cost-effective procedure.

Reference

1. Tong, M.T.; Singhal, S.N.; and Chamis, C.C.: Computational Simulation of the Formation and Material Behavior of Ice. NASA TM–106702, 1994.

Lewis contact: Christos C. Chamis, (216) 433–3252

Adaptive Intraply Hybrid Fiber Composites Optimized With Reliability Considerations

Aerospace structures are complex assemblages of structural components that operate under severe and often uncertain service environments. They require durability, high reliability, light weight, high performance, and affordable cost. Composite materials are potential candidates that meet these requirements because they possess outstanding mechanical properties with excellent fatigue strength and corrosion resistance. Their mechanical properties are derived from a wide variety of variables, such as constituent material properties and laminate characteristics (fiber and void volume ratios, ply orientation, and ply thickness). These variables are known to be uncertain.

A new challenge is to further enhance structural performance by investigating other advanced concepts. Recent developments in smart-structure concepts that use actuation materials, such as piezoelectric ceramics, have the potential to improve structural performance, durability, and reliability (ref. 1). The control device in smart structures consists of (1) a polarized material, (2) an electric field parallel to the direction of polarization, and (3) the expansion-contraction effects of the polarized material. When a control voltage is applied, the actuation material expands or contracts so that the structural behavior is altered by a desired amount and its reliability is changed. Present piezoelectric technology has been successfully applied to small-scale, low-stress structures. However, there are inevitable difficulties when current technology is applied to

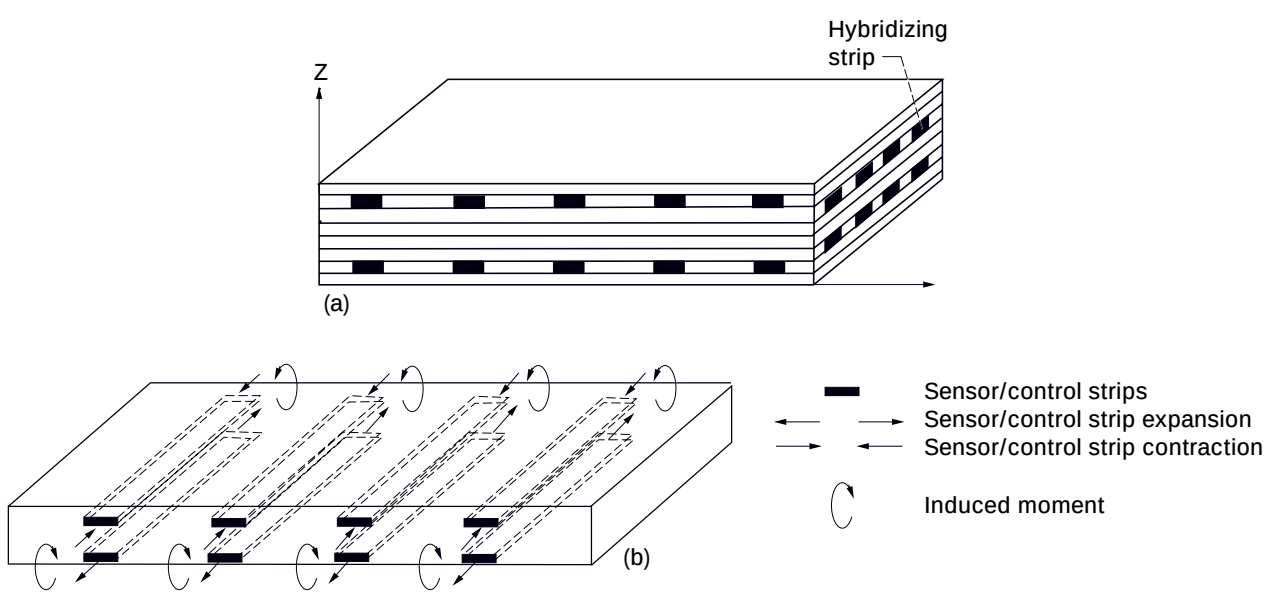

Figure 1.—Adaptation of intraply hybrid to smart composite system. (a) Intraply hybrid composite system. (b) Structural control using sensor/control material.

large-scale, high-stress composite structures. These difficulties can be alleviated if the following concept is adopted: combine special piezoelectric fibers that have a fast actuation capability and relatively high-strength, high-modulus fiber to form an adaptive intraply hybrid composite. This composite can be readily integrated into a smart composite structure by using combinations of intraply and intraply hybrid composites to ascertain that smart composite structures will operate in the design-specified range.

The adaptation of the intraply hybrid composite concept to smart composite structures is depicted schematically in figure 1, which shows that the smart composite comprises (1) regular plies that consist of regular composite materials and (2) control plies that consist of strips of regular composite materials and strips of mixed regular and actuation materials. Actuators, containing actuation materials, such as piezoelectric ceramics or piezoelectric fibers, are used to control composite structural behavior by expanding or contracting the actuation strips to achieve the requisite design and operational goals. However, the strains induced by the actuator are affected by uncertainties in several factors that can only be quantified probabilistically. These factors include (1) inaccurate measurements made by sensors, (2) deviation from the intended electric field, (3) uncertain relationship between actuation strain and electric field strength, (4) uncertain material properties for actuation materials, (5) uncertain electric field strength, and (6) improper location of sensor and/or control materials. Because of these factors the use of control devices increases the uncertainty in already uncertain composite structural behavior.

To account for various uncertainties and to satisfy design requirements, knockdown (safety) factors are used extensively. These knockdown factors result in a substantial weight increase but without a quantifiable measure of reliability. An alternative method for determining structural reliability has been investigated at NASA Lewis. This method is embedded in the computer code Integrated Probabilistic Assessment of Composite Structures (IPACS).

The investigation was accomplished by integrating probabilistic methods and smart composite concepts into the IPACS code. Probabilistic sensitivity factors from the probabilistic assessment of composite structures were used in the optimization procedure. The reliability for actuated change in the angle of attack of an airfoil-like composite structure with an adaptive torque plate was maximized to 0.9999 probability with constraints on the mean and standard deviation of the actuation material volume ratio (percentage of actuation composite material in a ply) and the actuation strain coefficient. This demonstrated that structural reliability with constraints on the distribution parameters could be maximized. The reliability-based cost for an

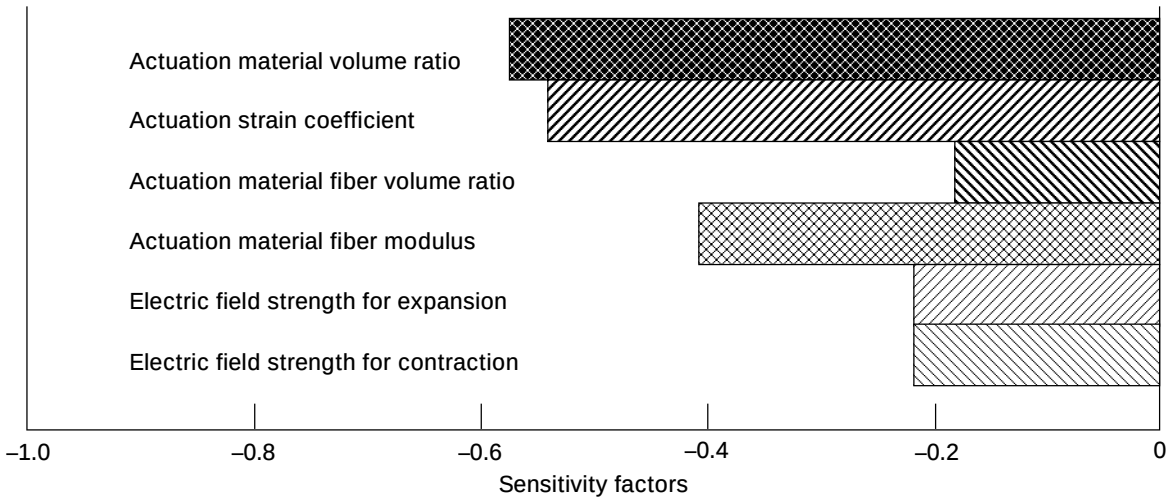

Figure 2.—Sensitivity factors of uncertain variables to reliability for lower bound of change in angle of attack.

airfoil-like composite shell structure with adaptive skin was also minimized with the mean actuation material volume ratio as the design parameter. The minimum cost was found when the mean actuation material volume ratio was equal to 0.91. The sensitivities at that minimum cost were also evaluated (fig. 2).

Reference

1. Shiao, M.C.; and Chamis, C.C.: Optimization of Adaptive Intraply Hybrid Fiber Composites With Reliability Considerations. NASA TM–106632, 1994.

Lewis contact: Christos C. Chamis, (216) 433–3252

Structural Probability Concepts Adapted to Electrical Engineering

Complex systems are often composed of subsystems involving more than one engineering discipline (e.g., electrical, mechanical, chemical, nuclear, fluid, and structural). Although each subsystem can affect the total system and often affect other subsystems, the components that comprise the subsystems may vary. For example, a structural subsystem has material property, load, and dimension components, whereas a simple electrical subsystem has resistance, voltage, and current components. Each component in each subsystem varies in magnitude and/or direction. Because of the variability of the components and the various levels of sensitivity of their coupling, the complete system varies in its operations. In order to analyze the variability of such a complex system, the subsystems must be evaluated probabilistically (stochastically). Probabilistic evaluation of multidisciplinary systems requires computer codes that can analyze structural, thermal, chemical, fluid, and electrical subsystems. However, it is only through such an evaluation that critical subsystems and components can be identified, leading, in turn, to possible reduced cost and improved reliability of complex systems.

One probabilistic code used to evaluate structural subsystems is Numerical Evaluation of Stochastic Structures Under Stress (NESSUS), developed for NASA Lewis by Southwest Research Institute. This code can be used to evaluate structural subsystems with variable material properties, dimensions, and loadings. Possible failure modes can be combined through fault-tree analysis to determine the reliability (probability of failure) of the subsystem. Risk analysis that includes subsystem costs can also be performed with the code. However, this probabilistic structural code is limited to the analysis of structural and thermal-structural subsystems.

Analogies between the variables of electrical and structural subsystems were used to analyze several simple electrical circuits. These equivalent variables allowed an electrical subsystem to be probabilistically analyzed with the NESSUS computer code. This ability to analyze the subsystem probabilistically allowed us to evaluate the reliability of systems having both structural and electrical subsystems. In the future, identification of the critical components, whether structural or electrical, will make possible more reliable systems at reduced costs.

Common examples of such systems are a structural subsystem integrated with a health-monitoring subsystem and smart structures. These systems have electrical subsystems that directly affect the operation of the overall system. For example, in a health-monitoring subsystem, electrical sensors inform system operators to

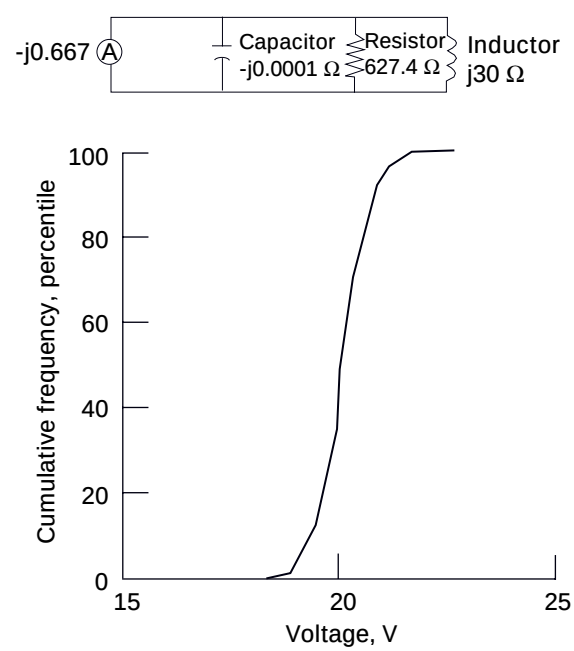

Figure 1.—Probability of occurrence for real voltage of alternating-current circuit.

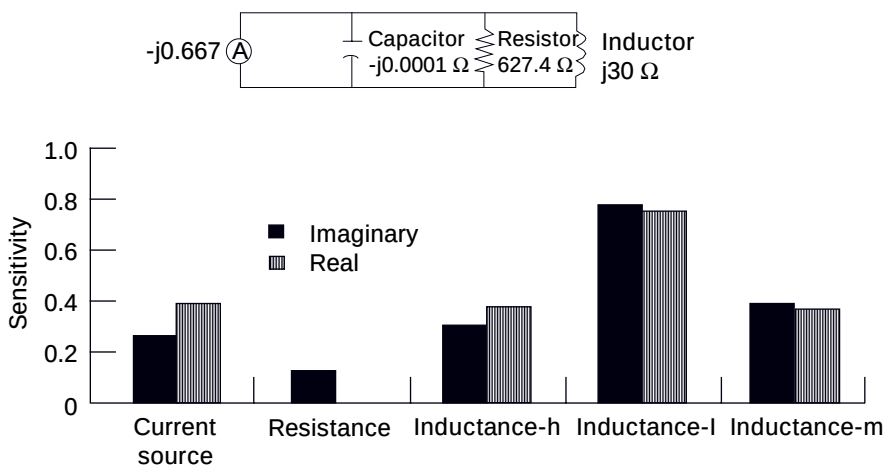

Figure 2.—Sensitivities (relative units) for voltages of alternating-current circuit.

make proper adjustments. If the monitoring system fails, the structural subsystem can be damaged or it can fail. Similarly, in smart structures that have an electrical subsystem in the form of piezoelectric sensors and/or actuators, failure of the piezoelectric system can also result in failure of or damage to the structural subsystem. Analogies between other disciplines and the structures discipline can be demonstrated so that such subsystems can be probabilistically analyzed with a single code.

We have shown that an electrical circuit can be probabilistically analyzed by using equivalent variables in the structural analysis code NESSUS (figs. 1 and 2). Therefore, system reliability analysis can be performed on systems containing both structural and electrical subsystems. There are other analogies that exist between engineering disciplines that should allow other types of subsystem to be probabilistically analyzed with the same code. The end result would be system reliability analysis of a complete system, including such subsystems as electrical, thermal, hydraulic, and structural. Analyses of coupling between subsystems could eventually be included, thereby leading to realistic modeling of the assembled system. Such improved system analysis would lead to increased system reliability and reduced cost.

Bibliography

Steinberg, E.P.; and Chamis, C.C.: Structural Probability Concepts Adapted to Electrical Engineering. NASA TM–106499, 1994.

Lewis contact: Christos C. Chamis, (216) 433–3252

Reliability of Composite Structures With Multiple Design Criteria Studied

Aerospace structures are complex assemblages of structural components that operate under severe and often uncertain service environments. They require durability, high reliability, light weight, and high performance at an affordable cost. Composite materials are potential candidates for meeting these requirements. Some polymer-matrix composite materials possess outstanding mechanical properties with excellent fatigue strength and corrosion resistance. Their mechanical properties are derived from a wide variety of variables, such as constituent material properties and laminate characteristics (fiber and void volume ratios, ply orientation, and ply thickness). These parameters are known to be uncertain.

To account for various uncertainties and to satisfy design requirements, knockdown (safety) factors are used extensively. These knockdown factors significantly reduce the design load of composite structures, resulting in substantial weight increase without a quantifiable measure of reliability. An alternative method that determines the structural reliability for a single design requirement is embedded in the computer code Integrated Probabilistic Assessment of Composite Structures (IPACS) for a comprehensive probabilistic assessment of composite structures.

A composite structure can be certified when all the design criteria are satisfied. For structural

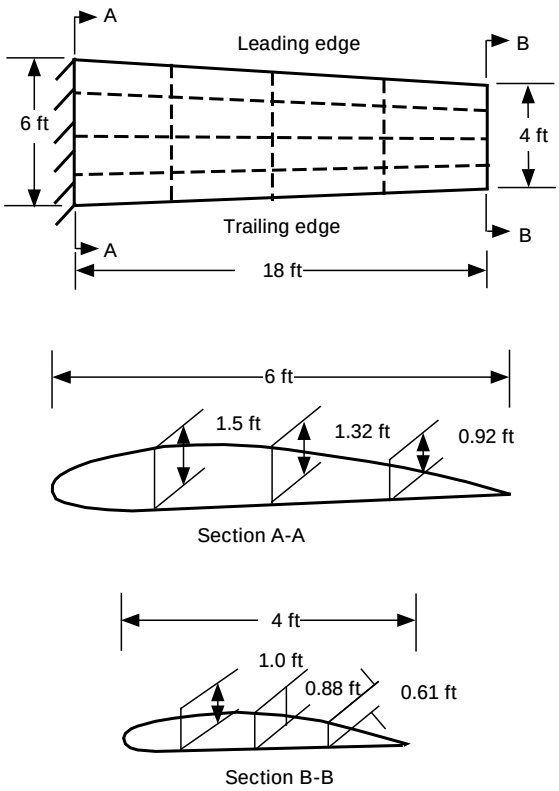

Figure 1.—Geometry of composite wing.

certification using probabilistic methods, not only the reliability of individual design (performance) criterion is needed, but also the system (combined) reliability for the entire structure considering all the necessary criteria needs to be calculated. Several methods for calculating system reliability of composite structures are described in reference 1. The computational simulation was conducted on a UNIX workstation. System reliability calculation was achieved by using probabilistic fault-tree analysis (PFTA) and adaptive important sampling (AIS) simulation methods. PFTA provides a way to deal with a structural system with multiple failure paths due to multiple components or multiple design criteria. The AIS method minimizes the number of simulations. Random samples are generated by using approximate limit state functions. Once sampling points are generated, two options for AIS simulations can be performed. One option is to perform a simulation with the approximate failure (limit state) functions. The other option is to create and analyze finite element models for each sample point. The performance criteria used for demonstration were structural frequency range, safety margin for stress, and displacement constraint. An example of PFTA considering failure function dependency was demonstrated. The accuracy and computational efficiency for different AIS options are discussed in reference 1.

A probabilistic fault-tree analysis using AIS methods for system reliability calculation considering failure function dependency was demonstrated (figs. 1 and 2). For this specific example the system reliabilities calculated by using both AIS approaches agreed well with each other. However, the computational time for AIS with approximate failure function was one-tenth that for AIS with finite element analysis. Also, the sum of individual failure probability may not be a good approximation for the system reliability if the correlations between the failure (basic) events are significant (table I).

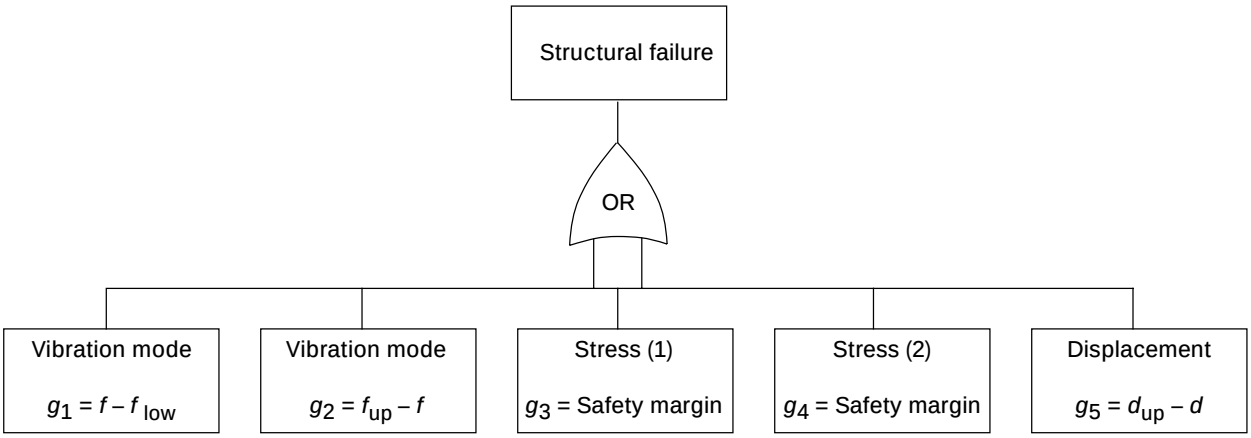

Figure 2.—Fault-tree representation of system reliability analysis for composite wing with multiple design criteria.

TABLE I.—SYSTEM RELIABILITY RESULTS WITH FIVE FAILURE FUNCTIONS

[P_f = Prob {[g_1<0] ∪ [g_2<0] ∪ [g_3<0] ∪ [g_4<0] ∪ [g_5<0]}.]

Reliability analysis method	Structural model	Number of random system samples	Probability of failure, P_f	Total CPU time, hr
AIS	Approx. functions (using advanced mean value +)	107 (86 failures)	0.0171	2.5
AIS	Approx. functions and finite element	113 (84 failures)	0.0163	22.0
Prob(g_1<0)+Prob(g_2<0)+ Prob(g_3<0)+Prob(g_4<0)+ Prob(g_5<0)	----------	----------	0.0207	2.5
Prob(g_1<0)+Prob(g_2<0)+ Prob(g_3<0)+Prob(g_5<0)	----------	----------	0.0165	2.5

Reference

1. Shiao, M.C.; and Chamis, C.C.: Reliability of Composite Structures With Multiple Design Criteria. NASA TM–106716, 1994.

Lewis contact: Christos C. Chamis, (216) 433–3252

Space Nuclear Propulsion System Nozzle Probabilistically Assessed

A space nuclear propulsion system (SNPS) nozzle was designed to generate the required thrust with the desired level of reliability. Nozzle system reliability is largely governed by structural integrity and behavior. Variables associated with structural behavior are geometry, boundary conditions, material behavior, and incident loads. Manufacturing a large nozzle with accurate design dimensions is very difficult because of loose tolerances in the machinery. Therefore, there are always variations in the geometry and thickness of the material used. The nozzle is connected to the pressure vessel at the top; the difficulty in determining the degree of its fixity to the pressure vessel results in modeling variations. Thus, the boundary conditions at the attachment are not certain. Also, the grain structure of the material is never uniform because of variations in the material processing. Therefore, the behavior of the material is never certain either and has a scatter associated with it. Additional uncertainties are attributed to irregularities in the combustion reaction, variations in the fuel mixture ratio, in the gas temperature from time to time and from location to location, and, consequently, in the magnitude of the gas pressure on the nozzle.

All the variables governing the structural design of the nozzle have uncertainties associated with them as just described. The conventional deterministic design approach accounts for these variations in the form of an upper bound or a lower bound as the case may be. Because such an approach results in an overconservative or sometimes unconservative design, it is difficult to assess the degree of conservatism, although the safety factor is known. Accurately quantifying the reliability and the associated risk with a given design is an impossible task for deterministic methods.

Probabilistic structural analysis is an approach that, in a rational way, accounts for the effects of uncertainties on the structural response. Furthermore, it determines the structural reliability and quantifies the risk. For more than a decade NASA Lewis has been engaged in developing probabilistic structural analysis methods. The methodology characterizes design variable uncertainties in the form of probability density functions. A finite element structural analysis and reliability algorithms are used to numerically integrate these probability density

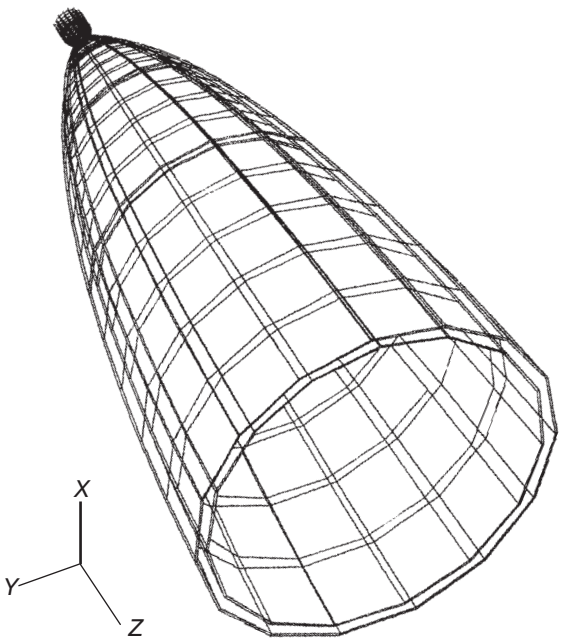

Figure 1.—SNPS nozzle second mode of vibration. Frequency, 198.63 Hz.

functions in order to evaluate the structural response distribution. The methodology developed to design propulsion system components probabilistically has been integrated into the computer code Numerical Evaluation of Stochastic Structures Under Stress (NESSUS).

An investigation was conducted to demonstrate the effectiveness of this methodology when applied to the reliability assessment of an SNPS nozzle and its extension (fig. 1). The design requirements for this nozzle are for very high pressures and thermal loads to achieve high thrust and good performance.

The results obtained demonstrated that the NESSUS computer code could be used to perform a probabilistic structural analysis of these types of structure. The sensitivity of the structural response and its respective reliability were quantified, and its role in the design process was discussed (ref. 1). The results showed that the stresses in the stiffener are higher than those in the shell because of the higher thermal gradient

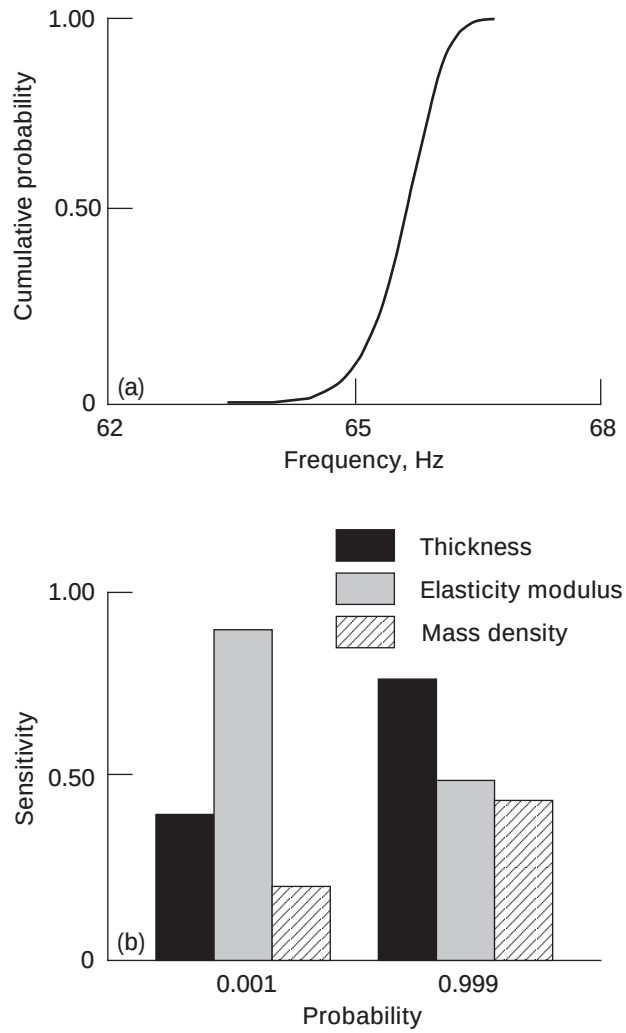

Figure 2.—Results of probabilistic assessment of nozzle. (a) First natural frequency. (b) Sensitivity of first natural frequency.

in the stiffener. The stresses at lower probability levels are governed by the temperature on the inner wall surface. The scatter of the natural frequency of the nozzle is small and is dominated by the uncertainties in the thickness of the shell at high probability levels (fig. 2).

Reference

1. Shah, A.S.; Ball, R.D.; and Chamis, C.C.: Probabilistic Assessment of Space Nuclear Propulsion System Nozzle. NASA TM–106539, 1994.

Lewis contact: Christos C. Chamis, (216) 433–3252

Stress-Strain Behavior of Fiber-Reinforced, Ceramic-Matrix Composites Modeled Including Stress Redistribution

Ceramic-matrix composites (CMC's) currently are the subject of a great deal of research interest due to the requirement for new high-temperature materials for use in high-speed engine structural components and other applications. Continuous-fiber-reinforced, ceramic-matrix composites offer promise in this area, and hence considerable effort is being devoted to their development. They offer several advantages: high specific stiffness and strength, higher toughness and nonbrittle failure relative to monolithic ceramics, and environmental stability and wear resistance for both room- and elevated-temperature applications.

There are several differences between ceramic-matrix and, say, polymer-matrix composites. In polymer-matrix composites the fibers provide stiffness while the polymer matrix serves primarily as a binder and generally has a very low modulus. The ratio of Young's modulus between the fibers and the matrix in polymer-matrix composites is typically 10^2. In order to achieve high stiffness, it is usually desirable to have a strong interfacial bond between the fiber and matrix materials. On the other hand, a major role of fibers in ceramic-matrix composites, in addition to providing higher stiffness, is to enhance toughness as the matrix material is quite brittle and fails at relatively low strain levels. The ratio of Young's modulus between the fibers and the matrix in ceramic-matrix composites is typically 10^0. A weak fiber/matrix interfacial bond in CMC's enables such toughening mechanisms as fiber debonding, fiber bridging, fiber pullout, and crack deflection to eliminate catastrophic failures and to provide some ductility. Therefore, in spite of some similarities with polymer-matrix composites, the analysis of ceramic-matrix composites requires an entirely different approach.

The computer code Ceramic Matrix Composite Analyzer (CEMCAN, fig. 1) has been under continued development under the sponsorship of the High-Temperature Engine Materials Program at NASA Lewis. CEMCAN is based on composite micro-, meso-, and macromechanics and has been developed specifically to simulate aspects unique to CMC's. It incorporates a novel and unique fiber-substructuring technique that has many advantages, including more accurate micromechanical representation of interfacial conditions, both around the fiber and through the laminate thickness, and provision of greater detail in stress distribution within a ply at a very high computational efficiency relative to numerical analysis techniques used for micromechanical analyses.

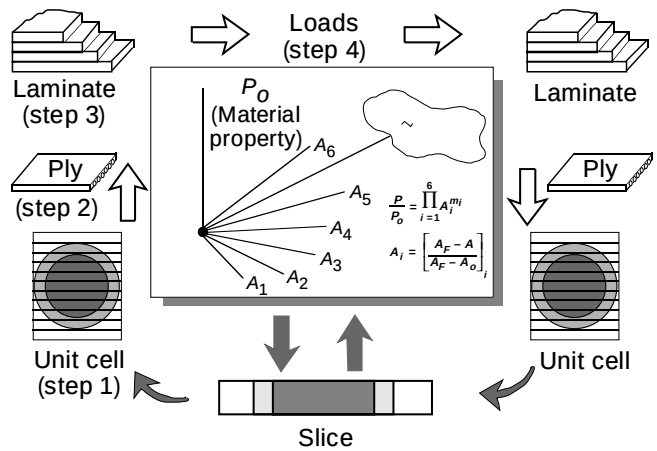

Figure 1.—Integrated analysis approach embedded in CEMCAN computer code.

Recent upgrades to the CEMCAN computer code included nonlinear analysis capability with microstress redistribution due to progressive fracture (ref. 1). Collectively, the results presented (fig. 2) show that CEMCAN provides sufficient

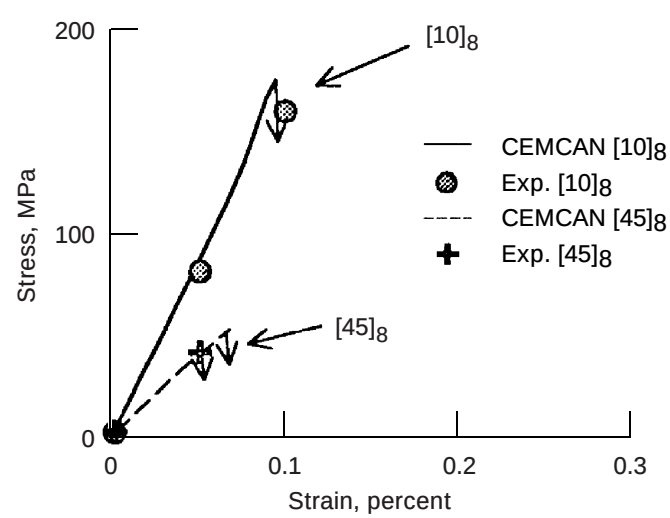

Figure 2.—Room-temperature, stress-strain curves to failure of $[10]_8$ and $[45]_8$ laminates.

flexibility for the user to study various aspects of the deformation and fracture behavior of ceramic-matrix composites. A unidirectional $[0]_8$ composite loaded along the longitudinal direction displayed linear stress-strain behavior up to first matrix cracking stress. Beyond this point the matrix was ineffective, and all the load was carried by the fibers until fracture. Off-axis and angle-ply laminate tensile strength was governed by a combination of matrix and shear failure. There was probable fiber damage or breakage due to processing in the cross-ply $[0_2/90_2]_s$ laminate.

The CEMCAN computer code provides the user with a "virtual test laboratory" in that new candidate materials and different laminate configurations or service environments can be evaluated in a fraction of the usual time and cost because only a minimum number of tests are needed to calibrate certain material properties for a given material system.

Reference

1. Mital, S.K.; Murthy, P.L.N.; and Chamis, C.C.: Modeling of Stress/Strain Behavior of Fiber-Reinforced Ceramic Matrix Composites Including Stress Redistribution. NASA TM–106789, 1994.

Lewis contact: Christos C. Chamis, (216) 433–3252

Technology Benefit Estimator (T/BEST) Users Manual Published

Improvements in technology have contributed to the advancement of research into aerospace propulsion systems. To efficiently take advantage of these advances, the benefits must be communicated. As a result, NASA Lewis has undertaken to develop a computational simulation, Technology Benefit Estimator (T/BEST), that successfully integrates several disciplines in aerospace propulsion systems to yield the benefits in emissions, noise, weights, thrust, range, specific fuel consumption, cost, etc.

T/BEST is an executive system developed for the benefit analysis of aerospace propulsion systems. Figure 1 depicts the computational simulation modules of T/BEST. The executive system controls the execution of all modules as well as the flow of information between modules. A computational module is defined here as a FORTRAN (other language may be included) program with a specified analysis capability. All modules intercommunicate by a data file system named neutral file.

The disciplines integrated in T/BEST are

1. Thermodynamics
2. Structures
3. Fluid flow
4. Cost
5. Mission
6. Emissions
7. Noise

The T/BEST executive system conforms with three levels of user expertise:

1. Beginner, should execute T/BEST by using the example

2. Intermediate, a user who has executed T/BEST several times; must be able to modify many neutral file default parameters

3. Expert, a user with extensive experience in executing T/BEST; must be able to modify all neutral file default parameters; can add or remove modules to or from T/BEST

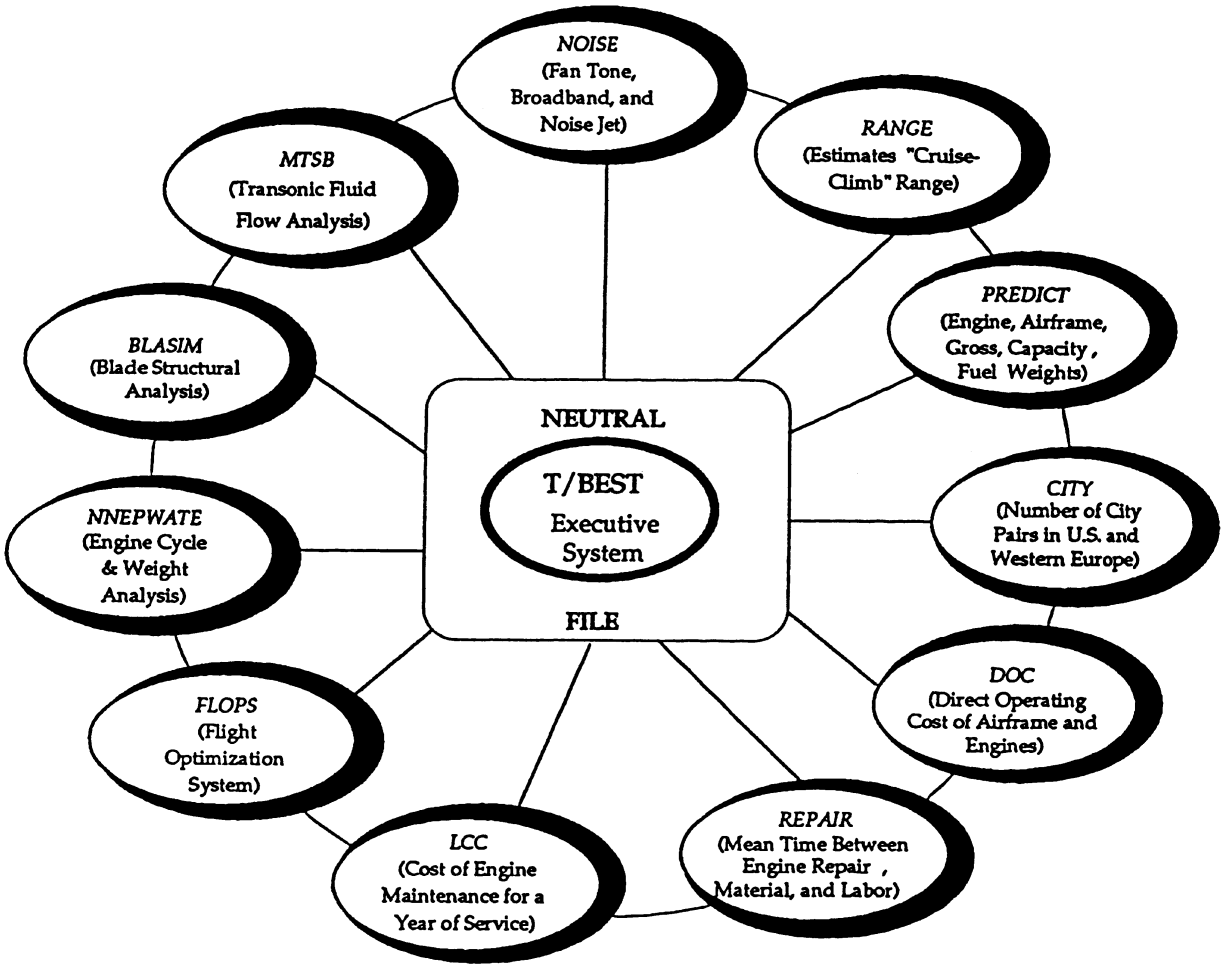

Figure 1.—Default computational simulation modules of T/BEST executive system.

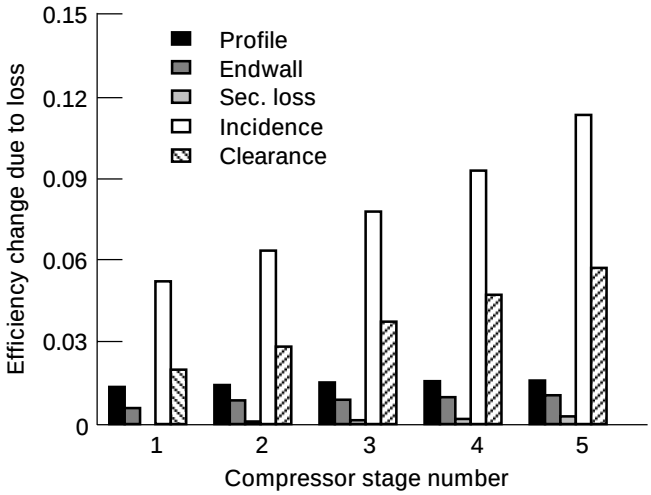

Figure 2.—Compressor efficiency changes due to loss. Blade type, NACA 64–206 fan; engine component number, 5; high-pressure compressor.

The T/BEST system is a formal method for assessing advanced technologies and quantifying the benefit contributions for ranking. T/BEST may be used to provide guidelines to identify and rank high-payoff research areas, to help manage research and limited resources, to show the link between advanced concepts and the bottom line (i.e., accrued benefit and value), and to credibly communicate the benefits of research (fig. 2).

Bibliography

Generazio, E.R.; Chamis, C.C.; and Abumeri, G.: Technology Benefit Estimator (T/BEST) Users Manual. NASA TM–106785, 1994.

Lewis contact: Christos C. Chamis, (216) 433–3252

Fatigue and Fracture

Thermal and Structural Analysis Performed on Hollow Core Space Shuttle Main Engine Turbine Blade

Hot-section components of spacecraft engines are exposed to severe thermal-structural loading conditions, especially during engine startup and shutdown. For instance, the thermal transient during startup conditions within the space shuttle main engines (SSME) can lead to a gas temperature of over 3000 ^{o}C (5432 ^{o}F), which causes high stresses and strains that affect the operating life of key components, such as the turbine blades. To improve the durability of these components, in particular the turbine blade, single-crystal superalloys are being considered. PWA–1480, a nickel-based superalloy, has been used as the turbine material for the SSME Alternate Turbopump Development Program.

Turbine blades made of single-crystal superalloys, including PWA–1480, are directionally solidified along the low modulus [001] crystallographic direction. The directional solidification process usually generates a secondary crystallographic direction, [010], that is randomly oriented with respect to fixed geometric axes in the turbine blade. Moreover, because of the anisotropic nature of the single crystal, the stress-strain response and the dynamic characteristics of any component made of single crystal, such as the turbine blade, would depend on both the secondary and primary orientation angles. This work addresses the influence of primary and secondary orientations on the elastic response of an SSME hollow core, [001]-oriented, nickel-based, single-crystal superalloy (PWA–1480) turbine blade, under combined thermal and mechanical loading conditions. The results from a previous study (ref. 1) involving flat plates of single-crystal material subjected to thermal loading showed that the influence of the secondary orientation on the elastic stress response is substantial. Highest stresses occurred at 45° secondary orientation, which identified it as the most critical secondary orientation. Also, the influence of the primary orientation angle, when constrained between 0° and 10°, on the elastic stresses generated within the turbine blade is much lower than the influence of the secondary orientation angle, which is not usually controlled.

This study consisted of thermal-structural analysis of an SSME type of turbine blade subjected to thermal and mechanical loading characteristic of engine use. The objective was to assess the influence of secondary crystallographic orientation on the stresses developed and to apply understanding obtained from earlier analyses of simpler structures (ref. 2) to this problem. Figures 1 and 2 show the results obtained, demonstrating that secondary crystallographic orientation has strong influence on the stresses in the turbine blade, which is consistent with earlier findings on much simpler structures.

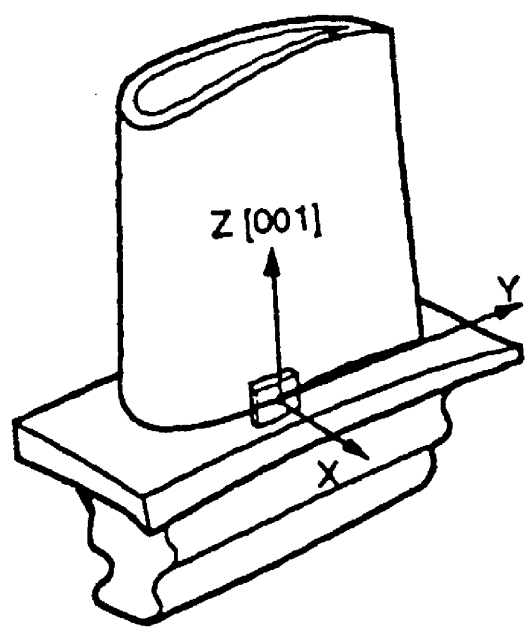

Figure 1.—Schematic of SSME hollow core turbine blade.

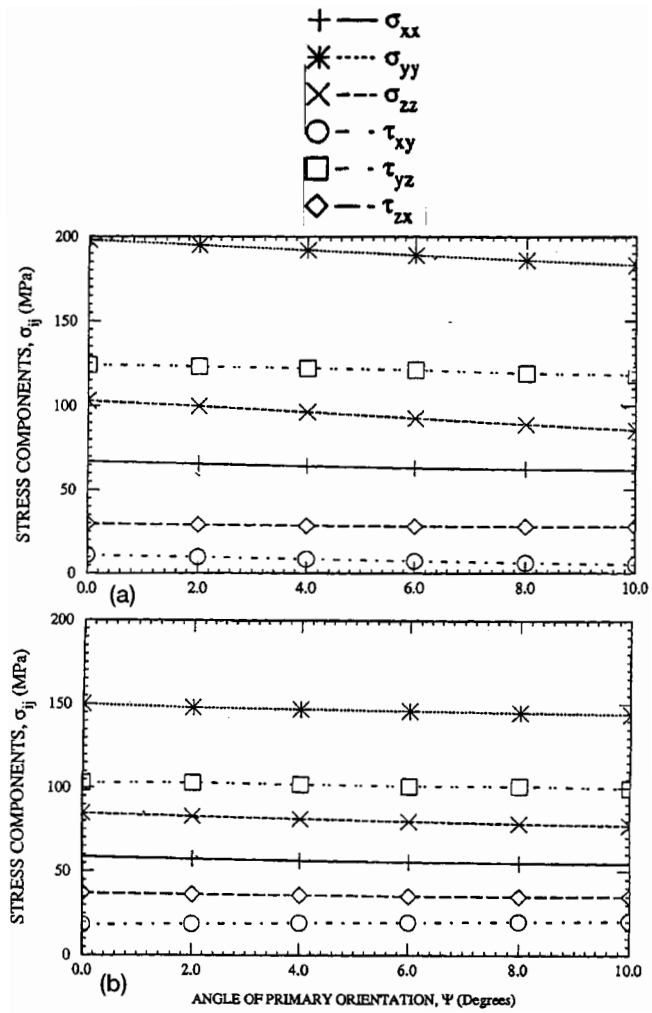

Figure 2.—Influence of primary and secondary orientation angles under combined thermal and mechanical loading. Element 430. (a) Secondary orientation, $\theta = 45°$. (b) Secondary orientation, $\theta = 0°$.

References

1. Kalluri, S.; Abdul-Aziz, A.; and McGaw, M.: Elastic Response of [001]-Oriented PWA–1480 Single Crystal—The Influence of Secondary Orientation. SAE Transaction Paper 911111, vol. 100 (sect. 1, part 1), 1991, pp. 273–283.

2. Abdul-Aziz, A.; Kalluri, S.; and McGaw, M. A.: The Influence of Primary and Secondary Orientations on the Elastic Response of a Nickel-Based Single-Crystal Superalloy. ASME Paper 93–GT–376, 1993.

Lewis contacts: Ali Abdul-Aziz, (216) 433–6729; Sreeramesh Kalluri, (216) 433–6727; Michael McGaw, (216) 433–3308

Fully Associative, Nonisothermal, Potential-Based Unified Viscoplastic Model Developed for Titanium-Based Matrices

A number of titanium-matrix composite (TMC) systems are being investigated for high-temperature airframe and propulsion system applications. As a result numerous computational methodologies for predicting both deformation and life for this class of material are under development. An integral part of these methodologies is an accurate and computationally efficient constitutive model for the metallic matrix constituent. Furthermore, because of the proposed elevated operating temperatures for which these systems are designed, the required constitutive models must account for both time-dependent and time-independent deformations. To accomplish this, we employ a recently developed, complete, potential-based framework (ref. 1) using internal state variables that was put forth for the derivation of reversible and irreversible constitutive equations. This framework, and consequently the resulting constitutive model, is termed complete because the existence of the total (integrated) form of the Gibbs complementary free-energy and complementary dissipation potentials is assumed. The specific forms selected here for both the Gibbs and complementary dissipation potentials result in a fully associative, multiaxial, nonisothermal, unified viscoplastic model with nonlinear kinematic hardening. This model (refs. 2 and 3) is one of many models in the Generalized Viscoplasticity With Potential Structure (GVIPS) class of inelastic constitutive equations.

A unique aspect of this GVIPS model is the inclusion of nonlinear hardening through the use of a compliance operator (derived from the Gibbs potential) in the evolution law for the backstress. This nonlinear tensorial operator is significant in that it allows both the flow and evolutionary laws to be fully associative (and therefore easily integrated (ref. 4)), greatly influences the multiaxial response under nonproportional loading paths (refs. 1, 5, and 6), and in the case of nonisothermal histories, introduces an instantaneous thermal softening mechanism proportional to the rate of change in temperature (ref. 3). In addition to this nonlinear compliance operator the new (ref. 2) consistent, potential-preserving, internal unloading criterion has been used to prevent abnormalities in the predicted

stress-strain curves, which are present with nonlinear hardening formulations, during unloading and reversed loading. This nonisothermal GVIPS model was characterized for Timetal 21S, an advanced titanium-based matrix commonly used in TMC's. Results (see figs. 1 and 2) illustrated the very good overall correlation and predictive capability of the model for a wide range of loading conditions (i.e., tensile, cyclic, creep, step creep, step temperature, creep-plasticity interaction and relaxation tests) performed over the temperature range 23 to 704 °C (72 to 1300 °F). Finally, the proposed model was also compared with a commonly accepted and employed Bodner-Partom (BP) viscoplastic model and found to be superior in both its predictive capabilities and numerical performance.

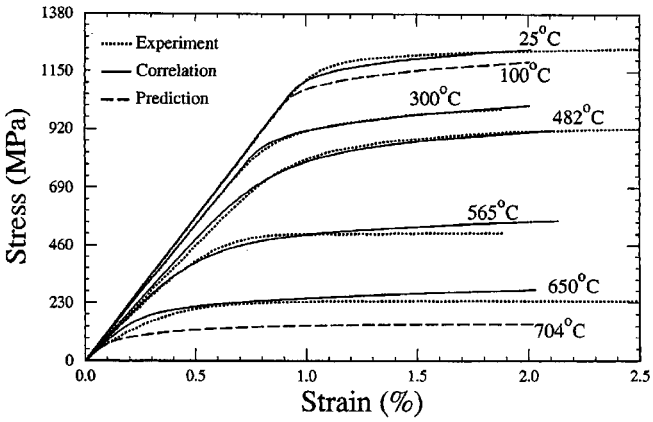

Figure 1.—GVIPS correlation with experimental tensile data at 25, 300, 482, 565, and 650 °C (80, 580, 900, 1050, and 1200 °F) for a total strain rate of 8.33×10^{-5}.

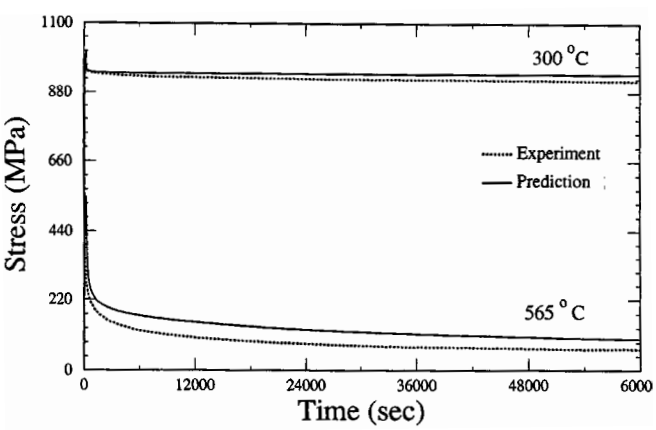

Figure 2.—Stress-time response of GVIPS prediction given relaxation tests at 300 and 565 °C (580 and 1050 °F). Total strain, 1.9%.

References

1. Arnold, S.M.; and Saleeb, A.F.: On the Thermodynamic Framework of Generalized Coupled Thermoelastic Viscoplastic-Damage Modeling. NASA TM–105349, 1991.

2. Arnold, S.M.; Saleeb, A.F.; and Castelli, M.G.: A Fully Associative, Nonlinear Kinematic, Unified Viscoplastic Model for Titanium-Based Matrices. NASA TM–106609, 1994.

3. Arnold, S.M.; Saleeb, A.F.; and Castelli, M.G.: A Fully Associative, Nonisothermal, Nonlinear Kinematic, Unified Viscoplastic Model for Titanium Alloys. NASA TM–106926, 1994.

4. Saleeb, A.F.; and Wilt, T.E.: Analysis of the Anisotropic Viscoplastic-Damage Response of Composite Laminates—Continuum Basis and Computational Algorithms. Int. J. Num. Meth. Eng., vol. 36, 1993, pp. 1629–1660.

5. Arnold, S.M.; Saleeb, A.F; and Wilt, T.E.: A Modeling Investigation of Thermal and Strain Induced Recovery and Nonlinear Hardening in Potential-Based Viscoplasticity. NASA TM–106122, 1993.

6. Saleeb, A.F.; Seif, Y.; and Arnold, S.M.: Fully Associative Viscoplasticity With Anisotropic and Nonlinear Kinematic Hardening. Submitted Int. J. Plasticity, 1994.

Lewis contact: Steven M. Arnold, (216) 433–3334

Micromechanics Analysis Code Predicts Thermomechanical Deformation of Advanced Composites

The ability to accurately predict the thermomechanical deformation response of advanced composite materials continues to play an important role in the development of these strategic materials. Analytical models that predict the effective behavior of composites are used not only by engineers performing structural analysis of large-scale composite components but also by material scientists in developing new material systems. For an analytical model to fulfill these two distinct functions it must be based on a micromechanics approach, which uses physically based deformation and life constitutive models and allows one to generate the average (macro) response of a composite material given the properties of the individual constituents and their geometric arrangement. Only then can such a model be used by a materials scientist to investigate the effect of different deformation

mechanisms on the overall response of the composite in order to identify the appropriate constituents for a given application. However, if a micromechanical model is to be used in a large-scale structural analysis, it must be computationally efficient, able to generate accurate displacement and stress fields at both the macro- and microlevels, and compatible with the finite element method. Additionally, new advances in processing and fabrication techniques now make it possible to engineer the architectures of these advanced composite systems.

Full utilization of these emerging manufacturing capabilities requires the development of a computationally efficient micromechanics analysis tool that can accurately predict the effect of microstructural details on the internal and macroscopic behavior of composites. Computational efficiency is required for two reasons: a large number of parameters must be varied in the course of engineering (or designing) composite materials, and optimizing a material's microstructure will require integrating the micromechanics model with optimization algorithms. From this perspective analytical approaches that produce closed-form expressions which describe the effect of a material's internal architecture on the overall material behavior are preferable to numerical methods, such as the finite element or finite difference schemes.

A number of models presently exist that can fulfill some aspect of these tasks. However, few working models are both computationally efficient and sufficiently accurate at the micro- and macrolevels. One such micromechanics model with the potential of fulfilling both tasks is the method of cells (ref. 1) and its generalization (ref. 2). The comprehensive capabilities and efficiency of this method have been documented in references 3 and 4. Consequently, NASA Lewis recently developed the computationally efficient and comprehensive Micromechanics Analysis Code (MAC) whose predictive capability rests entirely upon a fully analytical micromechanics model called the generalized method of cells (GMC) (refs. 2 and 3). MAC is a versatile form of research software that "drives" the doubly or triply periodic micromechanics constitutive models based on GMC. GMC can predict the response of both continuous and discontinuous multiphase composites with an arbitrary internal microstructure and reinforcement shape. GMC is a continuum-based micromechanics model that provides closed-form expressions for the macroscopic composite response in terms of the properties, size, shape, distribution, and response of the individual constituents or phases that make up the material. GMC also uses physically based viscoplastic deformation and life models for each constituent. MAC enhances the basic capabilities of GMC by providing a modular framework wherein (1) various thermal, mechanical (stress or strain control) and thermomechanical load histories can be imposed, (2) different integration algorithms can be selected, (3) a variety of constituent constitutive models can be implemented, and (4) a variety of fiber architectures can be easily accessed through their corresponding representative volume elements. Figure 1 illustrates the basic flow diagram for this modular framework. Figure 2 illustrates MAC's ability to describe the influence of hybrid architectures on the transverse inelastic response of MMC's.

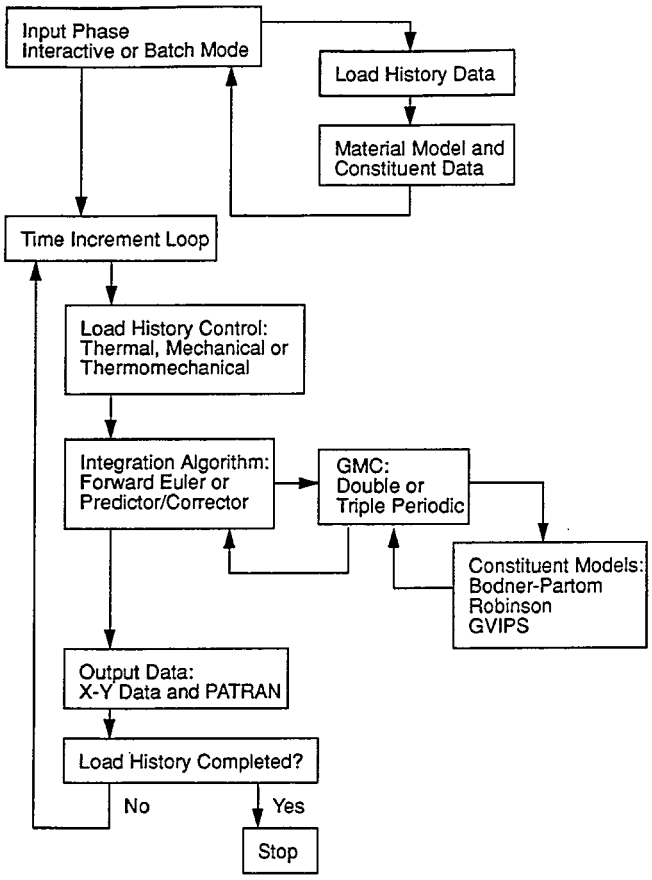

Figure 1.—MAC flowchart.

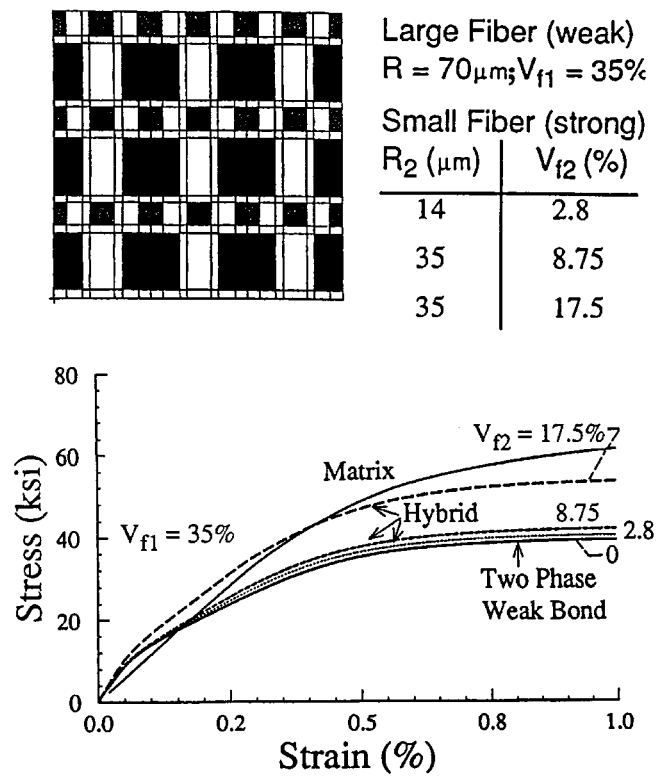

Figure 2.—Influence of hybrid architecture and bond strength on transverse inelastic response, where V_f denotes fiber volume fraction and the subscripts 1 and 2 denote fibers 1 and 2.

References

1. Aboudi, J.: Mechanics of Composite Materials: A Unified Micromechanical Approach. Elsevier, Amsterdam, 1991.

2. Paley, M.; and Aboudi, J.: Micromechanical Analysis of Composites by the Generalized Method of Cells Model. Mechanics of Materials, vol. 14, 1992, pp. 127–139.

3. Arnold, S.M.; Wilt, T.E.; Saleeb, A.F.; and Castelli, M.G.: An Investigation of Macro- and Micromechanical Approaches for a Model MMC System. Proceedings of the 6th Annual HiTemp Review, NASA CP–19117, Vol. II, 1993, pp. 52–1 to 52–12.

4. Arnold, S.M.; Wilt, T.E.; and Pindera, M.J.: Influence of Fiber Architecture on the Elastic and Inelastic Response of Metal Matrix Composites. NASA TM–106705, 1994.

5. Wilt, T.E.; and Arnold, S.M.: Micromechanics Analysis Code (MAC) User Guide: Version 1.0. NASA TM–106706, 1994.

Lewis contact: Steve M. Arnold, (216) 433–3334

Thermomechanical Multiaxial Fatigue Testing Capability Developed

Structural components in aeronautical gas turbine engines typically experience multiaxial states of stress under nonisothermal conditions. To estimate the durability of the various engine components, it is necessary to characterize the cyclic deformation and fatigue behavior of the materials used under thermal and complex mechanical loading conditions (refs. 1 and 2). To this end, a testing protocol and associated test control software have been developed for performing thermomechanical axial-torsional fatigue tests. These tests are to be performed on thin-walled, tubular specimens fabricated from the cobalt-based superalloy Haynes 188. The software is written in C and runs on an MS–DOS-based microcomputer. Several innovations incorporated into the test control software include a successive approximation algorithm for constant-rate temperature control; dynamic compensation for changes in the specimen dimensions due to changes in the coefficient of thermal expansion times temperature $\alpha \Delta T$, including the extensometer gage length; synchronization of all command and acquisition events using the personal computer's 8254 timer chip; high data acquisition rate oversampling to reduce noise while minimizing signal time averaging; polynomial interpolation of temperature versus thermal strain; and control of the axial mechanical strain ($\varepsilon_{tot} - \alpha \Delta T$), where ε_{tot} is the total strain. In addition, to avoid crack initiation from thermocouple spot welds, the gage section temperature is monitored by a light-pipe infrared probe. The test control software allows for arbitrary phasing between temperature and axial and torsional command waveform signals. Axial and torsional load, strain, and stroke as well as specimen temperature data are acquired 1000 times per cycle. Tests are performed in 600-sec cycles (dictated by the slowest free-convection cooling rate at the low end of the temperature cycle). Graphical output of axial and torsional stress response, temperatures, and additional pertinent information is displayed on the computer monitor in real time.

The test matrix will include (1) axial in-phase and out-of-phase thermomechanical force (TMF) tests, (2) torsional in-phase TMF tests, (3) mechanically and thermally in-phase tests (MIPTIP), (4) mechanically in-phase and thermally out-of-phase

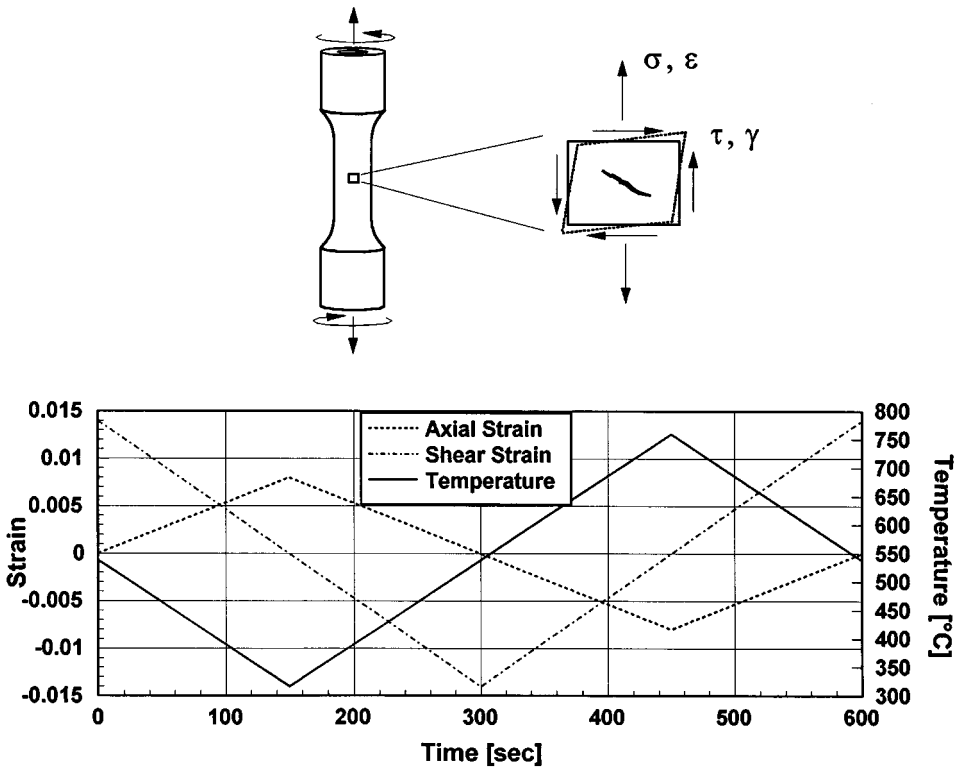

Figure 1.—Mechanically and thermally out-of-phase (MOPTOP) cycle of axial-torsional thermomechanical fatigue, where σ denotes axial stress, ε denotes axial strain, τ denotes shear stress, and γ denotes shear strain.

tests (MIPTOP), (5) mechanically out-of-phase and thermally in-phase tests (MOPTIP), and (6) mechanically and thermally out-of-phase tests (MOPTOP) (fig. 1). The maximum and minimum temperatures for all tests will be 760 and 316 °C (1400 and 600 °F), respectively. The results of these experiments will be used to assess multiaxial fatigue life models for their applicability to cyclic thermomechanical loading conditions. This program has been preceded by baseline experiments establishing the axial-torsional fatigue and deformation characteristics of Haynes 188 at 760 and 316 °C (1400 and 600 °F).

References

1. Kalluri, S.; and Bonacuse, P.J.: Estimation of Fatigue Life Under Axial-Torsional Loading. Material Durability/Life Prediction Modeling: Materials for the 21st Century, PVP–Vol. 290, S.Y. Zamrik and G.R. Halford, eds., American Society of Mechanical Engineers, New York, 1994.

2. Bonacuse, P.J.; and Kalluri, S.: Cyclic Axial-Torsional Deformation Behavior of a Cobalt-Base Superalloy. Cyclic Deformation, Fracture and Nondestructive Evaluation of Advanced Materials Symposium, ASTM STP–1184, Vol. 2, M.R. Mitchell and O. Buck, eds., American Society for Testing and Materials, Philadelphia, PA, 1994, pp. 204–229.

Lewis contacts: Peter J. Bonacuse, (216) 433–3309; Sreeramesh Kalluri, (216) 433–6727

High-Temperature Extensometer and Palladium-Chromium Temperature-Compensated Wire Resistance Strain Gages Compared

A detailed experimental evaluation is under way at NASA Lewis to compare and contrast the performance of the palladium-chromium/platinum (PdCr/Pt), dual-element, temperature-compensated, wire resistance strain gage with that of conventional high-temperature extensometry (ref. 1). The advanced PdCr gage, developed by researchers at NASA Lewis, exhibits desirable properties and a relatively small and repeatable apparent strain to 800 °C (1475 °F) (refs. 2 and 3). This gage represents a significant advance in technology, as existing commercial

resistance strain gages are not reliable for quasi-static strain measurements above ~400 °C (760 °F). The two strain measurement systems are being evaluated by applying various thermal and mechanical loading spectra using a high-temperature thermomechanical uniaxial testing system. In this way the applicability of the PdCr strain gage to the coupon-level specimen testing environment typically employed when characterizing high-temperature mechanical behaviors of structural materials can be investigated. Strain measurement capabilities to 800 °C (1475 °F) are investigated with a nickel-based superalloy (Inconel 100, or IN100) substrate material, and application to titanium-matrix composites (TMC's) is examined with the model system silicon carbide-reinforced/titanium-15 wt% vanadium–3 wt% chromium–3 wt% aluminum–3 wt% tin (SCS–6/Ti-15-3). Further, two gage application techniques are investigated in the comparison study, flame spraying and spot welding.

The apparent strain responses of both the weldable and flame-sprayed PdCr wire strain gages were found to be cyclically repeatable on both IN100 and SCS–6/Ti-15-3 $[0]_8$. In general, each gage exhibited some uniqueness with respect to apparent strain behavior. Gages mounted on the IN100 specimens tended to show a repeatable apparent strain within the first few cycles, as the thermal response of the IN100 was stable. This was not the case, however, for the TMC, which typically required several thermal cycles to stabilize the thermal strain response. Thus, progressive changes in the apparent strain behavior were corroborated by the extensometer, which, unlike the mounted gage, can distinguish quantitative changes in the material's thermal strain response. One specimen was instrumented with both a fixed and floating gage. From the difference in output of these two gages the thermal expansion strains were calculated. These data are given in figure 1, exhibiting excellent agreement with the values measured by the high-temperature extensometer.

In general, the mechanical strain measurements from the gages and extensometer on both the IN100 (to 800 °C; 1475 °F) and TMC (to 600 °C; 1115 °F) were in relatively good agreement (within 10%) to 2000 με. However, a slightly larger variation was found in the low-temperature measurements on the IN100 specimen with the weldable gage. The weldable gage mounted on the TMC experienced an effective failure with initial loading caused by a crack in the Timetal 21S shim at a spot weld location. Data obtained from this gage were therefore erroneous, as poor contact existed between the shim and the substrate composite. Subsequent to mechanical loading cycles, the specimens were subjected to thermal cycles to measure changes in the apparent strain responses. In general, the apparent strain responses of both the weldable and flame-sprayed gages were repeatable. As a final aspect of mechanical performance in the present work the specimens were subjected to progressively increasing mechanical loads to measure the maximum mechanical strain threshold of the gages at room temperature. Preliminary results indicate that the gages tended to lose reliable strain measurement capabilities at

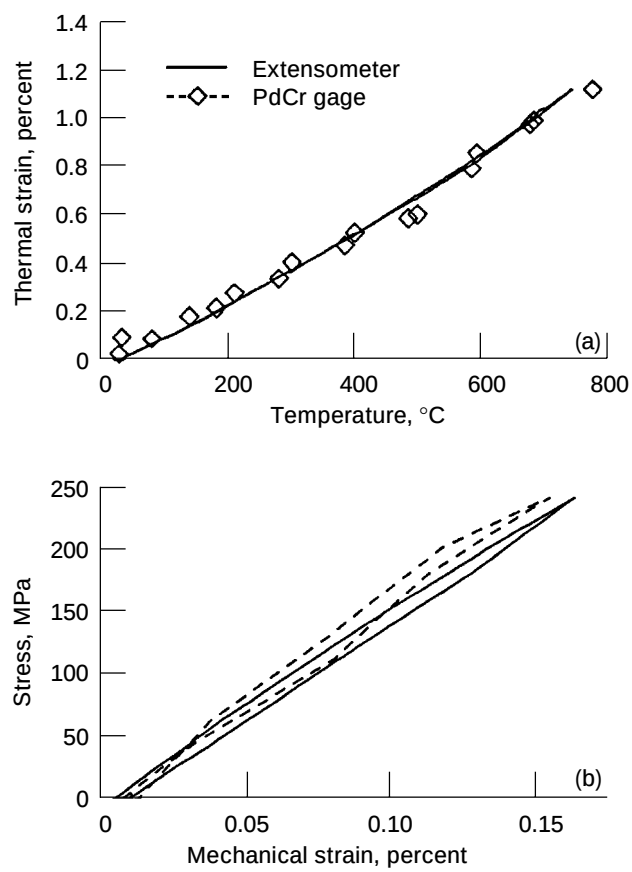

Figure 1.—Gage and extensometer output showing excellent agreement under thermal and mechanical loadings. (a) Thermal strain of Inconel 100 as function of temperature. (b) Stress of Inconel 100 as function of mechanical strain at 750 °C (1385 °F).

approximately 4500 με.

References

1. Castelli, M.G.; and Lei, J.–F.: A Comparison Between High Temperature Extensometry and PdCr-Based Resistance Strain Gages With Multiple Application Techniques. Proceedings of the 7th Annual HiTEMP Review, NASA CP–10146, Vol. II, 1994, pp. 36–1 to 36–12.

2. Lei, J.–F.: A Resistance Strain Gage With Repeatable and Cancelable Apparent Strain for Use to 800 °C. NASA CR–185256, 1990.

3. Lei, J.–F.: Palladium-Chromium Static Strain Gages for High Temperatures. Proceedings of the 1992 NASA Langley Measurement Technology Conference, NASA CP–3161, 1992, pp. 189–209.

Lewis contacts: Michael G. Castelli, (216) 433–8464; Jih-Fen Lei, (216) 433–3922

Temperature-Dependent Effects Studied on Mechanical Behavior and Deformation Substructure of Haynes 188 Under Low-Cycle Fatigue

The mechanical behavior of a cobalt-nickel-chromium-tungsten superalloy, Haynes 188, is presently undergoing critical examination at NASA Lewis. This dynamic strain aging (DSA) alloy is used in many military and commercial aircraft turbine engines for combustor liners and in the main injectors of the space shuttle main engines for the liquid oxygen posts. Its attractive features include a good combination of high monotonic yield and tensile strength and excellent fabricability, weldability, and resistance to high-temperature oxidation for prolonged exposures. One of the current research activities on Haynes 188 is investigating the effects of temperature on the mechanical behavior and deformation substructure under low-cycle fatigue (LCF) conditions over the temperature range 25 to 1000 °C (80 and 1840 °F) at a constant strain rate of 10^{-3} sec^{-1}. Particular attention is given to the effects of DSA on the stress-strain response and LCF life. Although DSA is found to occur over a wide temperature range between 300 and 750 °C (570 and 1385 °F), the microstructural characteristics and the deformation mechanisms responsible for DSA vary considerably and depend on temperature. Further, DSA is not consistently evidenced through serrated yielding; however, specialized tests where the strain rate is changed at specific cycles reveal a negative strain rate sensitivity, indicative of DSA. A correlation between the cyclic deformation behavior and the microstructural processes is enabled through detailed transmission electron microscopy investigations on material tested at the various temperatures.

As shown in figure 1, Haynes 188 exhibits a relatively complex temperature-dependent stress response. Below 300 °C (570 °F) the material exhibits a short period of cyclic hardening followed by an extended period of essentially stable stress response until the onset of failure. Here, cyclic deformation occurs by simultaneous activation of two slip systems. In the midtemperature regime from 400 to 750 °C (760 to 1385 °F), where DSA occurs, the material exhibits marked cyclic hardening prior to the onset of failure. In this regime two slip systems are also activated, with the deformation substructure exhibiting much higher dislocation densities than those revealed at 300 °C (570 °F) and below. Between 650 and 750 °C (1200 and 1385 °F) dislocations are distributed more homogeneously and are pinned by fine chromium-rich carbides, leading to enhanced cyclic hardening. Above approximately 800 °C (1475 °F) the tendency for cyclic hardening declines, and

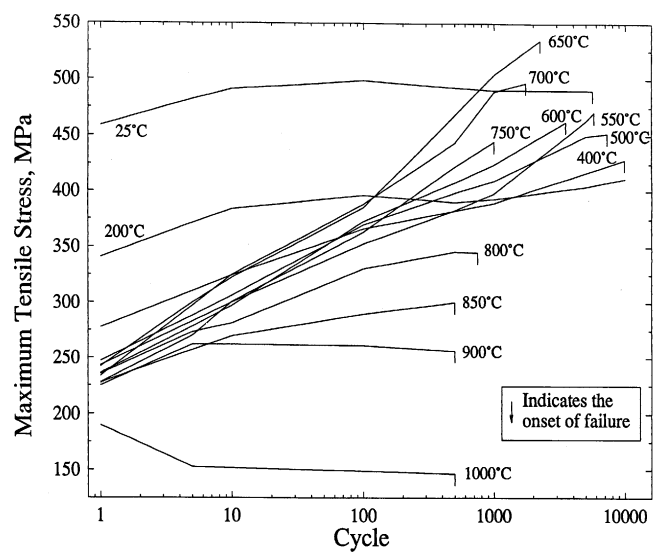

Figure 1.—Cyclic stress response of Haynes 188 under low-cycle fatigue conditions with strainrange of 0.4% and strain rate of 10^{-3} sec^{-1}.

cyclic softening is displayed above 900 °C (1650 °F). At 900 °C (1650 °F) and above dynamic recovery by thermally activated climb becomes prominent and leads to the formation of cells and subgrains.

The crack initiation and propagation modes are also found to be temperature dependent in Haynes 188 under LCF conditions. Below 600°C (1115 °F) crack initiation and propagation occur in a transgranular mode. Between 650 and 750 °C (1200 and 1385 °F) crack propagation occurs in a mixed transgranular plus intergranular mode, despite the fact that the crack initiation occurs by transcrystalline mechanisms. For specimens fatigued above approximately 800 °C (1475 °F) the fracture surfaces are covered with a thick oxidation layer. At these relatively high temperatures the apparent predominant mechanism for crack initiation and propagation is environmentally assisted intergranular cracking.

Lewis contact: Michael G. Castelli, (216) 433–8464

Fatigue Behavior and Deformation Mechanisms Studied in Inconel 718 Superalloy

The nickel-based superalloy Inconel 718 (IN718) is used as a structural material for a variety of components in the space shuttle main engines (SSME) and accounts for more than half the total weight of the SSME. IN718 is also the bill of materiel for the pressure vessels of nickel-hydrogen batteries for the space station. SSME structural components are typically subjected to startup and shutdown load transients and occasional overloads in addition to the high-frequency vibratory loads from routine operation. The nickel-hydrogen battery cells are proof tested before service and are subjected to fluctuating pressure loads during operation. In both these applications the structural material is subjected to a monotonic load initially that is subsequently followed by fatigue. To assess the life of these structural components, it is necessary to determine the influence of a prior monotonic load on the subsequent fatigue life of the superalloy. An insight into the underlying deformation and damage mechanisms is also required to properly account for the interaction between the prior monotonic load and the subsequent fatigue loading.

An experimental investigation was conducted to establish the effect of prior monotonic straining on the subsequent fatigue behavior of wrought, double-aged IN718 at room temperature (ref. 1). First, monotonic strain tests and fully reversed, strain-controlled fatigue tests were conducted on uniform-gage-section IN718 specimens. Next, fully reversed fatigue tests were conducted under strain control on specimens monotonically strained in tension. Results from this investigation (fig. 1) indicated that prior monotonic straining reduced the fatigue resistance of the superalloy, particularly at the lowest strain range. Some tested specimens were sectioned and examined by transmission electron microscopy to reveal typical microstructures as well as the active deformation and damage mechanisms under each loading condition (ref. 2). In monotonically strained specimens deformation during the subsequent fatigue loading was mainly confined to the deformation bands initiated during the prior monotonic straining. This confinement can cause dislocations to move more readily along the previously activated deformation bands and pile up near grain boundaries, which eventually makes the grain boundaries susceptible to fatigue cracking. The mechanisms inferred from the microstructural investigation were extremely valuable in interpreting the influence of prior monotonic straining on the subsequent fatigue life of IN718 superalloy.

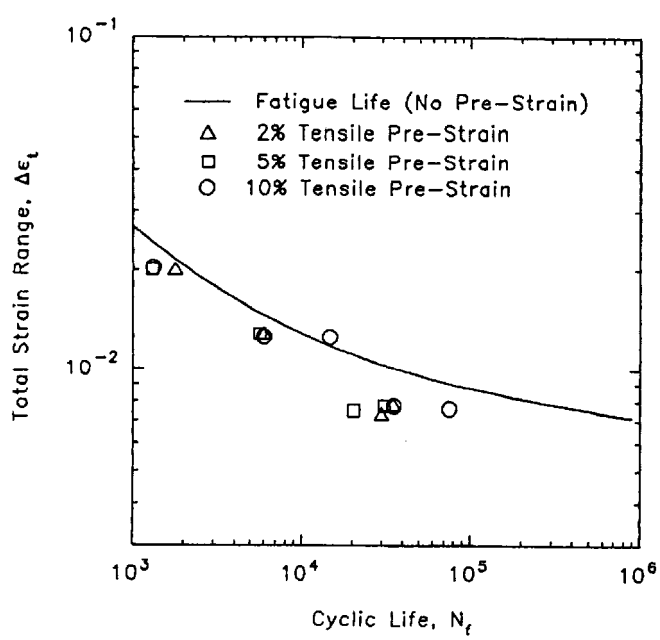

Figure 1.—Influence of prior monotonic straining on subsequent fatigue life of Inconel 718 superalloy.

References

1. Kalluri, S.; Halford, G.R.; and McGaw, M.A.: Fatigue Behavior of Inconel 718 Superalloy Subjected to Monotonic Tensile and Compressive Strains. Advanced Earth-To-Orbit Propulsion Technology, R.J. Richmond and S.T. Wu, eds., Vol. 2, 1994, pp. 287–294.

2. Kalluri, S.; Bhanu Sankara Rao, K.; Halford, G.R.; and McGaw, M.A.: Deformation and Damage Mechanisms in Inconel 718 Superalloy. Proceedings of the Symposium on Superalloys 718, 625, 706 and Various Derivatives, E.A. Loria, ed., The Minerals, Metals, and Materials Society, 1994, pp. 593–606.

Lewis contacts: Sreeramesh Kalluri, (216) 433–6727; Gary R. Halford, (216) 433–3265; Michael A. McGaw, (216) 433–3308

Effects of Control Mode and *R*-Ratio on Fatigue Behavior of Metal-Matrix Composites Studied

Continuously reinforced metal-matrix composites (MMC's) are under consideration for future-generation aeropropulsion systems because of their high specific stiffness and strength at elevated temperatures. Since components in aeropropulsion systems experience substantial cyclic thermal and mechanical loads, the fatigue behavior of MMC's is of great interest. Almost without exception previous investigations of the fatigue behavior of MMC's have been conducted in a zero-tension, load-controlled ($R_\sigma = 0$) mode. The reason is that available material is typically less than 2.5 mm (0.1 in.) thick and, therefore, unable to withstand high compressive loads without buckling. This testing mode may be appropriate for MMC's to be used in aircraft skins. However, unlike aircraft skins most engine components are thick. Additionally, the transient thermal gradients experienced in an aircraft engine will impose tension-compression loading on engine components, requiring the designer to understand how the MMC will behave under fully reversed loading conditions. The greater thickness of the engine MMC may also affect the fatigue life.

Traditionally, low-cycle fatigue (LCF) tests on MMC's have been performed in load control. For monolithic alloys LCF tests are more typically performed in strain control. Two reasons justify this choice: (1) the critical volume from which cracks initiate and grow is generally small and elastically constrained by the larger surrounding volume of material and (2) load-controlled LCF tests of monolithics invariably lead to unconstrained ratchetting and localized necking—an undesired material response because the failure mechanism is far more severe than, and unrelated to, the fatigue mechanism being studied. It is not known if this is the proper approach to composite testing. However, there is a lack of strain-controlled data on which to base any decisions. Consequently, this study addresses the isothermal LCF behavior of a $[0]_{32}$ MMC tested under strain- and load-controlled conditions for both zero-tension ($R_\sigma = 0$) and tension-compression ($R_\sigma = -1$) loading. These tests were run at 427 °C (800 °F) on thick specimens of silicon-carbide-reinforced titanium–15 wt% vanadium–3 wt% chromium–3 wt% aluminum–3 wt% tin (SCS–6/Ti-15-3).

For the fully reversed tests no difference was observed in life between the load- and strain-controlled tests. However, for the zero-tension tests the strain-controlled tests resulted in three times longer life than the load-controlled tests. The reason is that under strain control the specimens cyclically softened, reducing the cracking potential. In contrast, the load-controlled tests ratchetted toward larger tensile strains, leading to an eventual overload of the fibers.

Fatigue tests revealed that specimens tested under fully reversed conditions had approximately 10 times longer lives than specimens tested under zero tension. The fully reversed specimens had similar, but still shorter, lives than the unreinforced matrix material when examined on a strain range basis (fig. 1(a)). However, the composite had a strain limitation at low life because of the limited strain capacity of the brittle ceramic fiber. The composite also suffered at very high life because of the lack of apparent fatigue limit relative to the unreinforced matrix. The value of adding fibers to the matrix is apparent when the fatigue lives are plotted as a function of stress range (fig. 1(b)). Here, the composite is far superior to the unreinforced matrix because of the additional load-carrying capacity of the fibers.

Lewis contacts: Bradley A. Lerch, (216) 433–5522; Gary R. Halford, (216) 433–3265

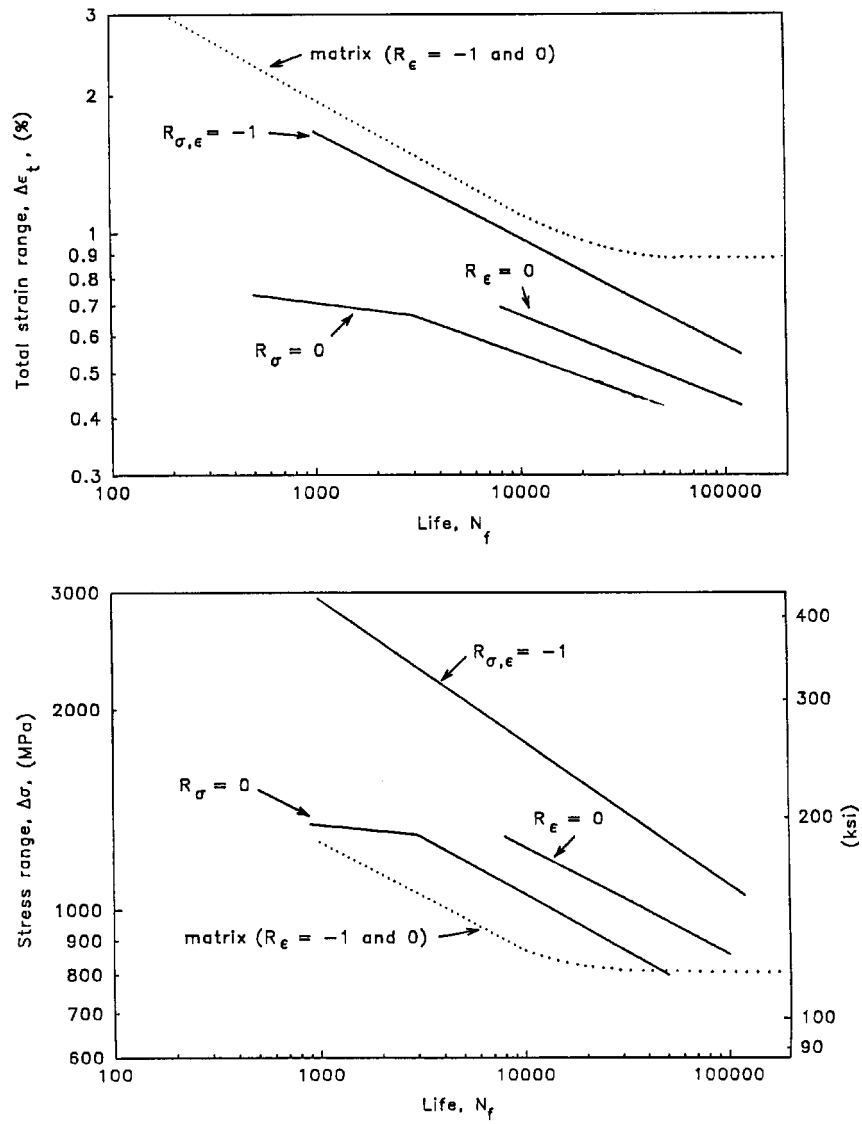

Figure 1.—Summary of fatigue life on strain range (a) and stress range (b) for SCS–6/Ti 15-3 composite and unreinforced matrix tested at 427 °C (800 °F), where R_ϵ denotes strain-controlled tests and R_σ denotes load-controlled tests.

Effects of Microalloying on Low-Cycle Fatigue Behavior of Powder-Extruded Nickel Aluminides Investigated

There is considerable interest in developing new structural materials in which high use temperatures and high strength, coupled with low density, are minimum requirements. The goal for these new materials is to provide operational capability well beyond the working range of conventional superalloys. Of the many intermetallics under consideration, nickel aluminum (NiAl) is one of the few systems that has emerged as a promising candidate for further development. It has a number of property advantages, including low density, high melting temperature, high thermal conductivity, and excellent environmental resistance. However, binary NiAl lacks strength and creep resistance at elevated temperatures. Poor high-temperature strength also results in worse than predicted low-cycle fatigue (LCF) life at low strain ranges at 727 °C (1341 °F) due to accelerated creep damage mechanisms that result in significant intergranular cracking (ref. 1). One approach for improving these properties involves microalloying with either zirconium (Zr) or nitrogen (N). As an integral part of this alloy development program

the LCF behavior of Zr- and N-doped nickel aluminides produced by extrusion of prealloyed powders has been investigated and compared with the LCF behavior of similarly processed binary NiAl.

The fatigue-life behavior of the various NiAl alloys is plotted in figure 1. The two stages in the total strain-life plot of NiAl(Zr) result from the change in fracture behavior from slow, stable intergranular crack growth at strain ranges of 0.38% or less to brittle, cleavage-dominated overload fracture above this value. At strain ranges above 0.38% the peak tensile stress reached the monotonic cleavage fracture stress of the Zr-doped alloy at 1000 K (328 MPa; 47 ksi) in less than 100 cycles, enabling fast crack growth by cleavage. At total strain ranges of 0.38% or less the peak tensile cyclic stress remained at a much lower level than the tensile cleavage fracture stress. In general, fatigue life is governed by the ductility of the material at high strains and by its strength at low strains. The longer lives of NiAl(Zr) at low strain ranges result from its basic capacity to resist the applied strains on the basis of high strength. Both the NiAl and NiAl(N) have shorter lives at low strain ranges because of the synergistic interaction between fatigue and creep. To improve the fatigue resistance of the binary and N-doped alloys, the grain boundaries need to be strengthened to reduce grain boundary sliding and associated intergranular wedge cracking. Since Zr segregates to the grain boundaries in NiAl (ref. 2) and apparently strengthens the boundary regions, preventing grain boundary sliding, NiAl(Zr) does not suffer from the same problem as the other two alloys.

Previously, it has been shown that binary NiAl materials have superior fatigue life relative to conventional superalloys when compared on a plastic strain range basis (ref. 1). This holds true for the additional NiAl alloys studied. The problem was that the NiAl alloys compared poorly with superalloys on a stress range basis. However, the current results show that even the extremely small Zr addition (approximately 0.1 at.%) significantly improved fatigue life on a stress range basis, approaching that of the superalloys (fig. 2). Furthermore, although Ni-based superalloys are highly alloyed materials, the NiAl alloy has significant upside potential in both strength and fatigue life by the incorporation of higher levels of alloying additions.

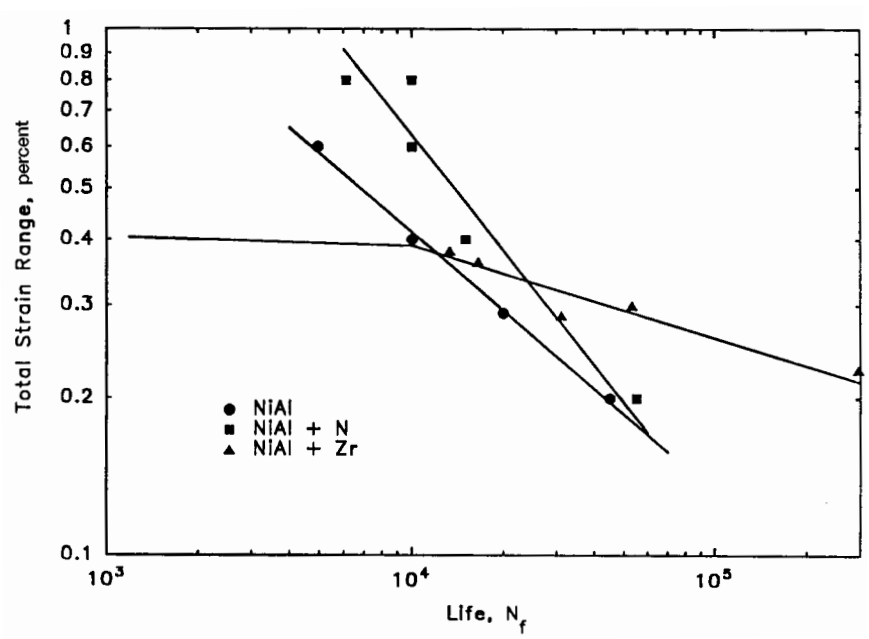

Figure 1.—Fatigue life of three NiAl alloys.

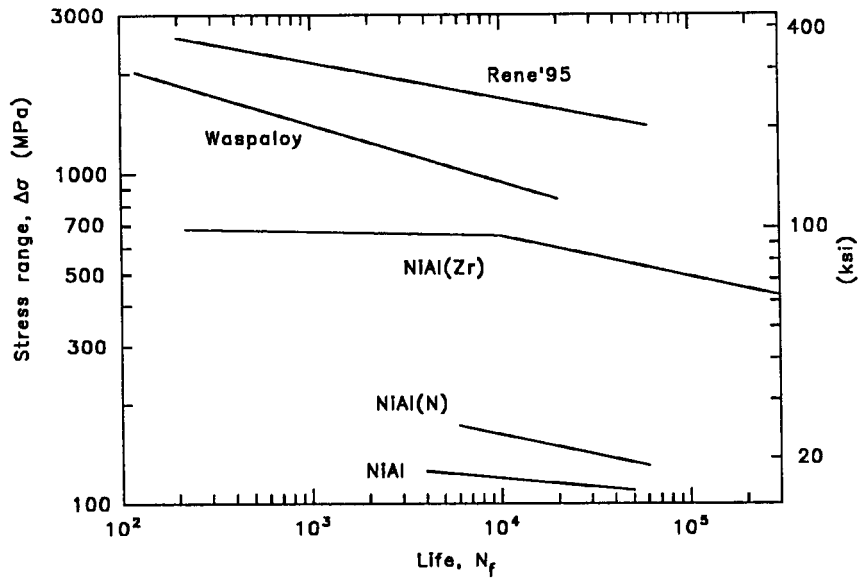

Figure 2.—Comparison of NiAl Alloys with typical superalloys tested at nominally 727 °C (1341 °F).

References

1. Lerch, B.A.; and Noebe, R.D.: Low-Cycle Fatigue Behavior of Polycrystalline NiAl at 1000 K. Metall. Maters. Trans. A, vol. 25A, 1994, pp. 309–319.

2. Zeller, M.V.; Noebe, R.D.; and Locci, I.E.: Grain Boundary Segregation Studies of NiAl and NiAl(Zr) Using Auger Electron Spectroscopy. Proceedings of the 3rd Annual HiTEMP Review, NASA CP–10051, 1990, pp. 21–1 to 21–17.

Lewis contacts: Bradley A. Lerch, (216) 433–5522; Ronald D. Noebe, (216) 433–2093

Thermomechanical Fatigue Behavior of Coated and Uncoated Enhanced SiC/SiC Studied

Thermomechanical fatigue (TMF) testing provides a method of evaluating continuous-fiber-reinforced ceramic composites (CFCC's) under thermal and mechanical loading conditions. Although these tests are complicated, they provide a reasonable approximation of the combined thermal and mechanical loads to be experienced by the material in service. These data will be used to develop life prediction models as well as to aid the materials development.

Previous TMF results on the silicon carbide (SiC)/SiC composite demonstrated that enhancing the oxidation resistance of the matrix by a proprietary process increased TMF life (ref. 1). This improvement allowed the continued application of maximum cyclic stresses at or above the level where microcracking occurs (ref. 2). In contrast, the unenhanced composite developed microcracks that led to rapid failure. The enhanced composite thus has improved damage tolerance. Further improvements in TMF life were realized by using an oxidation-resistant coating, which also permitted an increase in the maximum temperature by at least 100 °C (ref. 3).

The composite with the enhanced matrix (both coated and uncoated) cracked through the formation of periodic microcracks. These cracks began on the edge of the sample at interbundle regions where only matrix material (which also contained uninfiltrated regions) existed (fig. 1). These interbundle regions are weak, unreinforced areas very susceptible to crack formation. This cracking subsequently allowed oxygen to penetrate into the interior of the composite, leading to the formation of a glass-like phase, which is intended to seal the cracks. However, this phase also formed at the fiber/matrix interface and is suspected of degrading the strength of the fibers.

These results (fig. 2) indicate that an improvement in the TMF behavior of the material can be gained by improving the oxidation resistance of the matrix and by applying an oxidation-resistant coating. However, these improvements may only be marginal, since the material still suffers from the weak interbundle regions. These regions are

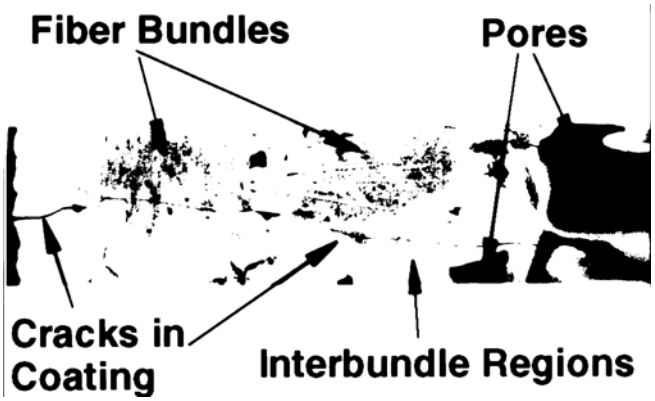

Figure 1.—Optical micrograph showing composite microstructure and propagation of cracks from edge of sample.

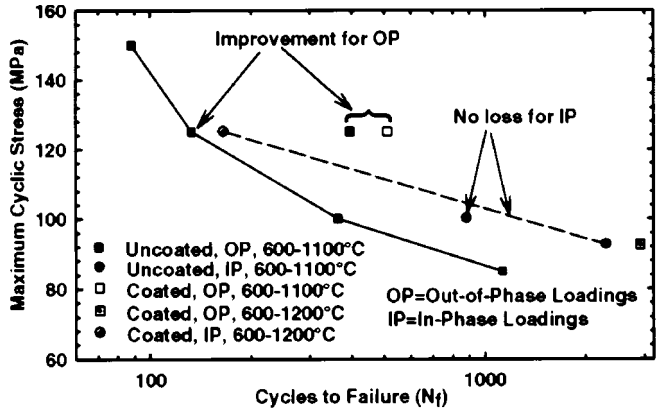

Figure 2.—Maximum cyclic stress versus cycles to failure.

manifestations of the woven character of the material. Also, the matrix enhancements and the oxidation-resistant coating may be chemically incompatible with the fibers, leading to strength degradations during long-term tests.

References

1. Worthem, D.W.: Thermomechanical Fatigue of Three Ceramic-Matrix Composites. Proceedings of the 6th Annual HiTEMP Review, NASA CP–19117, 1993, Vol. III, pp. 79–1 to 79–11.

2. Marshall, D.B.; and Evans, A.G.: Failure Mechanisms in Ceramic-Fiber/Ceramic-Matrix Composites. J. Am. Ceram. Soc., vol. 68, no. 5, 1985, pp. 225–231.

3. Worthem, D.W.: Thermomechanical Fatigue Behavior of Coated and Uncoated Enhanced SiC/SiC[PW]. Proceedings of the 7th Annual HiTEMP Review, NASA CP–10146, Vol. 3, 1994, pp. 66–1 to 66–12.

Lewis contact: Dennis Worthem, (216) 433–3209

Structural Dynamics

Active Rotor Blade Tip Clearance Controlled With Embedded Piezoelectric Layers

Controlling the clearance between the aircraft turbine engine blade tips and the engine casing is a vital issue in engine performance and health monitoring in the NASA Advanced Subsonic Technology Program. Smart structure technology has been used to actively control tip clearance and thus dramatically improve engine efficiency and health-monitoring capabilities. A finite element code has been developed to predict casing radial displacement that incorporates the system dynamics, smart materials, and controller. The simulation result showed that smart structure technology could be a simple, effective, reliable way to actively control the tip clearance.

Variation in blade tip clearance is influenced by a number of factors, such as blade deformations, uneven deflections of the engine shaft, uneven thermal distortions of blades, and unknown factors. This research was focused on controlling radial casing displacement by using embedded piezoelectric layers (PZT). A smart engine casing incorporates piezoelectric layers to transform radial casing deformation into electrical voltage signals (acting as sensors), a neural control package to process those signals (the smart part), and other piezoelectric layers to convert the processed signals into applied forces on the casing (acting as actuators). To simulate the elastic deformation shape of the casing with a 1-mm (0.04-in.) thick single piezoelectric layer, we selected the Pratt & Whitney (P&W) T2037 casing

model. All geometric data, material properties, and boundary conditions of P&W T2037 and PZT were plugged into the developed finite element code.

The simulation result (fig. 1) shows the capability to actively induce significant radial displacement (about 1 mm (0.04 in.) maximum) even with a single 1-mm (0.04-in.) thick PZT layer. As compared with the thermal method currently used by P&W, this method is advantageous because of fast response, compensation for static and dynamic loading, and mode shape control. Also, this method requires very low power because the integrated current is low and improves reliability because it is simple and efficient. Since this method can significantly reduce weight and be used for tip clearance control at takeoff, cruise, and landing speeds, fuel consumption can be reduced by 2 to 3%.

Considering the success of the initial staged smart structure application for controlling blade tip clearance, future studies may address the active control of smart engine casing with discretely embedded piezoelectric patches for the next generation of turbine engines.

Lewis contacts: Benjamin B. Choi, (216) 433–6040; Dimitris A. Saravanos, (216) 433–8466; Charles Lawrence, (216) 433–6048

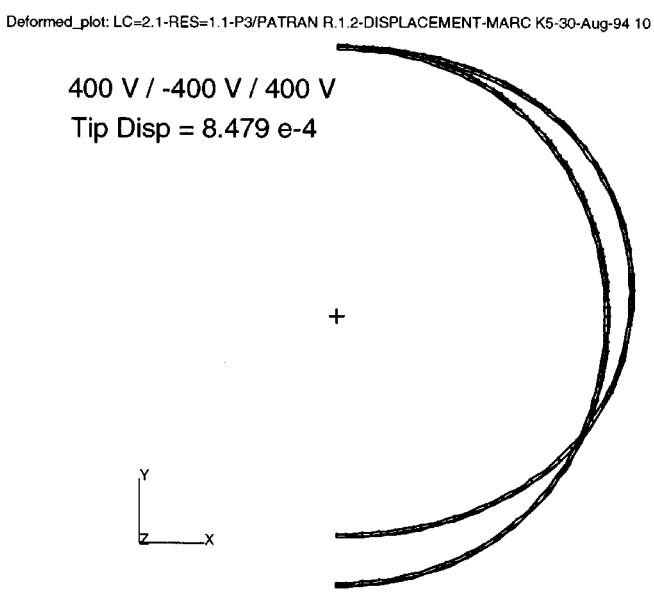

Figure 1.—Computer simulation of radial deformation of Pratt & Whitney T2037 engine casing model actuated by 1-mm (0.04-in.) thick piezoelectric layer (400 V applied). Tip displacement, 8.479×10^{-4}.

Shape Memory Alloy May Control Gas Turbine Engine Blade Tip Clearances

NASA Lewis is sponsoring a research effort to experimentally examine the feasibility of using an innovative adaptive control technique to minimize blade tip clearances in gas turbine engines. The technique uses shape memory alloy (SMA; e.g., smart material) compensator rings. NASA Lewis has contracted with Memry Technologies, a recognized leader in shape memory alloys, and Allied Signal (formerly Textron Lycoming) to design and fabricate full-scale compressor compensator rings and to evaluate the performance improvements possible through compressor performance measurements.

The compensator rings are designed and the shape memory alloys selected to allow the rings to reduce the operating clearances in the T–55 engine from 0.043 cm to 0.013 cm (0.017 in. to 0.005 in.), resulting in an estimated increase in compressor efficiency of 0.3%. The compensator ring is fabricated of a copper-aluminum-nickel shape memory alloy whose martensitic-to-austenitic transformation temperature is tailored so that as the compressor reaches operating temperatures, tip clearances are reduced to their minimum.

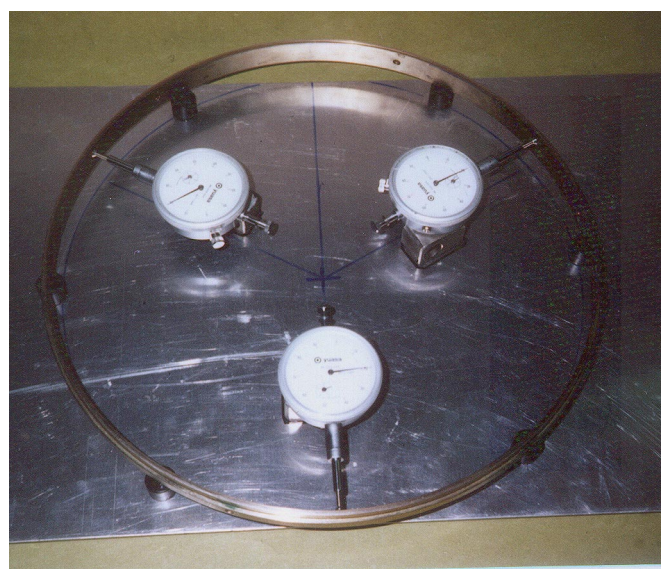

Figure 1.—Prototype compensator ring, phase I.

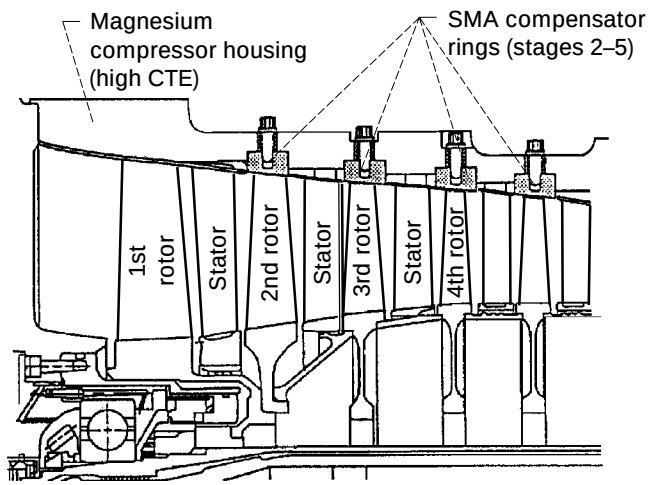

Figure 2.—Engine compressor development demonstration, phase II.

Phase I has been completed and has successfully demonstrated the ring's ability to change dimension at the correct rate to minimize clearances (fig. 1). The phase II contract has been awarded to perform a detailed design of the compensator rings, to fabricate rings for the first four stages of the compressor, and to demonstrate the performance improvements possible relative to the standard steel rings used conventionally in a T–55 compressor performance rig (fig. 2).

Lewis contact: Bruce M. Steinetz, (216) 433–3302

Engine Seal Technology Required To Meet NASA's Advanced Subsonic Technology Program Goals

NASA is working in close partnership with the aircraft industry under the Advanced Subsonic Technology (AST) Program to develop technology to reduce operating costs, reduce noise and emissions, and boost performance of the next generation of commercial aircraft. To reach the stated goals (ref. 1), significant improvements in engine components and subsystems are required to extract more useful work from these high-power-density engines. Improving engine seal technology shows great promise in helping engine manufacturers reach the required reductions in specific fuel consumption and ultimately direct operating costs. System-level studies have identified seals as having high benefit-to-development-cost ratios. Advanced engine seals show promise of reducing engine losses and maintaining these performance benefits over the service interval of the engine and are comparatively inexpensive to develop.

NASA and the Army commissioned Allison Engines to examine two modern engines and to identify performance benefits possible through implementing advanced engine seals. The study looked at a turbofan engine (AE3007) slated for growth to meet the 89-kN (20 000-lb) thrust requirement of the AST program and at a turboshaft engine (T–800 study basis) with

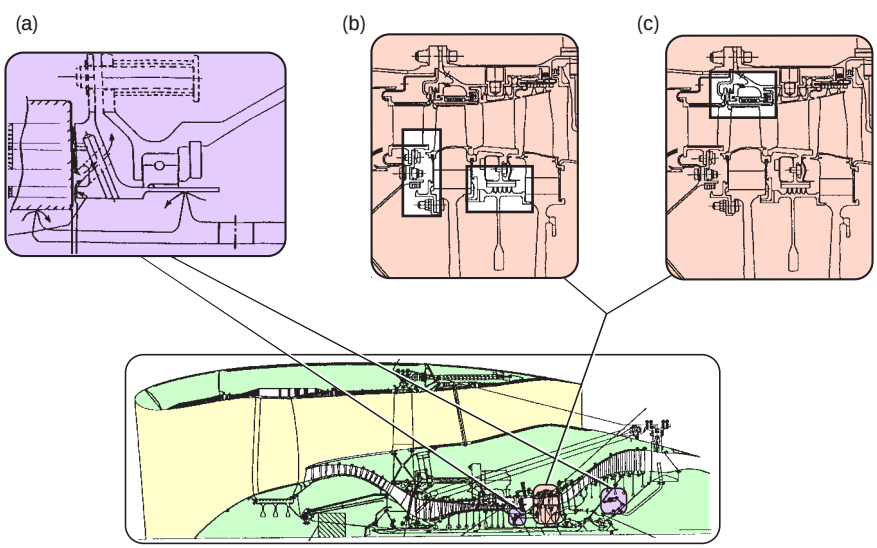

Figure 1.—Seal locations. (a) Compressor discharge and balance piston seal locations in face and brush seals. (b) Turbine rim and interstage seals. (c) Blade tip clearance control.

performance growth to meet the military Integrated High Performance Turbine Engine Technology (IHPTET) phase 2 goals. The study (ref. 2) demonstrated that implementing advanced seals within the engine (e.g., at the turbine rim, the compressor discharge, and the intershaft seals) would save 2 to 5% in engine efficiency.

References

1. Steinetz, B.M.; and Hendricks, R.C.: Engine Seal Technology Requirements to Meet NASA's Advanced Subsonic Technology Program Goals. AIAA Paper 94–2698, 1994. (Also NASA TM–106582.)

2. Munson, J.; and Steinetz, B.M.: Specific Fuel Consumption and Increased Thrust Performance Benefits Possible With Advanced Seal Technology. AIAA Paper 94–2700, 1994.

Lewis contact: Bruce M. Steinetz, (216) 433–3302

Multistage Aeroelastic Program Is Based on Two-Dimensional Euler Equations

An accurate analysis of blade row aerodynamic interaction that includes blade structural vibratory motion is essential for predicting both forced response and flutter characteristics of turbomachinery blade rows. Toward this goal a multistage aeroelastic program, MSAP2D, was developed. The program can be used to analyze single or multiple rows of blades. The blade rows can have unequal numbers of blades, and blades can be rigid or vibrating. The required unsteady aerodynamic forces are obtained from solving two-dimensional Euler equations by using a finite volume method with a combination of flux vector splitting and flux difference splitting. The Euler solution scheme is third-order accurate in space and second-order accurate in time. The flow equations are solved on one or more passage-centered H grids. The structural model is a typical section with bending and torsional motion degrees of freedom for each blade in the blade rows. The aeroelastic equations are solved by using Newmark's method. The program has been calibrated on two examples: a compressor in supersonic throughflow, and the space shuttle main engine (SSME) high-pressure fuel turbopump (HPFTP) in subsonic flow.

For the supersonic throughflow compressor two blade rows were considered. The front row was designated as the rotor and moved with a speed equal to Mach 0.10. The aft row was stationary and was designated as the stator. The airfoils were double circular-arc airfoils with 1% thickness-to-chord ratio t/c. The axial gap between the blade rows was 20% of the chord and the stagger angle was zero. The number of blades was varied in each blade row. The gap-to-chord ratio s/c was 0.5 for rows with two blades, 0.33 for rows with three blades, and 0.25 for rows with four blades. The free-stream Mach number was 1.5.

Figure 1 shows the variation of the aft stator's moment coefficient when the number of blades in the front rotor was varied from two to three to four (i.e., 2:2, 3:2, and 4:2 blade ratios). Both the amplitude and frequency of the moment changed as the number of blades was increased. The amplitude was higher because the front row's blades were closer, increasing the cascading effect. The frequency was different because the aft row was seeing more blades for the same pitch distance as the number of blades in the front row was increased. The frequency for the four-blade-row configuration was twice that of two-blade-row configuration. Also (not shown here), when the number of blades in the aft row was increased for a fixed number of blades in the front rotor, the amplitude of the force changed, but the frequency of the force remained the same. The amplitude was higher because the blades in the aft row were closer, increasing the cascading effect. The frequency was same because the aft row was seeing the same number of blades in the front at the same pitch distance. Note that the force on the front rotor remained steady, irrespective of the number of blades in the aft row, since in supersonic throughflow the aft row cannot have any influence on the front rotor.

Figure 2 shows the structural response of the stator blade row. The structural model for each blade (in each row) was a typical section with pitching degree of freedom. The elastic axis was at 30% from the leading edge. The mass ratio μ was 456.2, the radius of gyration r_α was 0.588, there was no offset between the elastic axis and the center of mass (i.e., $x_\alpha = 0.0$), the ratio of natural frequencies in bending and torsion ω_h/ω_α was 0.567. The reference reduced velocity for the time domain calculations was taken as $V^* (= M_\infty a_\infty / b\omega_\alpha) = 1.2$.

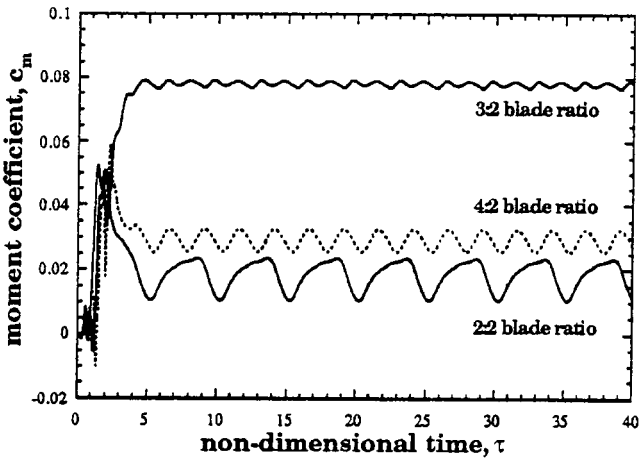

Figure 1.—Moment coefficient variation on stator airfoil surface. Double circular-arc airfoil cascade; thickness-to-chord ratio, t/c, 1%; stagger, 0°; free-stream velocity, Mach 1.5; rotor velocity, Mach 0.10.

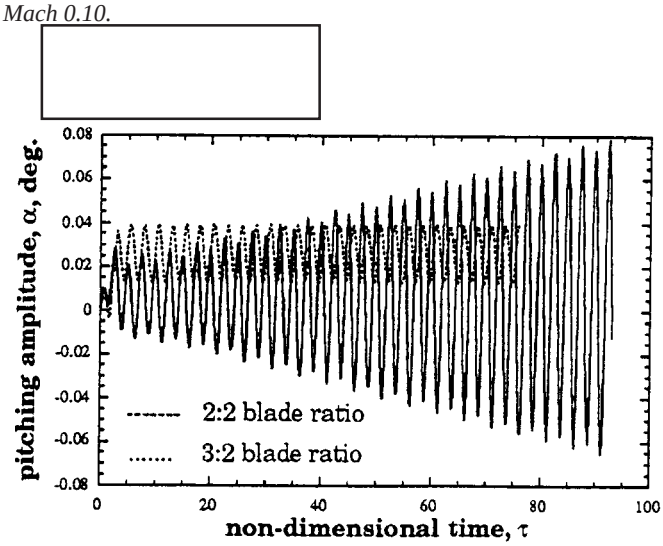

Figure 2.—Time response of pitching amplitude. Stator blade row; forcing function only; cascade parameters same as for figure 1; reduced velocity, V*, *1.2.*

The stator blade row is now subjected to a two-part aerodynamic force. One part is the force due to the wake of the front blade row (as seen in fig. 1, called forcing function), and the other part is the aerodynamic force generated by blade (self) vibration. Figure 2 shows the pitching response of the stator blade row for V^*=1.2 for the forcing function given in figure 1 for the 2:2 and 3:2 blade ratio cases. A Fourier analysis of the forcing function for 2:2 (and also for 4:2) blade ratio showed that it has frequencies near the natural frequency of the aeroelastic system for V^*=1.2. The response shows an unstable response for V^*=1.2, as expected, due to resonance. Blade forces due to self-vibration induced positive aerodynamic damping, even though the amount of damping from the blade vibration was not sufficient for the response to become stable.

The forcing function frequency can be moved away from the natural frequency of the aeroelastic system in two ways: by changing the rotor velocity and by increasing the number of blades in the front blade row (rotor). First, the number of blades in the front rotor was increased, and the response was again calculated. Figure 2 shows that the response for the 3:2 blade ratio was stable. The response was a typical forced response and was no longer divergent because the frequency of the forcing function was now away from the natural frequency of the aeroelastic system. The same type of behavior occurred when the rotor velocity was increased to 0.15 from 0.10. Thus, increasing the rotor velocity and/or increasing the number of blades moved the frequency of the forcing function away from the natural frequency.

The response from the 2:3 and 2:4 configurations showed a divergent trend (not included here), as the frequency of the force was the same as for the 2:2-blade-ratio configuration. The calculations for the SSME HPFTP turbine also showed the expected trends. These calculations validated the MSAP2D program for both compressor and turbine configurations.

Bibliography

Reddy, T.S.R.; and Srivastava, R.: Analysis of a Rotor-Stator Stage Using a Two-Dimensional Euler Aeroelastic Solver. AIAA Paper 94–1638–CP, 1994, pp. 2537–2551.

Lewis contacts: T.S.R. Reddy, (216) 433–6083; Rakesh Srivastava, (216) 433–6045; George Stefko (216) 433–3920

Flutter Analysis of Rotating Blades Used Three-Dimensional Euler Solver

Accurate analysis of unsteady airloads on rotating blades having high sweep and operating in transonic flow requires solution of three-dimensional unsteady Euler equations. Therefore, a three-dimensional structural model has been coupled with a time-accurate, three-dimensional Euler solver to investigate flutter of rotating blades. The aeroelastic equations are formulated

in normal mode and are solved for flutter by using both time domain and frequency domain methods. The analysis solves for instability for all possible interblade phase angles. For verification the analysis was applied to the SR3C–X2 propfan, for which experimental flutter data as well as analyses by other numerical methods are available.

The three-dimensional Euler equations are solved by using an implicit-explicit hybrid scheme. The scheme results in a large saving of central processing unit time as well as of memory requirements because only two matrix inversions are required as opposed to three for fully implicit schemes. The structural analysis is carried out by using the normal mode approach, assuming the hub or nacelle to be rigid. This results in structurally decoupling the blades from one another, requiring the modeling of only one blade in the analysis. At present the analysis is restricted to tuned rotors only. For the aeroelastic analysis a steady-state aerodynamic solution is first obtained. The steady-state solution is then used to start the time domain or frequency domain aeroelastic calculation.

In the time domain analysis the blades are perturbed from the steady state and the combined aeroelastic equations, aerodynamic and structural, are solved in a sequential fashion while marching in time. The response of the blades to initial perturbations is calculated. Increasing amplitude of the response implies instability. Any number of normal modes can be included in the analysis. Further, no knowledge of interblade phase angle or flutter frequency is required. A single run is sufficient to provide the blade aeroelastic characteristics for the particular flight condition. The response of the blades may be Fourier analyzed to provide flutter frequency and interblade phase angle.

In the frequency domain solution pulse vibration and influence coefficient techniques are used to reduce the computational time. This allows for analysis of all frequencies and all interblade phase angles of interest. In this method one blade is oscillated in a prescribed normal mode. The blade motion is defined by a pulse in the given normal mode. The pulse includes significant spectral content for the frequencies of interest. The unsteady aerodynamic force on all blades, arising from the motion of one blade, is recorded and Fourier analyzed to provide the unsteady aerodynamic coefficients for solving the aeroelastic equation in the frequency domain. Roots of the equation provide damping and frequency. A negative damping implies instability. This process needs to be repeated for all normal modes of interest.

The analysis was applied to a four- and eight-bladed SR3C–X2 propfan, which showed flutter in wind tunnel tests at free-stream Mach numbers of 0.62 for four blades and 0.60 for eight blades when operating at an advance ratio of 3.55 and a setting angle of 61.2°. Both cases were analyzed at Mach 0.5 and 0.7 using the first three normal modes. The blade was stable at Mach 0.5 and unstable at Mach 0.7, as expected. Time and frequency domain results correlated well with each other. Similar responses were observed for other modes as well. For the stable case (Mach 0.5) an initial perturbation rapidly increased, followed by increasing response of other blades, indicating an instability. Frequency domain results obtained from the present analysis were compared with numerical solutions obtained by using the panel and full potential methods. The three results compared well, as expected, as the flow Mach number fell in the linear range. It was also observed, from the analysis, that for exactly the same flight conditions, the eight-bladed propfan was more unstable than the four-bladed one. This implies that the cascading of the blades makes the rotor less stable (i.e., the closer the blades are spaced, the less stable the rotor is going to be). Both time and frequency domain analyses showed similar behavior.

Bibliography

Srivastava, R.; Reddy, T.S.R.; and Mehmed, O.: Flutter Analysis of Propfans Using a Three-Dimensional Euler Solver. AIAA Paper 94–1549–CP, 1994, pp. 1803–1813.

Lewis contacts: Rakesh Srivastava, (216) 433–6045; T.S.R. Reddy, (216) 433–6083; Oral Mehmed, (216) 433–6036

Blade Thickness Effects on Forced Response of Turbomachinery Blading Investigated

Turbomachinery blades operate in an inherently unsteady environment and are subjected to numerous excitations. Blade vibration due to these unsteady excitations is an important cause of fatigue in many aircraft engines and can lead to blade failure if the endurance limit is exceeded. These excitations cannot be removed by redesign because they arise from the very nature of turbomachinery operation. A frequent technique used to overcome vibratory problems is to thicken the blade, sacrificing some performance. The expectation is that a thicker blade will respond with lower amplitudes at resonance. In reality, however, the effect of blade thickness on forced response is not so simple. Larger blade thickness influences the vibration amplitude by two distinct mechanisms. First, it generally makes the blade structurally stiffer. Second, it modifies the aerodynamic flow in the blade passages. The aerodynamic effect on the vibration response is less obvious than the stiffening effect. The aerodynamic effect can itself be attributed to two mechanisms: variations in aerodynamic damping and in excitation force amplitude. The dependence of damping and excitation on blade thickness is complicated by the fact that both steady and unsteady flow are influenced by changes in thickness. Falling aerodynamic damping levels and rising excitation amplitudes with thickness lead to the counterintuitive result of the thicker blade having higher levels of stresses.

By using steady and unsteady aerodynamic analysis methods based on the full potential equation and structural analysis methods based on the finite element method, we investigated the effect of blade thickness on the aeroelastic forced response of turbomachinery rotors. The effect of blade thickness was considered on both structural and aerodynamic response. For the steady aerodynamic analysis we used the nonconservative form of the nonlinear potential flow equations together with an implicit, least-squares, finite difference approximation to solve for the steady flow field around a given isolated, infinite cascade of identical airfoils. The unsteady aerodynamic analysis used calculates the unsteady aerodynamic response of a cascade of airfoils to prescribed entropic, vortical, and acoustic gust excitations and blade motions. The unsteady flow is regarded as a small perturbation of a nonuniform mean flow. This linearization technique leads to very efficient predictions of unsteady aerodynamic loading. The aeroelastic analysis used calculates the dynamic stresses in the turbomachinery blades in response to the unsteady aerodynamic loading on the blade. The motion-dependent and motion-independent aerodynamic forces, respectively, provide the aerodynamic damping and excitation on which the dynamic stresses depend.

Test cases based on an artificial rotor were generated (fig. 1). The test rotors were all identical except for the thickness ratio of the blade cross sections. The cross sections were generated from the definitions of modified NACA four-digit-series airfoils, except that the thickness-to-chord ratio was varied for each rotor. Results indicated that, for these test rotors, a reduction in aerodynamic damping is possible for some engine-order excitations as blade thickness is increased. Also, a significant part of this reduction in aerodynamic damping is due to profile effects. This result shows that the counterintuitive behavior of a thicker blade having larger resonant stresses can occur in practice. In this investigation the beneficial effects of increasing stiffness and decreasing excitation outweighed the adverse effects of reduced damping. Nevertheless, turbomachinery blade designers must bear in

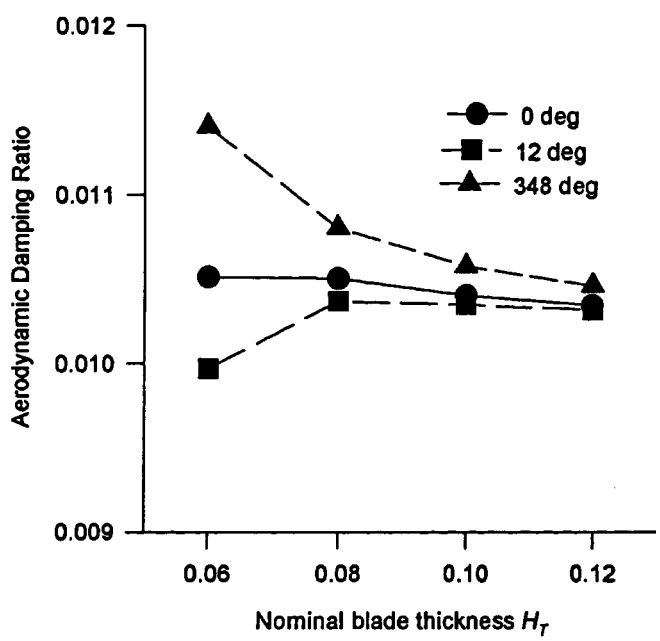

Figure 1.—Aerodynamic damping ratio as function of nominal blade thickness for three angles.

mind that redesigning turbomachinery blades by making them thicker will not necessarily solve forced response problems, unless unsteady aerodynamic effects are taken into account.

Lewis contacts: Durbha V. Murthy, (216) 433–6714; George Stefko, (216) 433–3920

Passive Vibration of Rotating Composite Plates Reduced by Using Built-in Damping Material

An analytical and experimental research program is in progress to investigate the use of built-in viscoelastic damping material to passively reduce vibrations of rotating composite fan blades. This work is being done cooperatively on a grant by NASA Lewis and the University of California, San Diego. Analyses, design, fabrication, and bench testing of the plates have been successfully completed at the university. Spin tests will be performed in the Lewis dynamic spin facility during the summer of 1995. The tests are to measure damping and natural frequencies, evaluate different designs, and verify the proof of concept for the spinning blades.

The proof-of-concept composite plates are simple blade structures. Figure 1 shows the components of a typical plate. A viscoelastic damping patch is surrounded by a border material and sandwiched between graphite/epoxy layers. A loose-weave E-glass scrim cloth is embedded in the damping material to keep the damping material from creeping outward under the large rotational forces.

The natural frequencies and damping levels of nonspinning plates were measured and it was found (1) that the bending and torsion natural frequencies were not significantly changed by border material and patch size, (2) that the patches can be designed to significantly increase damping in specific modes, (3) that a border composed of 90° graphite/epoxy material produced much higher modal damping than a border of 0° graphite/epoxy material, and (4) that the measured damping values were approximately 10 times greater than that of an undamped composite plate.

Lewis contact: Oral Mehmed, (216) 433–6036

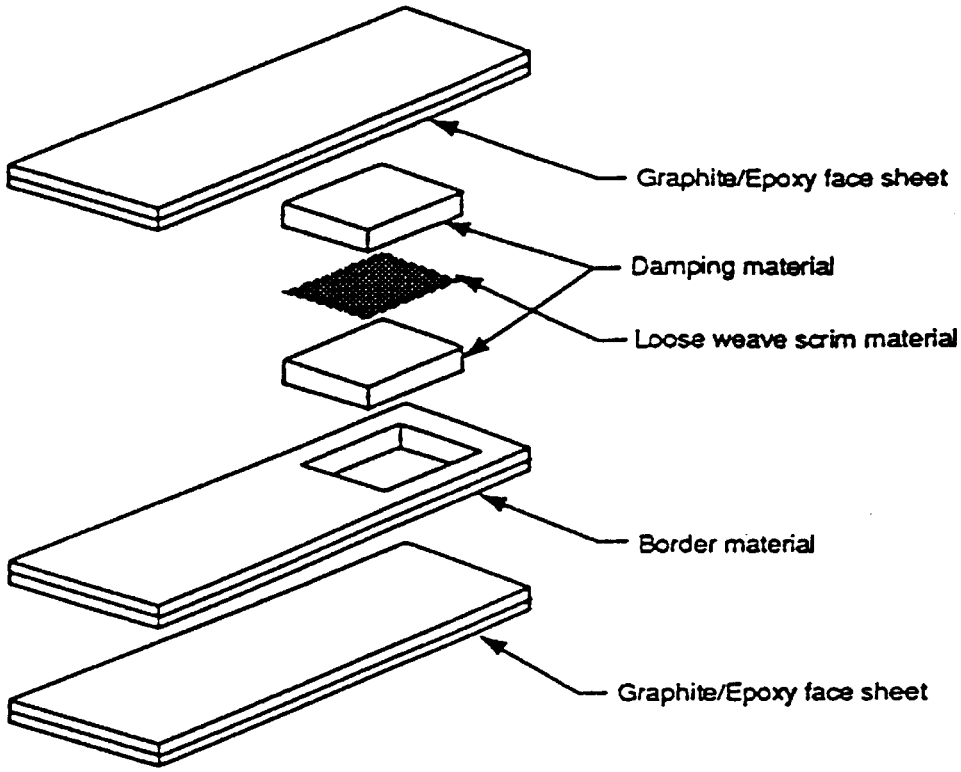

Figure 1.—Components of typical plate.

High-Temperature Magnetic Bearings Investigated for Gas Turbine Engines

A new NASA Lewis and Army thrust having significant industry participation and being coordinated with other Government agencies is in magnetic bearings. The NASA/Army emphasis is on high-temperature applications for future gas turbine engines. Using magnetic bearings could increase the reliability and reduce the weight of these engines by eliminating the lubrication system. It could also increase the DN (bearing speed times diameter) limit on engine speed and allow active vibration cancellation systems to be used. The result could be a more efficient, "more electric" engine. The Integrated High-Performance Turbine Engine Technology (IHPTET) Program, a joint Department of Defense/industry program, has identified a need for a high-temperature (as high as 650 °C (1200 °F)) magnetic bearing that could be demonstrated in a phase III engine.

A magnetic bearing is similar to a electric motor. The magnetic bearing has a laminated rotor and stator made of cobalt steel. A series of electrical copper wire coils wound around the stator form a series of electric magnets around the circumference. These magnets exert a force on the rotor. A probe senses the rotor position, and a feedback controller keeps it in the center of the cavity. The engine rotor, bearings, and case form a flexible structure that contains a large number of modes. The bearing feedback controller could cause some of these modes to become unstable. The controller could be adapted to varying flight conditions to minimize seal clearances and to monitor the health of the system. Cobalt steel has a Curie point greater than 925 °C (1700 °F), and copper wire has a melting point beyond that. Practical limitations associated with the maximum magnetic field strength in the cobalt steel and the stress in the rotating components limit the temperature to about 650 °C (1200 °F).

The objective of this effort is to determine the limits in temperature and speed of a magnetic bearing operating in an engine environment. Our approach is to use our in-house experience in magnets, mechanical components, high-temperature materials, and surface lubrication to build and test a magnetic bearing. Rig and engine tests will be done in-house or through cooperative programs in industrial facilities.

During the last year we have made significant accomplishments. We have a cooperative program with Allison Engine to work on a high-temperature magnetic thrust bearing. During this program we uncovered a problem with the conventional design of the magnetic thrust bearing. Because the thrust bearing is not laminated, eddy currents severely reduce the bandwidth. Also, we have worked at Allison to bring their high-temperature magnetic bearing rig to full speed. We have predicted both in-house and Allison magnetic bearing rig stability limits. We have performed tests on a high-temperature displacement probe. Our flexible casing rig is being converted to a high-temperature magnetic bearing rig. Testing should start next year.

Our plan is to develop a high-temperature, compact wire insulation and to fiber reinforce the core lamination to operate at higher temperature and DN values. We plan to modify our stability analysis and controller theory by including a nonlinear magnetic bearing model. We are developing a controller that has an expert system to adaptively change the controller with changing flight conditions and to diagnose the health of the system. Then, we will demonstrate the bearing on our rotor dynamics rig and finally in an engine test.

Lewis contact: Albert F. Kascak, (216) 433–6024

Performance of Power-Saving Magnetic Bearing Controls Analyzed

Most magnetic bearing control schemes use a bias current with a superimposed control current to linearize the relationship between the control current and the force it delivers. For most operating conditions the existence of the bias current requires more power than alternative methods that do not use conventional bias. With bias current, even in no-load conditions, there is always some power consumption.

Three alternative methods were examined that reduce electrical power loss: the zero bias method, the pseudozero bias method, and the adaptive variable bias method. These methods are not new methods for rotordynamic control but rather are modifications to the magnetic bearing operating mode, resulting in a more efficient control actuator. The methods were analyzed for their potential to save power as well as to produce a commanded force, in comparison with the conventional bias mode. Analytical, simulated, and experimental results were obtained. The analytical and simulated results are in good agreement with one another and are sufficiently validated by the experiments. All methods were compared and ranked according to their power loss and actuator performance tradeoff results.

The zero bias method used the least amount of power for operation, followed by the pseudozero bias method, the adaptive variable bias method, and lastly the conventional bias method. All proposed methods used less power for a commanded force than the conventional bias method (see fig. 1). As force command levels approached the maximum force level, the adaptive variable bias method used as much power as the conventional bias method, but the zero bias and pseudozero bias methods were more than 30% better. Only the adaptive variable bias method was comparable to the conventional bias method at producing a commanded force. The zero bias method accurately produced the desired force only for low commanded force levels with the pseudozero bias method being effective in the low-to-middle command force range. The adaptive variable bias method was the best of the proposed methods based on a performance calculation that involved power, force, and phase components, proving it to be the method of choice.

The analytical work used the one-dimensional net force equation for a single magnetic bearing axis. The computer simulation was performed using Matlab/Simulink simulation software on a microcomputer. The experiment involved a magnetic bearing apparatus and supporting electronics. The magnetic bearing apparatus included a flexible shaft, two magnetic bearings, various disks used for rotational inertias, and a motor. Only one magnetic bearing was used for control purposes. The shaft was nonrotating.

Lewis contact: D. Johnson, (216) 433–3306

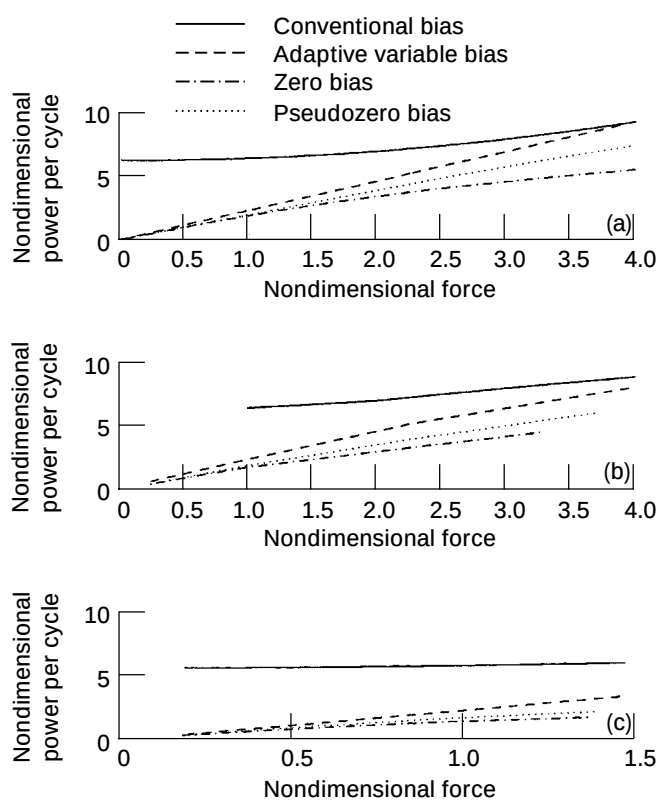

Figure 1.—Analytical, simulated, and experimental nondimensional power per cycle versus nondimensional force for conventional bias, adaptive variable bias, zero bias, and pseudozero bias operating methods. (a) Analytical. (b) Simulated. (c) Experimental.

Lubrication of Space Systems Studied

The space age brought with it many lubrication challenges that had not been experienced in the past, such as exposure to extremely low ambient pressures, radiation, atomic oxygen, and meteoroids, the absence of a gravitational field, imposed weight limitations, contamination by vapors, and the use of mechanical components that were not maintainable. The challenges for future spacecraft appear to be even greater because missions are being planned that will require mechanisms to last much longer. For example, the original design life for the space station was 30 years. Although we would like a space station to last 30 years, a 30-year, maintenance-free life may not be attainable because most mechanisms do not last that long on Earth without regular maintenance. The only mechanism with a long maintenance-free life that comes to mind is a refrigerator compressor. Other ventures such as long-lived Earth-orbiting spacecraft, lunar surface missions, and planetary surface missions are being planned that will require systems not only to have long, maintenance-free lives but be capable of operating under extreme conditions. On the Moon mechanical equipment will have to operate from 181 to 111 °C (355 to 235 °F), in a vacuum of 1012 torr, and under extremely dusty conditions. On Mars mechanisms must operate over wide temperature variations, in a low-oxygen atmosphere, in gusty winds, and in a dusty, corrosive environment.

In 1986 Kannel and Dufrane of Battelle Laboratory studied past and projected tribological problems in space. Figure 1 is a qualitative chart that illustrates the results of that study. Despite significant advances in tribology the demands on tribology for future space missions were projected to grow faster than the solutions. A Lewis study was conducted to determine if the state of the practice had improved since 1986 and to

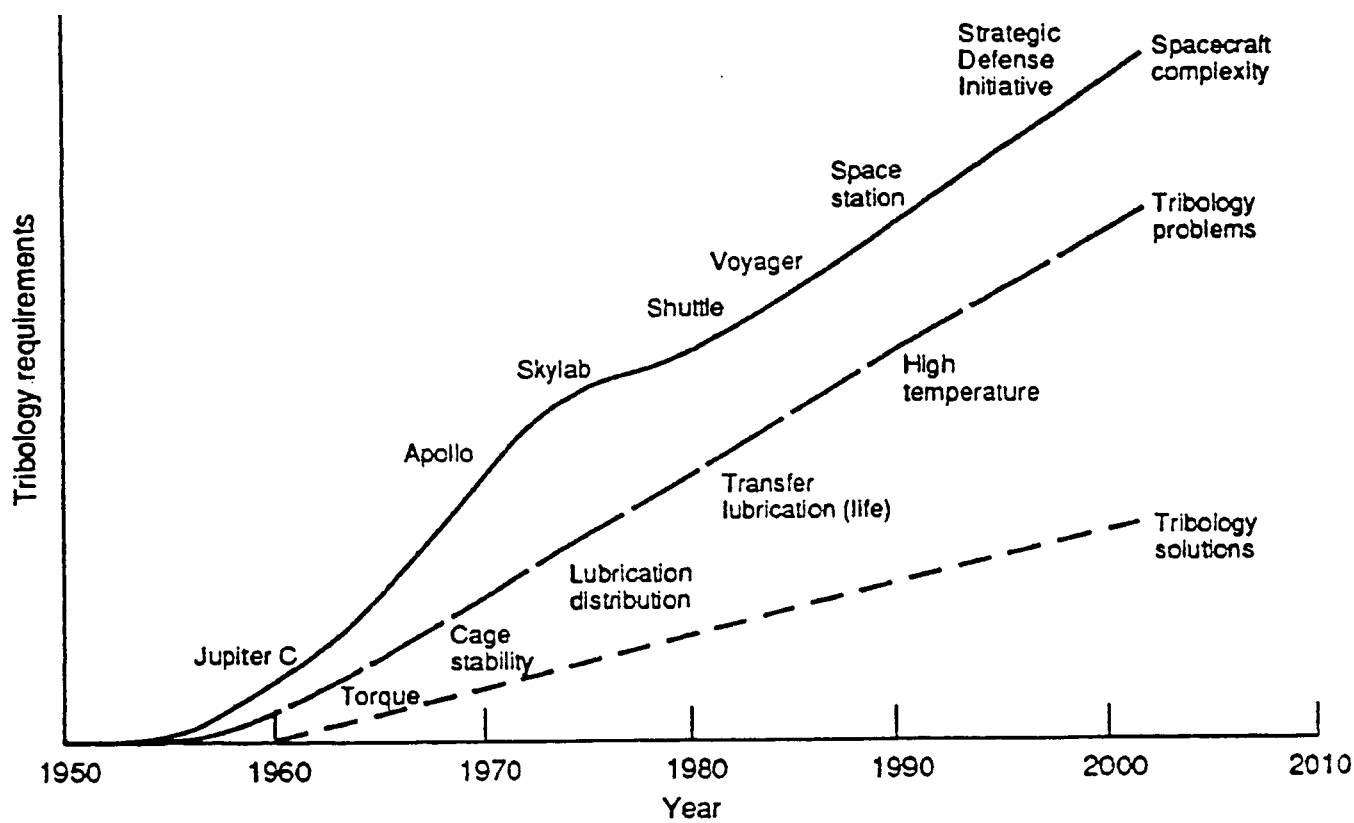

Figure 1.—Growth of tribology requirements with advances in space.

document the results. In general, it was concluded that the technology has not significantly advanced. A paper was written to document the current state of the art and the lubrication techniques used today and in the past (ref. 1). Some advantages and disadvantages of the various tribological techniques are discussed. In addition, tribology challenges for future NASA space missions are examined.

Reference

1. Fusaro, R.L.: Lubrication of Space Systems. NASA TM–106392, 1994.

Lewis contact: Robert L. Fusaro, (216) 433–6080

Wheel Abrasion Experiment Designed and Tested

The Microrover Flight Experiment will be delivered by the Mars Environmental Survey Pathfinder to the surface of Mars in July 1997. The rover will have experimental apparatus onboard to analyze soil chemistry and abrasiveness and the size and quantity of airborne dust. The wheel abrasion experiment (WAE), replacing one of the six wheels on the rover, will characterize the abrasiveness of Martian soil on metal coatings (platinum and aluminum). A photocell will measure the intensity of the reflected light from the metal coatings; as the metal coating wears revealing the black substrate, the reflected light decreases.

A ground test cell has been designed and built to test the WAE, housed within a 61-cm-diameter by 61-cm-long (24 by 24 in.) vacuum tank. A mechanical pump and a diffusion pump are used before backfilling the tank with Martian atmospheric simulant to 700 Pa (7 mbar). A variable-speed motor, external to the vacuum, drives the wheel through a rotary feedthrough in the chamber wall. The wheel rotates in place, turning an annular horizontal turntable filled with Martian soil simulant to 15-mm (0.6-in.) depth (fig. 1). The load on the wheel was counterbalanced to 500 g (1.1 lb). Not shown in figure 1 are a xenon arc lamp, providing the collimated light source through a quartz window, and an electrostatic probe to measure wheel charging.

Two wheels are available for testing, the test wheel (as shown in fig. 1) and the flight wheel (fig. 2). Thirty-two metal coupons are attached to the test wheel by screws in a unique pattern for coupon identification. The flight wheel is the flight design for the rover. The metal coupons on the flight wheel are to be glued between the rows of spiked cleats.

The flight wheel was rotated at rover wheel speeds (0.6 to 1.2 rpm) to assess the effects of electrostatic charging. The dust attracted to the wheel reduced the reflected intensity of the metal coupons by about 60%. To reduce the electrostatic charging, two types of discharge point were attached to the wheel, a point 0.0025 cm (0.001 in.) in diameter and a point 0.0002 cm (0.00008 in.) in diameter. The steady-state electrostatic voltage of the wheel was reduced by about 18 V with either point (fig. 3). The electrostatic charging of the simulant was measured by reorienting the probe. The magnitude of the voltage was about the same as for the wheel but the sense was opposite. The capacitance of the wheel was measured in the Martian atmosphere, and electrostatic voltage was used to find the charge on the wheel. Field strength at the discharge point was estimated from the charge. Ongoing tests will calibrate the rate of coupon coating wear when in contact with several different Martian soil simulants.

Lewis contacts: Mark Siebert, (216) 433–6012; Douglas A. Rohn, (216) 433–3325

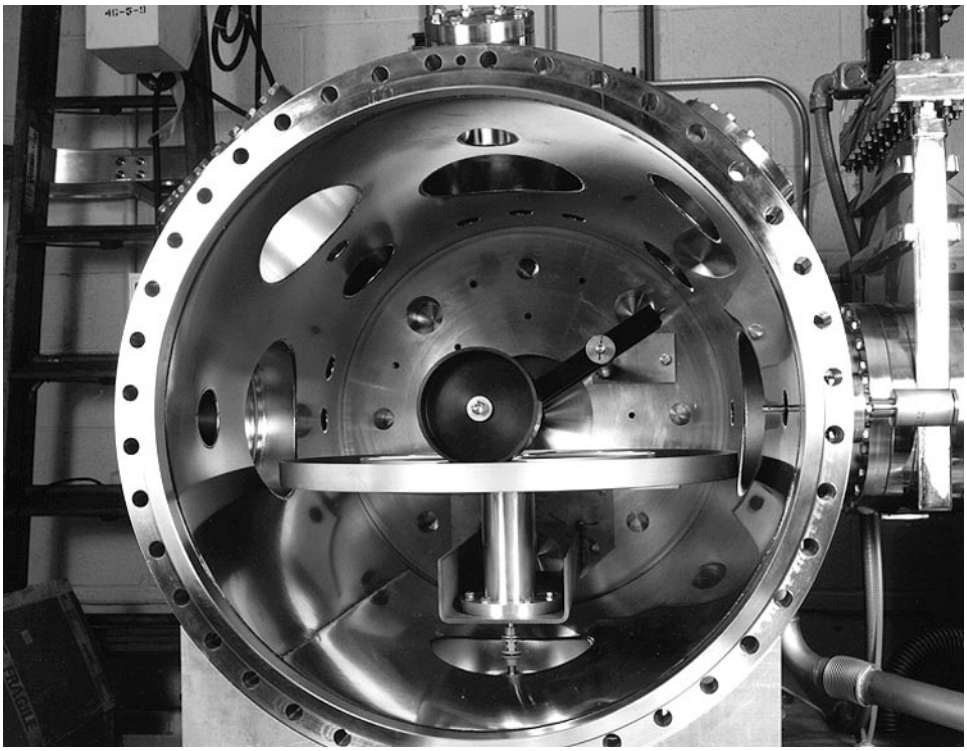

Figure 1.—WAE test fixture showing test wheel and turntable in vacuum tank.

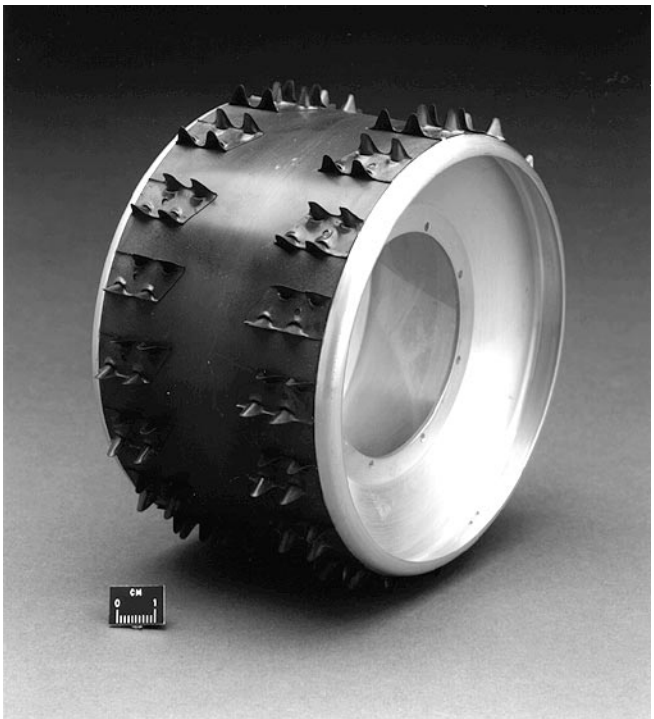

Figure 2.—Flight wheel without metal coupons attached.

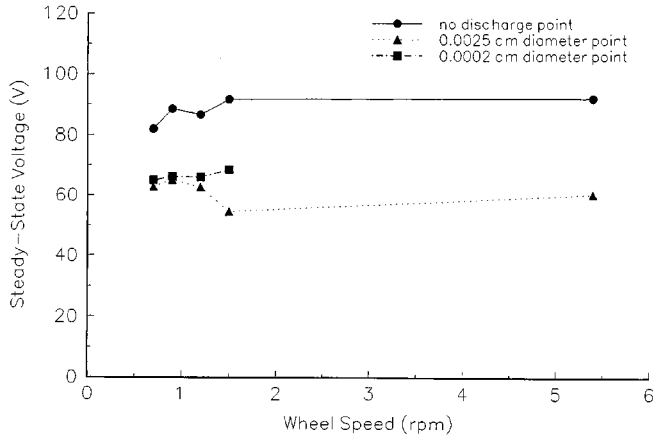

Figure 3.—Steady-state electrostatic voltage of flight wheel as function of type of discharge point. Wheel load, 500 g (1.1 lb); Martian simulant atmosphere, 700 Pa (7 mbar).

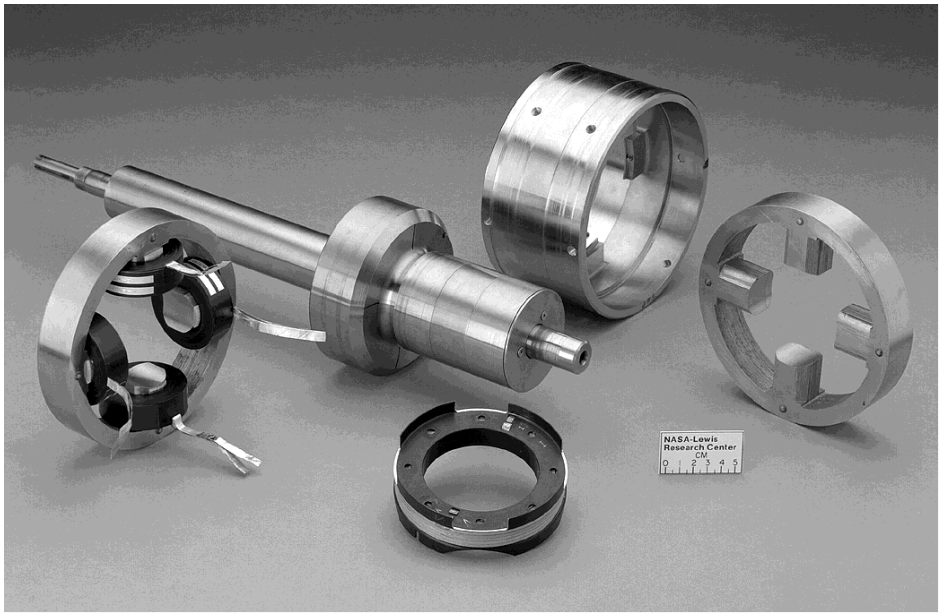

Figure 1.—Two stators, bias coil, external flux tube, and shaft with two sets of rotor laminations for cryogenic, high-load, homopolar magnetic bearing.

High-Load and Active High-Temperature Superconducting Magnetic Bearings Tested

High-load bearing.—A high-load, homopolar radial bearing (fig. 1) was tested in liquid nitrogen. In initial tests it produced 3600-N (800-lb) load in its linear range, far exceeding the 1600 N (350 lb) for previous bearings of the same external size (13.3-cm-outside-diameter, 11.4-cm-long, and 7.6-cm-inside-diameter journal; 5.25 by 4.5 by 3 in.). A maximum load in nonlinear operation of 5100 N (1150 lb) was reached for single-axis force, and with two axes active the bearing produced a resultant force of 6400 N (1440 lb). The increased load was due to tapered monolithic stator poles with improved coverage of the journal and a lower reluctance axial flux path.

Active superconducting bearing.—A high-temperature-superconducting (HTS), active magnetic bearing was designed and fabricated, using coils manufactured by two HTS vendors. This proof-of-feasibility demonstration showed that HTS coils can be used in a high-load, active magnetic bearing in liquid nitrogen. We found that HTS coils can operate stably with ferromagnetic cores in a feedback-controlled system at a current density similar to that in copper at liquid nitrogen temperature. The homopolar radial bearing (fig. 2) produced over 890-N (200-lb) radial load (measured nonrotating) and supported a shaft to 14 000 rpm. Design compromises permitted use of circular coils with rectangular cross section. Conductor improvements will eventually permit coil shape optimization, higher current density, and higher bearing load capacity. The bias coil, wound with nontwisted, multifilament HTS conductor, required negligible power to carry its direct current. The control coils, wound with

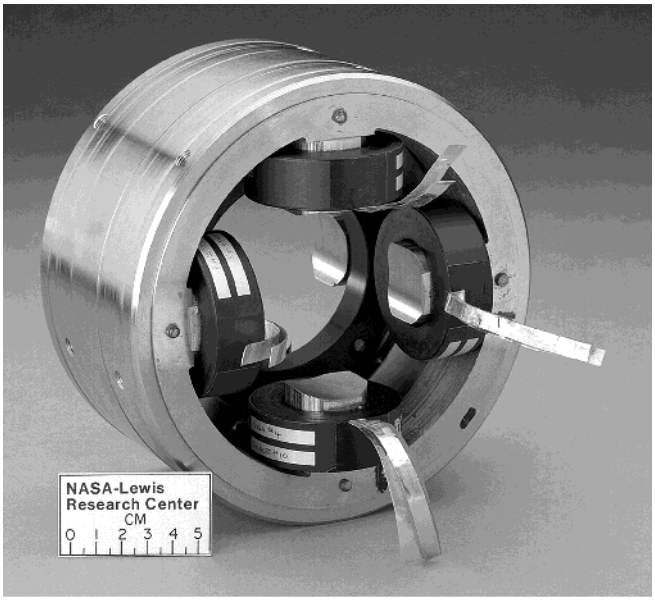

Figure 2.—Stator of homopolar magnetic bearing with high-temperature-superconducting bias and control coils.

monofilament HTS sheathed in silver, dissipated negligible power for direct current (i.e., for steady radial load components), even with superimposed alternating current (AC). The AC component, however, dissipated power, which increased rapidly with frequency and quadratically with AC amplitude. The results show that twisted multifilament conductor is not needed for stable levitation. However, twisted multifilaments will be required to reduce control power for sizable dynamic loads, such as those due to unbalance.

Lewis contact: Gerald V. Brown, (216) 433–6047

Electromagnet-Biased Homopolar Magnetic Bearing Tested

An electromagnet-biased, radial homopolar magnetic bearing was tested on the bench and in a rotating rig at room and liquid nitrogen temperatures. The bearing had most parts in common with a permanent-magnet-biased bearing previously tested and reported, but the midplane permanent magnet was replaced with an electromagnet and an external axial flux tube, all within the original bearing envelope.

Bench tests showed that, because of heat transfer limits, the electromagnet cannot match the bias field produced by the permanent magnet at room temperature. However, when submerged in liquid nitrogen the electromagnet-biased coil can produce a higher bias field than the permanent magnet.

Hall probe measurements showed substantial hysteresis of the field in the gap due to the iron-cobalt stator and rotor laminations, raising questions of phase lag and closed-loop controllability for this and other iron-cobalt core bearings that control current rather than field or flux. Transfer functions between control current and gap field and between control current and gap flux showed considerable phase lag at 100 to 1000 Hz, due mainly to eddy currents, and low-frequency phase lag due to the hysteresis.

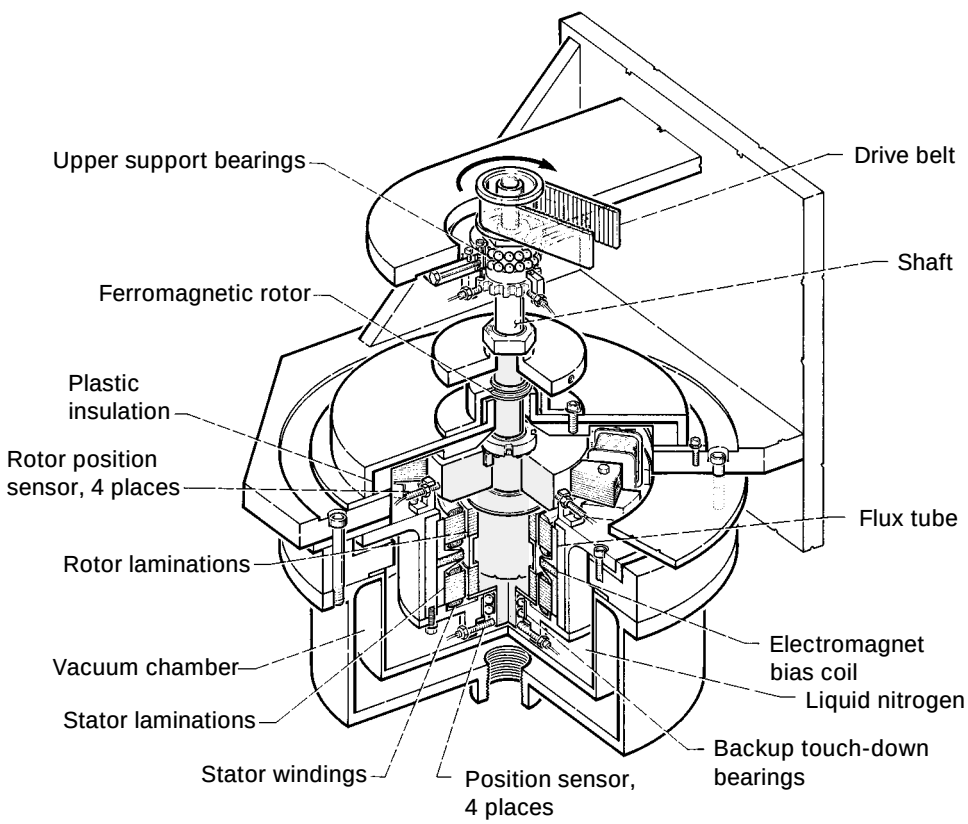

Figure 1.—Cryogenic magnetic bearing test rig with electromagnet bias coil.

Bias stiffness, actuator gain, and closed-loop stiffness and stability were all comparable to those of the permanent-magnet-biased bearing. Rotating tests to 14 000 rpm showed comparable behavior as well. Maximum steady radial load levels with one bearing axis active were nearly the same as for the permanent-magnet-biased bearing (approximately 2200 N (500 lb).

As with the permanent-magnet-biased bearing there were axis interaction effects. For a given control current and force on one axis, an increase in control current and force on the second axis reduced the force on the first axis. A maximum load of 3000 N (680 lb) was measured in the diagonal direction between axes with both axes energized.

At liquid nitrogen temperature greater nonlinearity of the eddy-current position probes reduced data quality somewhat relative to room-temperature results but did not affect performance noticeably.

Bibliography

Brown, G.V.: Tests of an Electromagnet-Biased Homopolar Magnetic Bearing. Advanced Earth-to-Orbit Propulsion Technology—1994, R.J. Richmond and S.T. Wu, eds., NASA CP–3282, Vol. II, 1994, pp. 385–394.

Lewis contact: Gerald V. Brown, (216) 433–6047

New Method Developed for Aeroelastic Stability Analysis

The development of advanced-design, ultra-high-bypass-ratio engines has led to renewed interest in the study of bladed-disk flutter. Previously, two fundamental approaches have been used in flutter calculations: frequency domain analysis and time domain analysis. With the development of time-marching computational fluid dynamics flow solvers, both approaches have been used with equal ease. We have achieved substantial computational savings by applying a numerical eigensolver to a nonlinear, time-marching, fluid-structure interaction system solver for flutter prediction.

The numerical eigensolver works with the steady-flow solution to determine the eigenvalues and eigenmodes corresponding to a fluid-structure interaction system directly. It does not require a time history of forces on blades and subsequent Fourier transformation to determine stability. Also, it avoids computationally expensive time domain simulations of small-perturbation responses, where several oscillation cycles are required to determine the growth or decay of perturbations. The computational savings due to this new method over the existing frequency and time domain nonlinear methods are on the order of 100 to 10 000. However, note that this is fundamentally a small-perturbation (linear) aeroelastic analysis, although steady-flow nonlinearities are taken into account (i.e., blade thickness, blade camber, shock waves, etc.).

We applied a numerical eigensystem solver, based on a Lanczos procedure, to a two-dimensional, full-potential cascade aeroelastic solver. Calculations were performed for a cascade geometry used in previous research, where frequency and time domain flutter calculations were performed. The steady solution was first obtained, as required in all such calculations. Then, the numerical eigensystem solver was used to calculate eigenvalues.

The eigenvalues obtained from this new approach indicate whether the aeroelastic system is stable or unstable. Comparing the results from this approach with those from existing flutter determination methods shows that the new approach predicts the correct flutter condition. It shows good agreement in flutter speed and flutter mode.

SAMPLE FLUTTER RESULTS FROM FULL-POTENTIAL AEROELASTIC CODE

[All values are nondimensional.]

Flutter parameter	Frequency domain	Time domain	New method
Frequency	0.265	0.262	0.239
Velocity	1.768	1.761	1.630

The numerical eigensystem analysis results in substantial computer time savings relative to the frequency and time domain solutions. It will allow the use of nonlinear, time-marching solvers in routine aeroelastic design analysis. Because of the modular nature of the numerical eigensystem solver, it can be readily adapted to other time-marching aeroelastic solvers with minimal additional effort required on the researcher's part.

Bibliography

Mahajan, A.J.; Bakhle, M.A.; and Dowell, E.H.: A New Method for Aeroelastic Stability Analysis of Cascades Using Nonlinear, Time-Marching CFD Solvers. AIAA Paper 94–4396, 1994.

Lewis contacts: Milind A. Bakhle, (216) 433–6037; George Stefko, (216) 433–3920

Users Guide Published for FPCAS2D, a Two-Dimensional Full-Potential Aeroelastic Solver

The FPCAS2D computer code has been developed for aeroelastic stability analysis of bladed disks, such as those in fans, compressors, turbines, propellers, or propfans. A users guide has been written to help the user prepare the input data file required by the FPCAS2D code.

In the users guide the input data are completely described. In addition, inputs and outputs are given for four examples from published papers. Detailed explanations of the aerodynamic analysis, the numerical algorithms, and the aeroelastic analysis are not given. Instead, the reader is directed to specific references that deal with each of these items.

The aerodynamic analysis used in this code is based on the unsteady, two-dimensional, full-potential equation. This equation is solved for a cascade of blades. A finite volume approach is adopted and a Newton iteration method is used to solve the nonlinear problem as a series of linear problems at each time step. The structural analysis is based on a two-degree-of-freedom, rigid, typical section model for each blade. Either a frequency domain or a time domain flutter analysis is possible with this code. The development of the time domain flutter analysis for cascades and the pulse response and influence coefficient method for cascades is described in the papers referenced in the users guide.

Bibliography

Bakhle, M.A.: FPCAS2D Users Guide, Version 1.0. NASA CR–195413, 1994.

Lewis contacts: Milind A. Bakhle, (216) 433–6037; George Stefko, (216) 433–3920

Structural Integrity

Acoustro-Ultrasonics and Fiber Features Studied in Metal-Matrix Composites

Advances in the processing and fabrication of metal-matrix composites require appropriate mechanical and nondestructive testing methods. These methods are needed to characterize properties, assess integrity, and predict life of engine components, such as compressor rotors, vanes, and blades. In order to interrogate local rather than global features in metal-matrix composites, the collected ultrasonic waveforms are limited to those that only pass through the region between the sending and receiving transducers. For example, for titanium alloys reinforced with silicon carbide (SCS–6) fibers the 10- to 20-µsec range of the acousto-ultrasonic signals need be studied.

Signals were collected with pairs of 5.0-MHz transducers. The higher frequency portion of the spectrum was sensitive to fiber features, as illustrated in figure 1 for a unidirectional SCS–6/titanium–15 wt% vanadium–3 wt% chromium–3 wt% aluminum–3 wt% tin (Ti-15-3) panel. Scatter, due to variations in coupling conditions, was minimized by calculating the fraction of the area of the magnitude spectrum that is contained between 2 and 3 MHz. This fraction is plotted against orientation with respect to fiber direction. This portion of the spectrum was strongly dependent on the SCS–6 fibers for propagation.

This same type of data was collected on SCS–6/Ti-6Al-4 rings, which are of significance in aerospace design. The 2- to 3-MHz fractions of the 10- to 20-µsec signals are displayed in figure 2 for circumferentially collected data on the fiber-reinforced region ([0] to the fiber direction) and also on the fiber-free Ti-6-4 inner margin. Data on the fiber-reinforced region were strongly dependent on ring position. The value at 220°, which is in the midst of the visible cracked region, is almost as low as the value on the Ti-6-4 margin. This result implies that loss of integrity at the crack is paralleled by loss of ability to propagate higher frequency ultrasound. This phenomenon is being studied as a possible monitor of fiber/matrix integrity for metal-matrix composite systems.

Lewis contact: Harold E. Kautz, (216) 433–6015

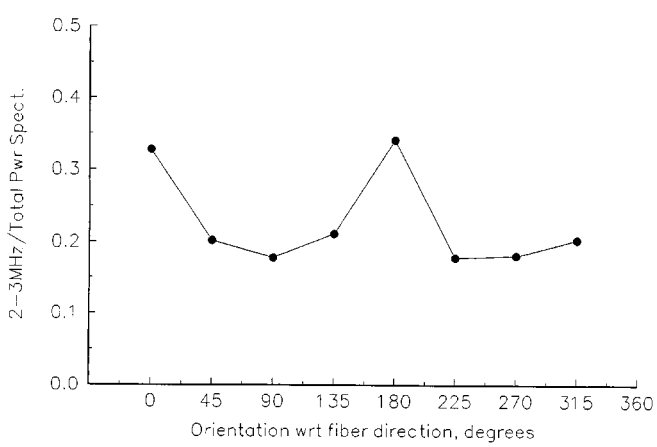

Figure 1.—Spectrum as function of fiber direction for SCS–6/Ti-15-3.

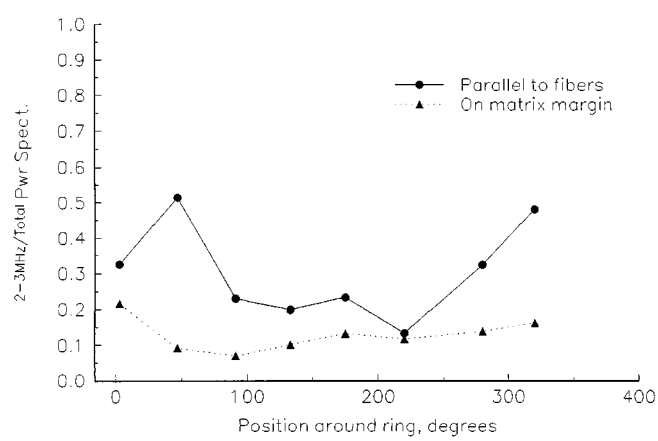

Figure 2.—Spectrum as function of fiber direction for SCS–6/Ti-6-4.

Nonuniformly Thick Polymer-Matrix Composites Analyzed Ultrasonically

Nonuniformity in polymer-matrix composite parts must be accurately characterized with regard to microstructural nature and severity and its resulting effect on physical properties. Only then (1) can a decision be made on whether such a part is unacceptable for further processing, testing, or application; (2) can the processing steps responsible for the nonuniformity be pinpointed and modified; and (3) can nondestructive evaluation (NDE) procedures be implemented, allowing quality decisions to be based primarily on nondestructive characterization.

In recent studies PMC materials were periodically identified. Although they appeared optically uniform, they contained a higher-than-normal level of global nonuniformity as indicated from preliminary ultrasonic C-scanning. One such panel was thoroughly examined by both NDE and destructive methods to quantitatively characterize the nonuniformity. The NDE analysis of the panel was complicated by the panel's nonuniform thickness, a common condition resulting from PMC manufacture. Because conventional ultrasonic C-scan results are affected by both thickness and microstructural variation, a novel NDE approach was required to determine whether a microstructural gradient existed in addition to the thickness variation.

This approach (fig. 1) required mapping of ultrasonic velocity across the panel in conjunction with an error analysis of the velocity mapping procedure. It revealed (1) that a microstructural (density) gradient, in addition to the thickness

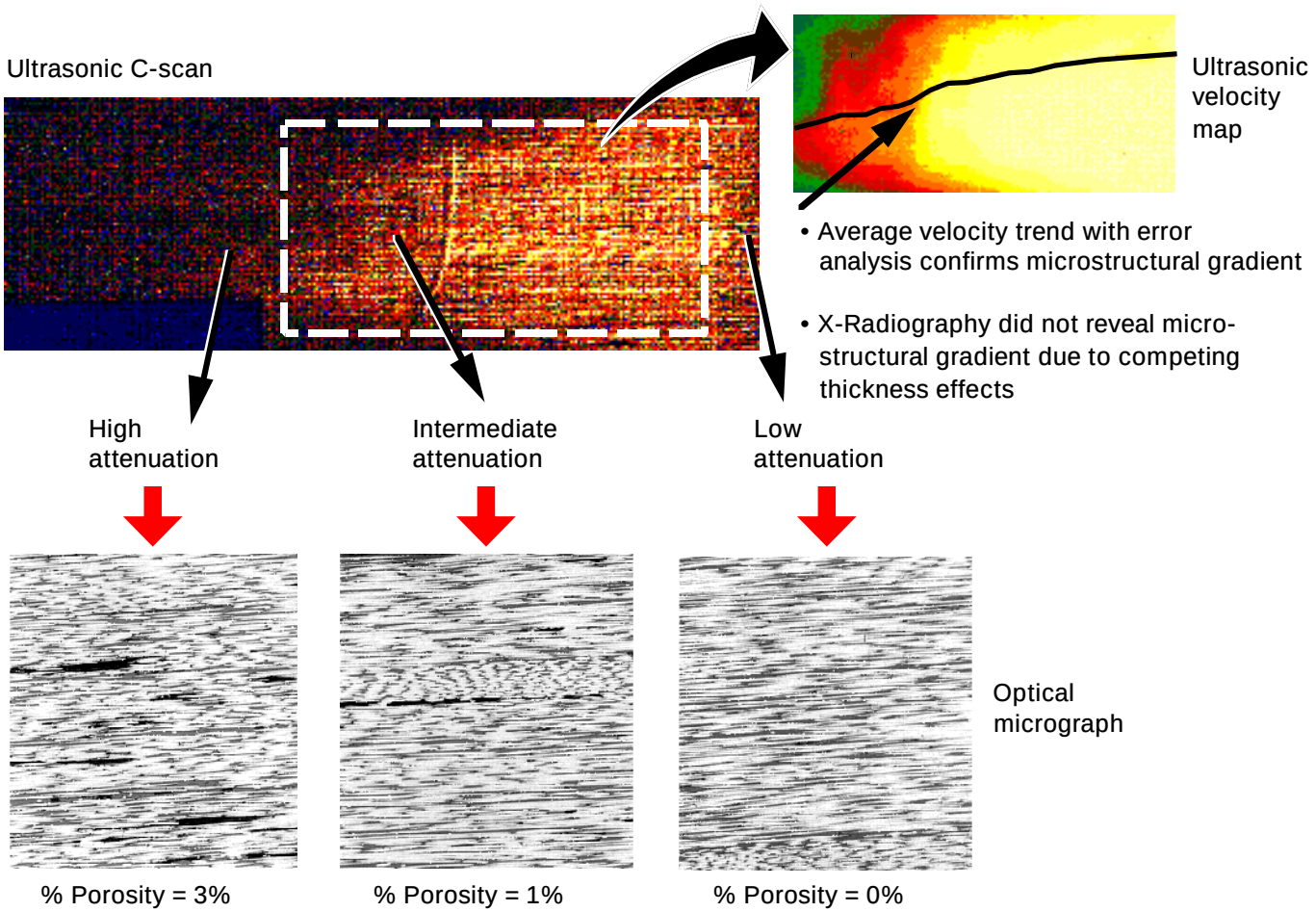

Figure 1.—Inhomogeneity of nonuniformly thick PMC's as characterized by ultrasonic analysis at NASA Lewis.

variation, did indeed exist in the panel and (2) that the percentages of velocity variation revealed in the velocity map that are assignable to thickness and microstructural variation can be estimated. Ideally, an ultrasonic imaging method that eliminates thickness variation effects would be desired. NASA Lewis and Sonix, Inc., of Springfield, Virginia, are involved in the development and commercialization of such a method.

Lewis contact: Don J. Roth, (216) 433–6017

Ceramics Durability Evaluation Software Predicts Useful Life of Components in Creep and Fatigue

Significant improvements in aerospace and terrestrial propulsion and power generation for the next century will require revolutionary advances in high-temperature materials and structural design. Advanced ceramics are relatively abundant materials that offer lighter weight and greater capacity to sustain loads at higher use temperatures than metals. However, ceramics are inherently brittle and have very low strain tolerance, low fracture toughness, and large variation in fracture strength caused by the variable size and random distribution of flaws. Ceramics also exhibit time-dependent degradation of load-carrying capability due to stress corrosion cracking, effects of elevated temperatures, cyclic fatigue, and creep. Successful application of advanced ceramics depends on proper characterization of material behavior and the use of an appropriate design methodology. This has been accomplished with the Ceramics Analysis and Reliability Evaluation of Structures fatigue life (CARES/LIFE) and forthcoming creep life (CARES/CREEP) integrated design computer programs.

Designing ceramic components requires specialized knowledge of statistics and fracture mechanics. Design accommodations for any given component shape and service environment require extensive numerical computational capabilities. CARES/CREEP incorporates damage mechanics with ANSYS finite element transient analysis to predict time-dependent material deformation and damage accumulation. CARES/LIFE combines multidisciplinary research in fracture mechanics and probabilistic modeling to determine the reliability of a monolithic ceramic component as a function of time in service. CARES/LIFE enables the design engineer to assess the risk of fracture from various competing failure mechanisms, including flaws introduced

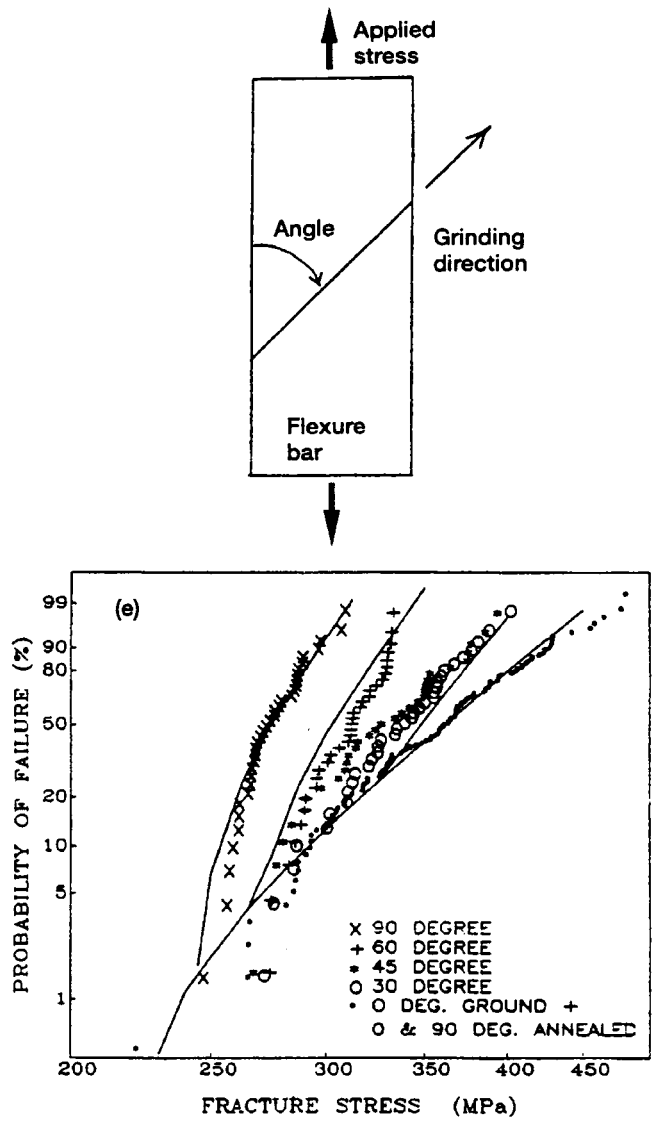

Figure 1.—Predicted versus experimental sensitivities of failure probability of unidirectionally ground ceramic relative to various loading orientations.

from finishing (grinding) operations, and to determine overall failure probability of a component over its life.

CARES/LIFE has been distributed to more than 75 U.S. companies for use in an extraordinarily wide array of product designs ranging from aerospace components to medical implants. It is the only public domain computer program of its kind available in the United States today. This technology applies to advanced ceramic materials (fig. 1), including silicon nitride and silicon carbide, and other brittle materials, such as glass and graphite. Many commercial products, such as turbocharger rotors, rocker arm pads, cam followers, poppet valves, radiant heater tubes, heat exchangers, and prototype ceramic turbines, are designed using this software. In addition, CARES/LIFE is used to design large infrared transmission windows, glass panels for skyscrapers, ceramic packaging for microprocessors, cathode ray tubes (fig. 2), and even ceramic tooth crowns and knee caps. The picture tube is in commercial production, and $1.5 million has been saved per year by using CARES/LIFE to optimize the design. Because of this demonstrated success CARES/LIFE won the first NASA Software of the Year Award for 1994.

Bibliography

Nemeth, N.N.; Powers, L.M.; Janosik, L.A.; and Gykenyesi, J.P.: Time-Dependent Reliability Analysis of Monolithic Ceramic Components Using the CARES/LIFE Integrated Design Program. Life Prediction Methodologies and Data for Ceramic Materials, ASTM STP–1201, C.R. Brinkman and S.F. Duffy, eds., American Society for Testing and Materials, Philadelphia, PA, 1993, pp. 390–408.

Nemeth, N.N.; Powers, L.M.; Janosik, L.A.; and Gykenyesi, J.P.: Lifetime Reliability Evaluation of Structural Ceramic Parts With the CARES/LIFE Computer Program. AIAA Paper 93–1497–CP, 1993, pp. 1634–1646.

Powers, L.M.; Janosik, L.A.; Nemeth, N.N.; and Gykenyesi, J.P.: Time-Dependent Reliability Analysis of Monolithic Ceramic Components Using the CARES/LIFE Integrated Design Program. Presented at the American Ceramic Society Annual Meeting and Exposition, Cincinnati, OH, April 19–22, 1993.

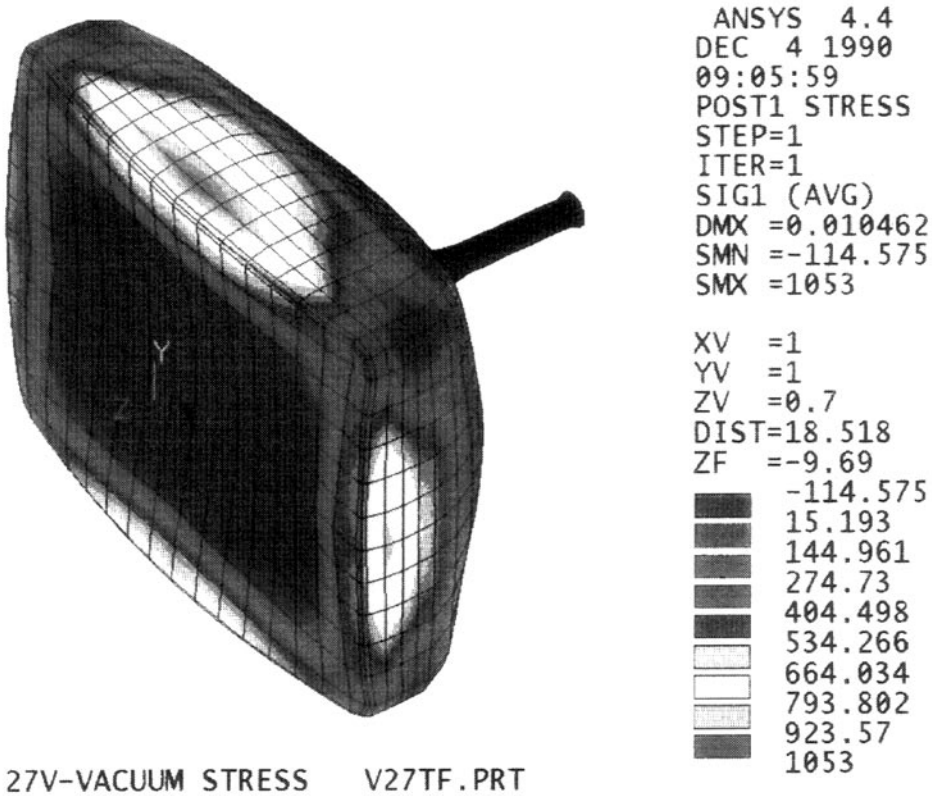

Figure 2.—Stress analysis of 27-in. television picture tube using CARES/LIFE.

Nemeth, N.N.; Powers, L.M.; Janosik, L.A.; and Gykenyesi, J.P.: Designing Ceramic Components for Durability. Am. Ceram. Soc. Bull., vol. 72, no. 12, Dec. 1993, pp. 59–69.

Nemeth, N.N.; Powers, L.M.; Janosik, L.A.; and Gykenyesi, J.P.: Durability Evaluation of Ceramic Components Using CARES/LIFE. ASME Paper 94–GT–362, 1994.

Lewis contact: Noel N. Nemeth, (216) 433–3215

X-ray Computed Tomography Monitors Damage in Composites

The Presidential Initiative in aeronautics and manufacturing identified critical technologies for solving key issues in materials and manufacturing. These technologies include high-quality processing of composites, rapid prototyping and reengineering, on-line sensors, and feedback controllers. The imperative is to reduce new product development cycle times and integration of new techniques, such as computed tomography (CT), smart materials with in-situ sensors, and controls. In this context CT can provide rapid reengineering and cost-effective prototyping.

Lewis recently codeveloped and installed a state-of-the-art x-ray CT facility (designated SMS SMARTSCAN model 100–112 CITATM). This multipurpose, modularized, digital, x-ray facility includes an imaging system for digital radiography, CT, and computed laminography. The system consists of a 160-kV microfocus x-ray source, a solid-state charge-controlled device (CCD) area detector, a five-axis object positioning subassembly, and a Sparc-based computer system that controls data acquisition and image processing. The x-ray source provides a beam spot size down to 3 mm (0.00012 in.). The area detector system consists of a 50- by 50- by 3-mm-thick (0.002 by 0.002 by 0.12 in.), terbium-doped, glass fiber optic scintillation screen; a right-angle mirror; and a scientific-grade, digital CCD camera. The camera has a resolution of 1000 by 1018 pixels and 10-bit digitization at ambient cooling. The digital output is recorded with a high-speed, 16-bit frame grabber that allows binning of data. The detector can be configured to provide a small field of view (SFOV) approximately 19 by 19 mm (0.75 by 0.75 in.) in cross section or a larger field of view (LFOV) approximately 45 by 45 mm (1.77 by 1.77 in.) in cross section. The SFOV is used whenever the highest spatial resolution is desired;

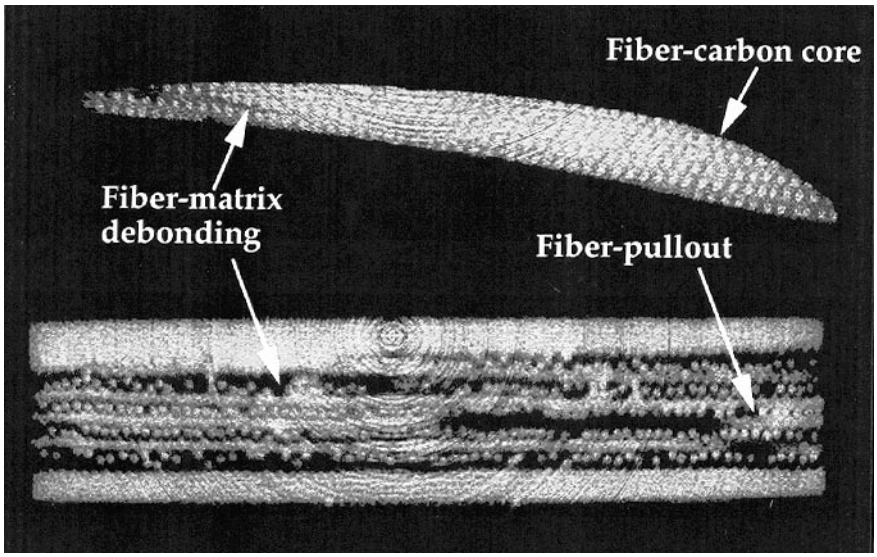

Figure 1.—Computed tomography of engine-tested vane.

the LFOV is used for larger samples with some reduction in spatial resolution.

This CT system demonstrated excellent resolution at 20 line pair per millimeter (lp/mm) (25 mm) with 20 to 40 % modulation in the SFOV mode, and 10 lp/mm (50 mm) with 50 to 70 % modulation in the LFOV mode. CT capabilities included fiber detecting, fiber-matrix debonding, fiber pullout in a $[0]_5$ silicon carbide/reaction-bonded silicon nitride (SiC/RBSN), and fiber-matrix debonding and the carbon core of oxidized SiC fibers in a engine-tested vane (fig. 1). CT evaluation of thermally cycled carbon/SiC revealed preexisting porosity, internal architecture, cracking, coating degradation, and loss of SiC materials.

The NASA Lewis CT facility can characterize critical manufacturing problems and compare as-designed with as-built metal-matrix composite engine subcomponents (rotors and rings). The facility was developed to provide rapid reengineering and to reduce new product development cycle times. Lewis is cooperating with industry to transform the CT technology from a nondestructive evaluation tool to a manufacturing and structural quality improvement tool for in-process modeling, structural modeling, and product safety assurance.

Bibliography

Baaklini, G.Y; and Engler, P.: Analysis of Ceramic Components by Computer Tomography. Invited paper to the American Ceramic Society Pacific Coast Regional Meeting, Los Angeles, Oct. 19–22, 1994.

Baaklini, G.Y.; Engler, P.; Castelli, M.G.; Bhatt, R.T.; Rauser, R.W.; and Eckel, A.J.: X-Ray Computed Tomography at LeRC—NDE of HiTEMP Composites. Proceedings of the 7th Annual HiTEMP Review, NASA CP–10146, 1994, pp. 32–1 to 32–12.

Baaklini, G.Y.; Engler, P.; Yancey, R.N.; Bhatt, R.T.; Fohey, W.R.; and Rauser, R.W.: CT Characterization of MMC and CMC Engine Subcomponents. Proceedings of the 7th Annual HiTEMP Review, NASA CP–10146, 1994, pp. 34–1 to 34–11.

Fohey, W.R.; Bhatt, R.T.; and Baaklini, G.Y.: Burner Rig, Stressed Oxidation and Engine Test Results of SCS–6/RBSN Composites. Proceedings of the 7th Annual HiTEMP Review, NASA CP–10146, 1994, pp. 21–1 to 21–12.

Hsu, D.K.; Liaw, P.K.; and Baaklini, G.Y.: Comparison of NDE Results and Correlation With Microstructural Characteristics of NiFeAl/W. ASME 94–GT–489, June 1994.

Hsu, D.K.; He, L.X.; Basart, J.P.; Liaw, P.K.; and Baaklini, G.Y.: Some Results on the NDE of Metal Matrix Composites. Review of Progress in Quantitative Nondestructive Evaluation (QNDE), D.O. Thompson and D.E. Chimenti, eds., Vol. 14B, Aug. 1994, pp. 1367–1374.

Rokhlin, S.I.; Chu, Y.C.; and Baaklini, G.Y.: Assessment of Damage in Ceramics and Ceramic Matrix Composites Using Ultrasonic Techniques. ASME Paper 94–GT–228, 1994.

Rokhlin, S.I.; Chu, Y.C.; Baaklini, G.Y.; and Bhatt, R.T.: Ultrasonic Characterization of Interphasial Stiffness and Oxidation in SiC/RBSN Composites. Proceedings of 7th Anual HiTEMP Review, NASA CP–10146, 1994, pp. 22–1 to 22–11.

Rokhlin, S.I.; Chu, Y.C.; Baaklini, G.Y.; and Bhatt, R.T.: Ultrasonic Assessment of Oxidation Damage in SiC/RBSN Composites. Ceram. Eng. Sci. Proc., vol. 15, no. 5, 1994, pp. 1164–1173.

Roth, D.J.; Baaklini, G.Y.; Sutteer, J.K.; Bodis, J.R.; Leonhardt, T.A.; and Crane, E.A.: NDE Methods Necessary for Accurate Characterization of Polymer Matrix Composite Uniformity. Proceedings of 7th Annual HiTEMP Review, NASA CP–10146, 1994, pp. 11–1 to 11–15.

Lewis contact: George Y. Baaklini, (216) 433–6016

Bibliography

Arnold, S.M.; Saleeb, A.F.; and Castelli, M.G.: A Fully Associative, Nonlinear Kinematic, Unified Viscoplastic Model for Titanium-Based Matrices. NASA TM–106609, 1994.

Arnold, S.M.; Saleeb, A.F.; and Castelli, M.G.: A Fully Associative, Nonisothermal, Nonlinear Kinematic, Unified Viscoplastic Model for Titanium Alloys. NASA TM–106926, 1994.

Arnold, S.M.; Wilt, T.E.; and Pindera, M.J.: Influence of Fiber Architecture on the Elastic and Inelastic Response of Metal Matrix Composites. NASA TM–106705, 1994.

Baaklini, G.Y; and Engler, P.: Analysis of Ceramic Components by Computer Tomography. Invited paper to the American Ceramic Society Pacific Coast Regional Meeting, Los Angeles, Oct. 19–22, 1994.

Baaklini, G.Y.; Engler, P.; Castelli, M.G.; Bhatt, R.T.; Rauser, R.W.; and Eckel, A.J.: X-Ray Computed Tomography at LeRC—NDE of HiTEMP Composites. Proceedings of the 7th Annual HiTEMP Review, NASA CP–10146, 1994, pp. 32–1 to 32–12.

Baaklini, G.Y.; Engler, P.; Yancey, R.N.; Bhatt, R.T.; Fohey, W.R.; and Rauser, R.W.: CT Characterization of MMC and CMC Engine Subcomponents. Proceedings of the 7th Annual HiTEMP Review, NASA CP–10146, 1994, pp. 34–1 to 34–11.

Bakhle, M.A.: FPCAS2D Users Guide, Version 1.0. NASA CR–195413, 1994.

Belegundu, A.D.; Murthy, D.V.; Salagame, R.R.; and Constans, E.W.: Multi-Objective Optimization of Laminated Ceramic Composites Using Genetic Algorithms. Presented at the 5th Symposium on Multidisciplinary Analysis and Optimization, Panama City Beach, FL, Sept. 7–9, 1994.

Bonacuse, P.J.; and Kalluri, S.: Cyclic Axial-Torsional Deformation Behavior of a Cobalt-Base Superalloy. Cyclic Deformation, Fracture and Nondestructive Evaluation of Advanced Materials Symposium, ASTM STP–1184, Vol. 2, M.R. Mitchell and O. Buck, eds., American Society for Testing and Materials, Philadelphia, PA, 1994, pp. 204–229.

Brown, G.V.: Tests of an Electromagnet-Biased Homopolar Magnetic Bearing. Advanced Earth-to-Orbit Propulsion Technology—1994, R.J. Richmond and S.T. Wu, eds., NASA CP–3282, Vol. II, 1994, pp. 385–394.

Castelli, M.G.; and Lei, J.–F.: A Comparison Between High Temperature Extensometry and PdCr-Based Resistance Strain Gages With Multiple Application Techniques. Proceedings of the 7th Annual HiTEMP Review, NASA CP–10146, Vol. II, 1994, pp. 36–1 to 36–12.

Chamis, C.C.; Liaw, D.G.; and Singhal, S.N.: Long-Term Behavior of Polymer Matrix Composites. Proceedings of 39th International SAMPE Symposium and Exhibition, 1994, pp. 2820–2828.

Chamis, C.C.; Murthy, P.L.N.; Singhal, S.N.; and Reddy, E.S.: Ice-Impact Analysis of Blades. Presented at the Propulsion and Energetics Panel, AGARD–CP–558, 1994.

Chamis, C.C.; and Shiao, M.C.: Integrated Probabilistic Composite Design, A Proposed New Approach. Proceedings of 39th International SAMPE Symposium and Exhibition, 1994, pp. 2806–2819.

Chamis, C.C.; and Singhal, S.N.: Coupled Multidiscipline Analysis Methods for Advanced Propulsion Systems. AIAA Paper 94–3094, 1994.

Chamis, C.C.; and Singhal, S.N.: Probabilistic Simulation of the Human Factor in Structural Reliability. NASA TM–106498, 1994.

Davy, D.T.; Saravanos, D.A.; Hopkins, D.A.; and Chamis, C.C.: Numerical Optimization and Composite Modeling Techniques Applied to Orthopedic Implants. Proceedings of 39th International SAMPE Symposium and Exhibition, 1994, pp. 1992–2003.

Ferri, R.; and Pereira, J.M.: Strength and Stiffness Properties of Graphite/Epoxy Laminates With Interlaminar Damping Layers. Proceedings of the 39th SAMPE Symposium, 1994, pp. 2544–2551.

Fohey, W.R.; Bhatt, R.T.; and Baaklini, G.Y.: Burner Rig, Stressed Oxidation and Engine Test Results of SCS–6/RBSN Composites. Proceedings of the 7th Annual HiTEMP Review, NASA CP–10146, 1994, pp. 21–1 to 21–12.

Fusaro, R.L.: Lubrication of Space Systems. NASA TM–106392, 1994.

Generazio, E.R.; and Chamis, C.C.: Technology Benefit Estimator for Aerospace Propulsion Systems. AIAA Paper 94–3096.

Generazio, E.R.; Chamis, C.C.; and Abumeri, G.: Technology Benefit Estimator (T/BEST): User's Manual. NASA TM–106785, 1994.

Heyliger, P.; Ramirez, G.; and Saravanos, D.: Coupled Discrete-Layer Finite Elements for Laminated Piezoelectric Plates. Communications in Numerical Methods in Engineering, vol. 10, 1994, pp. 971–981.

Hsu, D.K.; He, L.X.; Basart, J.P.; Liaw, P.K.; and Baaklini, G.Y.: Some Results on the NDE of Metal Matrix Composites. Review of Progress in Quantitative Nondestructive Evaluation (QNDE), D.O. Thompson and D.E. Chimenti, eds., Vol. 14B, Aug. 1994, pp. 1367–1374.

Hsu, D.K.; Liaw, P.K.; and Baaklini, G.Y.: Comparison of NDE Results and Correlation With Microstructural Characteristics of NiFeAl/W. ASME 94–GT–489, June 1994.

Kalluri, S.; Bhanu Sankara Rao, K.; Halford, G.R.; and McGaw, M.A.: Deformation and Damage Mechanisms in Inconel 718 Superalloy. Proceedings of the Symposium on Superalloys 718, 625, 706 and Various Derivatives, E.A. Loria, ed., The Minerals, Metals, and Materials Society, 1994, pp. 593–606.

Kalluri, S.; and Bonacuse, P.J.: Estimation of Fatigue Life Under Axial-Torsional Loading. Material Durability/Life Prediction Modeling: Materials for the 21st Century, PVP–Vol. 290, S.Y. Zamrik and G.R. Halford, eds., American Society of Mechanical Engineers, New York, 1994.

Kalluri, S.; Halford, G.R.; and McGaw, M.A.: Fatigue Behavior of Inconel 718 Superalloy Subjected to Monotonic Tensile and Compressive Strains. Advanced Earth-To-Orbit Propulsion Technology, R.J. Richmond and S.T. Wu, eds., Vol. 2, 1994, pp. 287–294.

Lerch, B.A.; and Noebe, R.D.: Low-Cycle Fatigue Behavior of Polycrystalline NiAl at 1000 K. Metall. Maters. Trans. A, vol. 25A, 1994, pp. 309–319.

Mahajan, A.J.; Bakhle, M.A.; and Dowell, E.H.: A New Method for Aeroelastic Stability Analysis of Cascades Using Nonlinear, Time-Marching CFD Solvers. AIAA Paper 94–4396, 1994.

Minnetyan, L.; Chamis, C.C.; and Murthy, P.L.N.: Effect of Adhesive Thickness on the Durability of a Stiffened Composite Panel. Proceedings of 39th International SAMPE Symposium and Exhibition, 1994, pp. 2044–2056.

Minnetyan, L.; Chamis, C.C.; and Murthy, P.L.N.: Damage Progression in Bent Composite Structural Members. AIAA Paper 94–1455–CP, pp. 1173–1180.

Minnetyan, L.; Chamis, C.C.; and Murthy, P.L.N.: Damage Tolerance of Thick Composite Shells Under External Pressure. Proceedings of the 10th Conference on Fibrous Composites in Structural Design, Report NAWCADWAR–94096–60, Vol. I, Apr. 1994, pp. 85–95.

Minnetyan, L.; Chamis, C.C.; and Murthy, P.L.N.: Damage Progression in Mechanical Fastened Composite Structural Joints. Proceedings of the American Society for Composites 9th Technical Conference, Technomic Publishing Co., Neward, Delaware, 1994, pp. 397–404.

Mital, S.K.; and Chamis, C.C.: Thermal and Mechnical Behavior of Particulate Composite Materials. Proceedings the Energy-Sources Technology Conference, American Society of Mechanical Engineers, New York, 1994, pp. 275–283.

Mital, S.K.; Murthy, P.L.N.; and Chamis, C.C.: Modeling of Stress/Strain Behavior of Fiber-Reinforced Ceramic Matrix Composites Including Stress Redistribution. NASA TM–106789, 1994.

Munson, J.; and Steinetz, B.M.: Specific Fuel Consumption and Increased Thrust Performance Benefits Possible With Advanced Seal Technology. AIAA Paper 94–2700, 1994.

Murthy, P.L.N.; Chamis, C.C.; and Minnetyan, L.: Design for Progressive Damage in Fibrous Composite Structures. Proceedings of 39th International SAMPE Symposium and Exhibition, 1994, pp. 1705–1715.

Nemeth, N.N.; Powers, L.M.; Janosik, L.A.; and Gykenyesi, J.P.: Durability Evaluation of Ceramic Components Using CARES/LIFE. ASME Paper 94–GT–362, 1994.

Pai, S.S.; and Chamis, C.C.: Probabilistic Progressive Buckling of Trusses. J. Space. Rock., vol. 31, no. 3, May-June 1994, pp. 466–474.

Pereira, J.M.; Kautz, H.E.; Roth, D.J.; and Duke, J.: Measurement of Mechanical Damage in Ceramic Matrix Composites Using Vibration and Acousto-Ultrasonic NDE. Proceedings of the 7th Annual HiTEMP Review, NASA CP–10146, Vol. I, 1994, pp. 23–1 to 23–12.

Reddy, T.S.R.; and Srivastava, R.: Analysis of a Rotor-Stator Stage Using a Two-Dimensional Euler Aeroelastic Solver. AIAA Paper 94–1638–CP, 1994, pp. 2537–2551.

Rokhlin, S.I.; Chu, Y.C.; and Baaklini, G.Y.: Assessment of Damage in Ceramics and Ceramic Matrix Composites Using Ultrasonic Techniques. ASME Paper 94–GT–228, 1994.

Rokhlin, S.I.; Chu, Y.C.; Baaklini, G.Y.; and Bhatt, R.T.: Ultrasonic Characterization of Interphasial Stiffness and Oxidation in SiC/RBSN Composites. Proceedings of 7th Anual HiTEMP Review, NASA CP–10146, 1994, pp. 22–1 to 22–11.

Rokhlin, S.I.; Chu, Y.C.; Baaklini, G.Y.; and Bhatt, R.T.: Ultrasonic Assessment of Oxidation Damage in SiC/RBSN Composites. Ceram. Eng. Sci. Proc., vol. 15, no. 5, 1994, pp. 1164–1173.

Roth, D.J.; Baaklini, G.Y.; Sutteer, J.K.; Bodis, J.R.; Leonhardt, T.A.; and Crane, E.A.: NDE Methods Necessary for Accurate Characterization of Polymer Matrix Composite Uniformity. Proceedings of 7th Annual HiTEMP Review, NASA CP–10146, 1994, pp. 11–1 to 11–15.

Saigal, A.; and Pereira, J.M.: Mechanical Behaviour and Residual Stresses in Unidirectional Tungsten Fibre-Reinforced Copper Matrix Composites. International Symposium on Recent Developments in Light Metals. Canadian Inst. Mining Met., 1994.

Saleeb, A.F.; Seif, Y.; and Arnold, S.M.: Fully Associative Viscoplasticity With Anisotropic and Nonlinear Kinematic Hardening. Submitted Int. J. Plasticity, 1994.

Saravanos, D.A.; Birman, V.; and Hopkins, D.A.: Detection of Delaminations in Composite Beams Using Piezoelectric Sensors. AIAA Paper 94–1754–CP, 1994, pp. 181–191.

Saravanos, D.A.; Heyliger, P.R.; and Hopkins, D.A.: Mechanics for the Coupled Dynamic Response of Active/Sensory Composite Structures. AIAA Paper 94–1756–CP, 1994, pp. 199–209.

Saravanos, D.A.; Lin, Y.J.; Choi, B.B.; and Hopkins, D.A.: On Smart Composite Structures for Active Tip Clearance Control. Adaptive Structures and Composite Materials: Analysis and Application. American Society of Mechanical Engineers, New York, 1994, pp. 145–150.

Shah, A.R.; Ball, R.D.; and Chamis, C.C.: Probabilistic Assessment of Space Nuclear Propulsion System Nozzle. NASA TM–106539, 1994.

Shah, A.R.; Singhal, S.N.; Murthy, P.L.N.; and Chamis, C.C.: Probabilistic Simulation of Long-Term Behavior in Polymer Matrix Composites. AIAA Paper 94–1445–CP, 1994, pp. 1095–1104.

Shiao, M.C.; and Chamis, C.C.: Optimization of Adaptive Intraply Hybrid Fiber Composites With Reliability Considerations. NASA TM–106632, 1994.

Shiao, M.C.; and Chamis, C.C.: Reliability of Composite Structures With Multiple Design Criteria. NASA TM–106716, 1994.

Shiao, M.C.; and Chamis, C.C.: Probabilistic Design of Smart Composite Structures. Proceedings of 39th International SAMPE Symposium and Exhibition, 1994, pp. 3112–1715.

Shiao, M.C.; and Chamis, C.C.: A Probabilistic Buckling Design of Stiffened Composite Structures With Cutouts. Proceedings of the 10th Conference on Fibrous Composites in Structural Design, Report NAWCADWAR–94096–60, Vol. I, April 1994, pp. 37–52.

Singhal, S.N.; Abumeri, G.H.; Shiao, M.C.; and Chamis, C.C.: Probabilistic Assessment of Tailored Composite Structures. AIAA Paper 94–1418–CP, pp. 871–881.

Singhal, S.N.; Shah, A.R.; Chamis, C.C.; and Murthy, P.L.N.: Computational Simulation of Fatigue Endurance Design for Composites. Proceedings of 39th International SAMPE Symposium and Exhibition, 1994, pp. 3283–3294.

Singhal, S.N.; Tong, M.T.; Murthy, P.L.N.; and Chamis, C.C.: Multi-Factor Interaction Model for Nonlinear Materials Behavior. ASME–Publications-vol. 62, 1994, pp. 261–274.

Srivastava, R.; Reddy, T.S.R.; and Mehmed, O.: Flutter Analysis of Propfans Using a Three-Dimensional Euler Solver. AIAA Paper 94–1549–CP, 1994, pp. 1803–1813.

Steinberg, E.P.; and Chamis, C.C.: Structural Probability Concepts Adapted to Electrical Engineering. AIAA Paper–94–1383–CP, pp. 616–632.

Steinetz, B.M.; and Hendricks, R.C.: Engine Seal Technology Requirements to Meet NASA's Advanced Subsonic Technology Program Goals. AIAA Paper 94–2698, 1994. (Also NASA TM–106582.)

Sutjahjo, E.; and Chamis, C.C.: Coupled Finite Element Analysis of Fluid Mechanics, Heat Transfer, and Solid Mechanics. AIAA Paper 94–1586–CP, 1994, pp. 2135–2145.

Tong, M.T.; Singhal, S.N.; and Chamis, C.C.: Computational Simulation of the Formation and Material Behavior of Ice. NASA TM–106702, 1994.

Wilt, T.E.; and Arnold, S.M.: Micromechanics Analysis Code (MAC) User Guide: Version 1.0. NASA TM–106706, 1994.

Worthem, D.W.: Thermomechanical Fatigue Behavior of Coated and Uncoated Enhanced SiC/SiC[PW]. Proceedings of the 7th Annual HiTEMP Review, NASA CP–10146, Vol. 3, 1994, pp. 66–1 to 66–12.

Zaretsky, E.V.; Chamis, C.C.; Murthy, P.L.N.; Singhal, S.N.; and Hopkins, D.: Modeling the Future With Metal-Matrix Composites. Machine Design, vol. 66, no. 5, Mar. 1994, pp. 124–132.

REPORT DOCUMENTATION PAGE

Form Approved
OMB No. 0704-0188

1. AGENCY USE ONLY (*Leave blank*)

2. REPORT DATE
May 1996

3. REPORT TYPE AND DATES COVERED
Technical Memorandum

4. TITLE AND SUBTITLE
Structures Division 1994 Annual Report

5. FUNDING NUMBERS
WU–505–63–5B

6. AUTHOR(S)

7. PERFORMING ORGANIZATION NAME(S) AND ADDRESS(ES)
National Aeronautics and Space Administration
Lewis Research Center
Cleveland, Ohio 44135–3191

8. PERFORMING ORGANIZATION REPORT NUMBER
E–9763

9. SPONSORING/MONITORING AGENCY NAME(S) AND ADDRESS(ES)
National Aeronautics and Space Administration
Washington, D.C. 20546–0001

10. SPONSORING/MONITORING AGENCY REPORT NUMBER
NASA TM–106989

11. SUPPLEMENTARY NOTES
Responsible person, Cindy Acquaviva, organization code 5200, (216) 433–3306.

12a. DISTRIBUTION/AVAILABILITY STATEMENT
Unclassified - Unlimited
Subject Category 00 or Categories 00 and 00

This publication is available from the NASA Center for Aerospace Information, (301) 621–0390.

12b. DISTRIBUTION CODE

13. ABSTRACT ***(Maximum 200 words)***

The NASA Lewis Research Center Structures Division is an international leader and pioneer in developing new structural analysis, life prediction, and failure analysis related to rotating machinery and more specifically to hot section components in air-breathing aircraft engines and spacecraft propulsion systems. The research consists of both deterministic and probabilistic methodology. Studies include, but are not limited to, high-cycle and low-cycle fatigue as well as material creep. Studies of structural failure are at both the micro- and macrolevels. Nondestructive evaluation methods related to structural reliability are developed, applied, and evaluated. Materials from which structural components are made, studied, and tested are monolithics and metal-matrix, polymer-matrix, and ceramic-matrix composites. Aeroelastic models are developed and used to determine the cyclic loading and life of fan and turbine blades. Life models are developed and tested for bearings, seals, and other mechanical components, such as magnetic suspensions. Results of these studies are published in NASA technical papers and reference publication as well as in technical society journal articles. The results of the work of the Structures Division and the bibliography of its publications for calendar year 1994 are presented.

14. SUBJECT TERMS
Structural mechanics; Structural fatigue; Structural dynamics; Structural integrity

15. NUMBER OF PAGES
73

16. PRICE CODE
A04

17. SECURITY CLASSIFICATION OF REPORT
Unclassified

18. SECURITY CLASSIFICATION OF THIS PAGE
Unclassified

19. SECURITY CLASSIFICATION OF ABSTRACT
Unclassified

20. LIMITATION OF ABSTRACT